THE UNIVERSITY OF CALGARY

Analysis of Eclipsing Binaries in the Globular Cluster M71

by

Jason Reed McVean

A THESIS

SUBMITTED TO THE FACULTY OF GRADUATE STUDIES

IN PARTIAL FULFILLMENT OF THE REQUIREMENTS FOR THE

DEGREE OF MASTER OF SCIENCE

DEPARTMENT OF PHYSICS AND ASTRONOMY

CALGARY, ALBERTA

SEPTEMBER, 1994

ISBN 0-315-99422-3

Canada

Name __Jason Read McLean__

Dissertation Abstracts International is arranged by broad, general subject categories. Please select the one subject which most nearly describes the content of your dissertation. Enter the corresponding four-digit code in the spaces provided.

__Astronomy and Astrophysics__

| 0 | 6 | 0 | 6 | U·M·I

Subject Categories

THE HUMANITIES AND SOCIAL SCIENCES

COMMUNICATIONS AND THE ARTS
Architecture 0729
Art History 0377
Cinema 0900
Dance 0378
Fine Arts 0357
Information Science 0723
Journalism 0391
Library Science 0399
Mass Communications 0708
Music 0413
Speech Communication 0459
Theater 0465

EDUCATION
General 0515
Administration 0514
Adult and Continuing 0516
Agricultural 0517
Art 0273
Bilingual and Multicultural 0282
Business 0688
Community College 0275
Curriculum and Instruction 0727
Early Childhood 0518
Elementary 0524
Finance 0277
Guidance and Counseling 0519
Health 0680
Higher 0745
History of 0520
Home Economics 0278
Industrial 0521
Language and Literature 0279
Mathematics 0280
Music 0522
Philosophy of 0998
Physical 0523

Psychology 0525
Reading 0535
Religious 0527
Sciences 0714
Secondary 0533
Social Sciences 0534
Sociology of 0340
Special 0529
Teacher Training 0530
Technology 0710
Tests and Measurements 0288
Vocational 0747

LANGUAGE, LITERATURE AND LINGUISTICS
Language
  General 0679
  Ancient 0289
  Linguistics 0290
  Modern 0291
Literature
  General 0401
  Classical 0294
  Comparative 0295
  Medieval 0297
  Modern 0298
  African 0316
  American 0591
  Asian 0305
  Canadian (English) 0352
  Canadian (French) 0355
  English 0593
  Germanic 0311
  Latin American 0312
  Middle Eastern 0315
  Romance 0313
  Slavic and East European 0314

PHILOSOPHY, RELIGION AND THEOLOGY
Philosophy 0422
Religion
  General 0318
  Biblical Studies 0321
  Clergy 0319
  History of 0320
  Philosophy of 0322
Theology 0469

SOCIAL SCIENCES
American Studies 0323
Anthropology
  Archaeology 0324
  Cultural 0326
  Physical 0327
Business Administration
  General 0310
  Accounting 0272
  Banking 0770
  Management 0454
  Marketing 0338
Canadian Studies 0385
Economics
  General 0501
  Agricultural 0503
  Commerce-Business 0505
  Finance 0508
  History 0509
  Labor 0510
  Theory 0511
Folklore 0358
Geography 0366
Gerontology 0351
History
  General 0578

Ancient 0579
Medieval 0581
Modern 0582
Black 0328
African 0331
Asia, Australia and Oceania 0332
Canadian 0334
European 0335
Latin American 0336
Middle Eastern 0333
United States 0337
History of Science 0585
Law 0398
Political Science
  General 0615
  International Law and
    Relations 0616
  Public Administration 0617
Recreation 0814
Social Work 0452
Sociology
  General 0626
  Criminology and Penology ... 0627
  Demography 0938
  Ethnic and Racial Studies 0631
  Individual and Family
    Studies 0628
  Industrial and Labor
    Relations 0629
  Public and Social Welfare 0630
  Social Structure and
    Development 0700
  Theory and Methods 0344
Transportation 0709
Urban and Regional Planning 0999
Women's Studies 0453

THE SCIENCES AND ENGINEERING

BIOLOGICAL SCIENCES
Agriculture
  General 0473
  Agronomy 0285
  Animal Culture and
    Nutrition 0475
  Animal Pathology 0476
  Food Science and
    Technology 0359
  Forestry and Wildlife 0478
  Plant Culture 0479
  Plant Pathology 0480
  Plant Physiology 0817
  Range Management 0777
  Wood Technology 0746
Biology
  General 0306
  Anatomy 0287
  Biostatistics 0308
  Botany 0309
  Cell 0379
  Ecology 0329
  Entomology 0353
  Genetics 0369
  Limnology 0793
  Microbiology 0410
  Molecular 0307
  Neuroscience 0317
  Oceanography 0416
  Physiology 0433
  Radiation 0821
  Veterinary Science 0778
  Zoology 0472
Biophysics
  General 0786
  Medical 0760

EARTH SCIENCES
Biogeochemistry 0425
Geochemistry 0996

Geodesy 0370
Geology 0372
Geophysics 0373
Hydrology 0388
Mineralogy 0411
Paleobotany 0345
Paleoecology 0426
Paleontology 0418
Paleozoology 0985
Palynology 0427
Physical Geography 0368
Physical Oceanography 0415

HEALTH AND ENVIRONMENTAL SCIENCES
Environmental Sciences 0768
Health Sciences
  General 0566
  Audiology 0300
  Chemotherapy 0992
  Dentistry 0567
  Education 0350
  Hospital Management 0769
  Human Development 0758
  Immunology 0982
  Medicine and Surgery 0564
  Mental Health 0347
  Nursing 0569
  Nutrition 0570
  Obstetrics and Gynecology .. 0380
  Occupational Health and
    Therapy 0354
  Ophthalmology 0381
  Pathology 0571
  Pharmacology 0419
  Pharmacy 0572
  Physical Therapy 0382
  Public Health 0573
  Radiology 0574
  Recreation 0575

Speech Pathology 0460
Toxicology 0383
Home Economics 0386

PHYSICAL SCIENCES
Pure Sciences
Chemistry
  General 0485
  Agricultural 0749
  Analytical 0486
  Biochemistry 0487
  Inorganic 0488
  Nuclear 0738
  Organic 0490
  Pharmaceutical 0491
  Physical 0494
  Polymer 0495
  Radiation 0754
Mathematics 0405
Physics
  General 0605
  Acoustics 0986
  Astronomy and
    Astrophysics 0606
  Atmospheric Science 0608
  Atomic 0748
  Electronics and Electricity 0607
  Elementary Particles and
    High Energy 0798
  Fluid and Plasma 0759
  Molecular 0609
  Nuclear 0610
  Optics 0752
  Radiation 0756
  Solid State 0611
Statistics 0463

Applied Sciences
Applied Mechanics 0346
Computer Science 0984

Engineering
  General 0537
  Aerospace 0538
  Agricultural 0539
  Automotive 0540
  Biomedical 0541
  Chemical 0542
  Civil 0543
  Electronics and Electrical 0544
  Heat and Thermodynamics ... 0348
  Hydraulic 0545
  Industrial 0546
  Marine 0547
  Materials Science 0794
  Mechanical 0548
  Metallurgy 0743
  Mining 0551
  Nuclear 0552
  Packaging 0549
  Petroleum 0765
  Sanitary and Municipal 0554
  System Science 0790
Geotechnology 0428
Operations Research 0796
Plastics Technology 0795
Textile Technology 0994

PSYCHOLOGY
General 0621
Behavioral 0384
Clinical 0622
Developmental 0620
Experimental 0623
Industrial 0624
Personality 0625
Physiological 0989
Psychobiology 0349
Psychometrics 0632
Social 0451

♻

Nom _____

Dissertation Abstracts International est organisé en catégories de sujets. Veuillez s.v.p. choisir le sujet qui décrit le mieux votre thèse et inscrivez le code numérique approprié dans l'espace réservé ci-dessous.

SUJET

□□□□ U·M·I

CODE DE SUJET

Catégories par sujets

HUMANITÉS ET SCIENCES SOCIALES

COMMUNICATIONS ET LES ARTS
Architecture	0729
Beaux-arts	0357
Bibliothéconomie	0399
Cinéma	0900
Communication verbale	0459
Communications	0708
Danse	0378
Histoire de l'art	0377
Journalisme	0391
Musique	0413
Sciences de l'information	0723
Théâtre	0465

ÉDUCATION
Généralités	515
Administration	0514
Art	0273
Collèges communautaires	0275
Commerce	0688
Économie domestique	0278
Éducation permanente	0516
Éducation préscolaire	0518
Éducation sanitaire	0680
Enseignement agricole	0517
Enseignement bilingue et multiculturel	0282
Enseignement industriel	0521
Enseignement primaire.	0524
Enseignement professionnel	0747
Enseignement religieux	0527
Enseignement secondaire	0533
Enseignement spécial	0529
Enseignement supérieur	0745
Évaluation	0288
Finances	0277
Formation des enseignants	0530
Histoire de l'éducation	0520
Langues et littérature	0279

Lecture	0535
Mathématiques	0280
Musique	0522
Orientation et consultation	0519
Philosophie de l'éducation	0998
Physique	0523
Programmes d'études et enseignement	0727
Psychologie	0525
Sciences	0714
Sciences sociales	0534
Sociologie de l'éducation	0340
Technologie	0710

LANGUE, LITTÉRATURE ET LINGUISTIQUE
Langues
Généralités	0679
Anciennes	0289
Linguistique	0290
Modernes	0291

Littérature
Généralités	0401
Anciennes	0294
Comparée	0295
Médiévale	0297
Moderne	0298
Africaine	0316
Américaine	0591
Anglaise	0593
Asiatique	0305
Canadienne (Anglaise)	0352
Canadienne (Française)	0355
Germanique	0311
Latino-américaine	0312
Moyen-orientale	0315
Romane	0313
Slave et est-européenne	0314

PHILOSOPHIE, RELIGION ET THÉOLOGIE
Philosophie	0422

Religion
Généralités	0318
Clergé	0319
Études bibliques	0321
Histoire des religions	0320
Philosophie de la religion	0322
Théologie	0469

SCIENCES SOCIALES
Anthropologie
Archéologie	0324
Culturelle	0326
Physique	0327
Droit	0398

Économie
Généralités	0501
Commerce-Affaires	0505
Économie agricole	0503
Économie du travail	0510
Finances	0508
Histoire	0509
Théorie	0511
Études américaines	0323
Études canadiennes	0385
Études féministes	0453
Folklore	0358
Géographie	0366
Gérontologie	0351

Gestion des affaires
Généralités	0310
Administration	0454
Banques	0770
Comptabilité	0272
Marketing	0338

Histoire
Histoire générale	0578

Ancienne	0579
Médiévale	0581
Moderne	0582
Histoire des noirs	0328
Africaine	0331
Canadienne	0334
États-Unis	0337
Européenne	0335
Moyen-orientale	0333
Latino-américaine	0336
Asie, Australie et Océanie	0332
Histoire des sciences	0585
Loisirs	0814

Planification urbaine et
régionale	0999

Science politique
Généralités	0615
Administration publique	0617
Droit et relations internationales	0616

Sociologie
Généralités	0626
Aide et bien-âtre social	0630
Criminologie et établissements pénitentiaires	0627
Démographie	0938
Études de l' individu et de la famille	0628
Études des relations interethniques et des relations raciales	0631
Structure et développement social	0700
Théorie et méthodes.	0344
Travail et relations industrielles	0629
Transports	0709
Travail social	0452

SCIENCES ET INGÉNIERIE

SCIENCES BIOLOGIQUES
Agriculture
Généralités	0473
Agronomie.	0285
Alimentation et technologie alimentaire	0359
Culture	0479
Élevage et alimentation	0475
Exploitation des péturages	0777
Pathologie animale	0476
Pathologie végétale	0480
Physiologie végétale	0817
Sylviculture et faune	0478
Technologie du bois	0746

Biologie
Généralités	0306
Anatomie	0287
Biologie (Statistiques)	0308
Biologie moléculaire	0307
Botanique	0309
Cellule	0379
Écologie	0329
Entomologie	0353
Génétique	0369
Limnologie	0793
Microbiologie	0410
Neurologie	0317
Océanographie	0416
Physiologie	0433
Radiation	0821
Science vétérinaire	0778
Zoologie	0472

Biophysique
Généralités	0786
Medicale	0760

SCIENCES DE LA TERRE
Biogéochimie	0425
Géochimie	0996
Géodésie	0370
Géographie physique	0368

Géologie	0372
Géophysique	0373
Hydrologie	0388
Minéralogie	0411
Océanographie physique	0415
Paléobotanique	0345
Paléoécologie	0426
Paléontologie	0418
Paléozoologie	0985
Palynologie	0427

SCIENCES DE LA SANTÉ ET DE L'ENVIRONNEMENT
Économie domestique	0386
Sciences de l'environnement	0768

Sciences de la santé
Généralités	0566
Administration des hipitaux	0769
Alimentation et nutrition	0570
Audiologie	0300
Chimiothérapie	0992
Dentisterie	0567
Développement humain	0758
Enseignement	0350
Immunologie	0982
Loisirs	0575
Médecine du travail et thérapie	0354
Médecine et chirurgie	0564
Obstétrique et gynécologie	0380
Ophtalmologie	0381
Orthophonie	0460
Pathologie	0571
Pharmacie	0572
Pharmacologie	0419
Physiothérapie	0382
Radiologie	0574
Santé mentale	0347
Santé publique	0573
Soins infirmiers	0569
Toxicologie	0383

SCIENCES PHYSIQUES

Sciences Pures

Chimie
Généralités	0485
Biochimie	487
Chimie agricole	0749
Chimie analytique	0486
Chimie minérale	0488
Chimie nucléaire	0738
Chimie organique	0490
Chimie pharmaceutique	0491
Physique	0494
PolymÇres	0495
Radiation	0754
Mathématiques	0405

Physique
Généralités	0605
Acoustique	0986
Astronomie et astrophysique	0606
Électronique et électricité	0607
Fluides et plasma	0759
Météorologie	0608
Optique	0752
Particules (Physique nucléaire)	0798
Physique atomique	0748
Physique de l'état solide	0611
Physique moléculaire	0609
Physique nucléaire	0610
Radiation	0756
Statistiques	0463

Sciences Appliqués Et Technologie
Informatique	0984

Ingénierie
Généralités	0537
Agricole	0539
Automobile	0540

Biomédicale	0541
Chaleur et ther modynamique	0348
Conditionnement (Emballage)	0549
Génie aérospatial	0538
Génie chimique	0542
Génie civil	0543
Génie électronique et électrique	0544
Génie industriel	0546
Génie mécanique	0548
Génie nucléaire	0552
Ingénierie des systèmes	0790
Mécanique navale	0547
Métallurgie	0743
Science des matériaux	0794
Technique du pétrole	0765
Technique minière	0551
Techniques sanitaires et municipales	0554
Technologie hydraulique	0545
Mécanique appliquée	0346
Géotechnologie	0428
Matières plastiques (Technologie)	0795
Recherche opérationnelle	0796
Textiles et tissus (Technologie)	0794

PSYCHOLOGIE
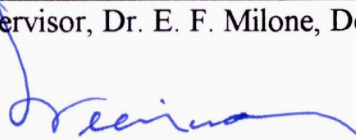|	
Généralités	0621
Personnalité	0625
Psychobiologie	0349
Psychologie clinique	0622
Psychologie du comportement	0384
Psychologie du développement	0620
Psychologie expérimentale	0623
Psychologie industrielle	0624
Psychologie physiologique	0989
Psychologie sociale	0451
Psychométrie	0632

THE UNIVERSITY OF CALGARY

FACULTY OF GRADUATE STUDIES

The undersigned certify that they have read, and recommend to the Faculty of Graduate Studies for acceptance, a thesis entitled "Analysis of Eclipsing Binaries in the Globular Cluster M71" submitted by Jason Reed McVean in partial fulfillment of the requirements for the degree Master of Science.

_____
Supervisor, Dr. E. F. Milone, Dept. of Physics and Astronomy

_____
Dr. S. R. Sreenivasan, Physics and Astronomy

_____
Dr. T. A. Clark, Physics and Astronomy

_____
Dr. D. L. Rod, Mathematics and Statistics

94/09/23
Date

ii

Abstract

The light curves of five eclipsing binary stars were analyzed using the University of Calgary's enhanced version of the Wilson-Devinney light curve modelling code and a simplex enhanced version of the same. Four of the binaries were found to be probable members of M71, while the fifth (V3) is less likely to be. Three of the probable members are contact binaries with contact parameters ranging from 0.06 to 0.27. The fourth probable member (V4) is a detached or semi-detached Algol-type system, the detached model being the more likely. The absolute parameters of all of the systems were calculated and the individual components were placed on the M71 colour magnitude diagram. The contact systems were used to check the recent colour-period-luminosity relationship for W UMa systems derived by Rucinski (1994). The possibility of mass exchange is discussed for V4 and it is concluded that mass exchange has probably not occurred.

Acknowledgements

TABLE OF CONTENTS

LIST OF TABLES

LIST OF FIGURES

1.0 INTRODUCTION

1.1 The unique astrophysical problem

The study of astrophysics suffers from a unique problem of scale. The size, distance and time scales of typical astrophysical phenomena render observation difficult and experimentation largely impossible. The limited data that can be collected from afar often lack crucial information that temporal variation would help supply, but little observable change can be expected in the vast majority of astrophysical structures in hundreds or thousands of years, so the sum of all modern astronomical observation essentially amounts to a single frame in the lifetime of the universe. As will be seen, the study of binary stars is one method of alleviating some of these problems.

A star's evolutionary path is traditionally thought to be determined primarily by its initial composition and mass, although other factors such as angular momentum are increasingly thought to be contributors as well. But without a doubt, the initial mass is the most important parameter. And yet, mass is also one of the most elusive characteristics of a star. This elusiveness is due, once again, to the problem of scale in astrophysics. If stars were not so far away, we could easily measure their mass once we arrived close enough to feel their gravitational pulls. Or alternatively, if events happened much more quickly, we could watch the path of a star among its comparatively close neighbors and deduce its mass from the interactions that take place.

Since mass is very important to a star's evolution, one expects its influence to be observable in many ways. Unfortunately, most of the means by which mass can be deduced rely on complicated processes. For instance, the gravitational acceleration felt by

atoms in a star's upper atmosphere has an observable effect. A more direct method of determining mass is through studying binary stars.

1.2 The importance of binary stars

Binary stars address the problem of mass determination because, by Newton's laws, they accelerate each other in a ratio proportional to the inverse of their masses. By virtue of the proximity of the two components, the time scale over which observation is necessary in order to see their interaction and hence deduce their masses is typically one of days or hours. Mass is not the only parameter that can be measured for binary stars. In fact, the study of binary stars is one of very few ways that many properties of stars can be determined in a direct fashion. Considering that roughly 50% of stars are in binary systems (Mihalas and Binney, 1981), if even a small fraction of binary stars yield their vital information, they act as a good sample of all the stars in the galaxy.

The amount of information that is extractable from the study of a binary star depends upon the type of binary star in question. Categorizing binaries according to how they are detected leads to three types: *visual, spectroscopic* and *eclipsing*.

A visual binary system consists of two gravitationally bound stars that can be individually resolved. The way in which the stars move around each other can be described by 8 orbital elements: the time of periastron passage, T; the time between periastron passages, P; the semimajor axis of the orbit, a; the eccentricity of the orbit, e; the position angle of the node, Ω; the inclination of the orbit, i; and the longitude of the periastron, ω. These orbital elements are illustrated and described in Figures 1a and 1b. Since the two stars can be resolved, it is possible to observe the period, P, and the projected orbits of the stars on the plane of the sky. The inclination, i, of the orbit can be
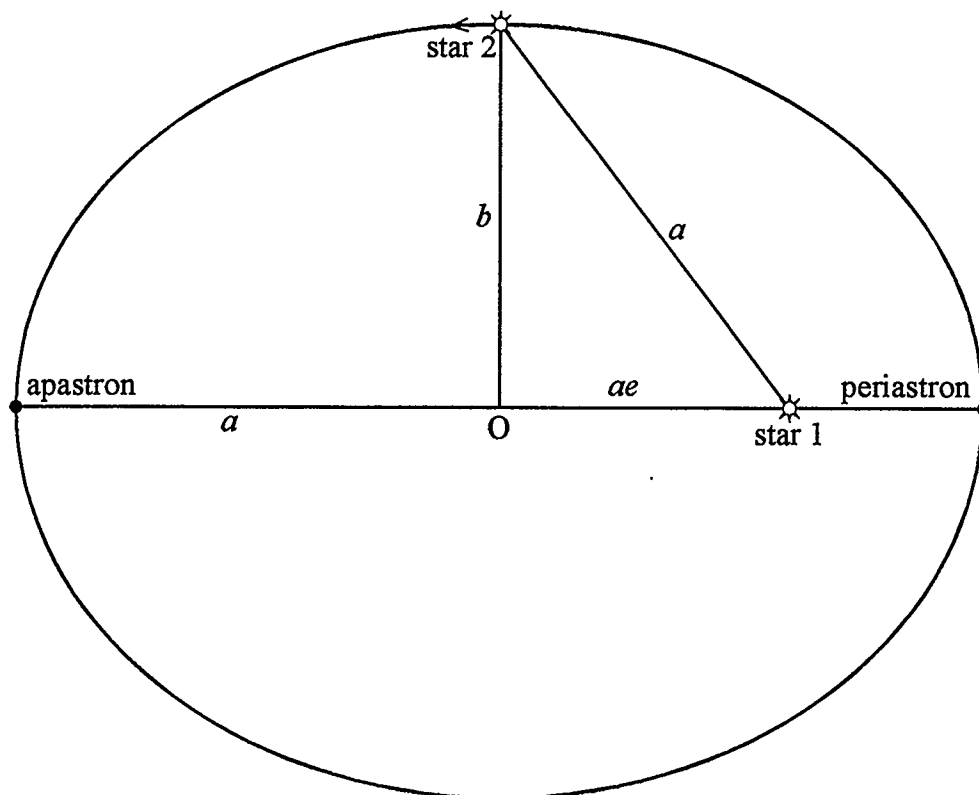
Figure 1a - The elliptical relative orbit of a binary system has the more massive star at its focus. The sum of the distances between any point on the ellipse and the two foci is equal to $2a$, where a is the semimajor axis of the ellipse, one of the elements necessary to describe a binary system orbit. The eccentricity e of the orbit, another orbital element, is equal to the ratio of the centre-to-focus distance and the semimajor axis. The semiminor axis b is measured perpendicular to the major axis from the centre O to the ellipse. The apastron is the point in the orbit at which the stars are at maximum separation. The periastron is the point of closest approach between the two stars. A third orbital element is the time of periastron passage T. The time between periastron passages is the fourth orbital element: the period P.
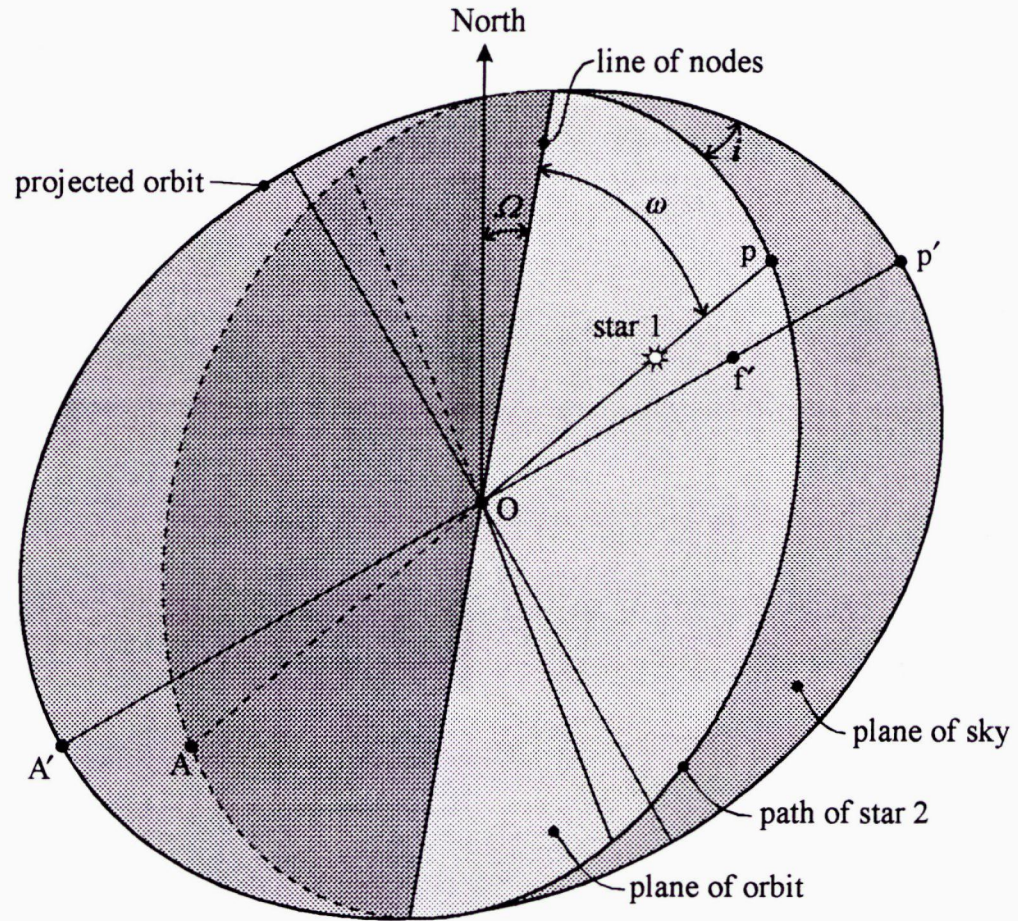
Figure 1b - The remaining elements necessary to describe a binary system orbit are illustrated. The position angle of whichever node is between zero and 180 degrees, measured eastward from north along the projected orbit, is designated Ω. The inclination i is the angle at which the plane of the true orbit tilts out of the plane of the sky. Finally, the longitude of the periastron ω is the angle between the line of nodes and the periastron p, measured along the true orbit.

deduced by measuring the apparent displacement of the more massive star from the focus of the less massive star's elliptical relative orbit. Once the inclination is known, the true orbits of the stars about the centre of mass of the system can be plotted. The mass ratio, q, of the components can then easily be found by the ratio of the distances, d_i, of the stars from the centre of mass:

$$\frac{d_1}{d_2} = \frac{m_2}{m_1} = q, \tag{1}$$

where m_1 and m_2 are the masses of the more massive star and less massive star respectively. The angular semimajor axis, a', can also be directly observed, and can be converted to the semimajor axis, a, provided that the distance, D, is known using

$$a = a'[\text{radians}] \cdot D \tag{2}$$

Knowing the distance is not an entirely unreasonable presumption since the visual binary must be reasonably nearby for the components to be resolved and still have an observably short period and an orbit small enough to resist disruption from passing stars[1]. The distances to nearby stars can be easily found by measuring their parallaxes using

$$d\,(\text{parsec}) = \frac{1}{p\,(\text{arcsec})}. \tag{3}$$

Once the semimajor axis is known, the total mass of the binary system can be calculated using Kepler's third law:

$$(m_1 + m_2) = \frac{4\pi^2}{GP^2}(a_1 + a_2)^3, \tag{4}$$

---

[1] Hills (1984) estimates that binaries with periods longer than 800 years would not survive star-star interactions in M71 but a stable system with an 800 year orbit would be very difficult to observe precisely due to incomplete coverage.

where a_1 and a_2 are the semimajor axes of the individual stars' orbits around the centre of mass such that

$$a = a_1 + a_2 . \tag{5}$$

Together, the total mass and the mass ratio allow the calculation of the individual component masses.

Of course, the precision of the individual mass determinations is strongly dependent on the precision of the measurements made. This can be quite low for distant systems since earth-based observing is limited by atmospheric fluctuations to angular resolutions of at best ~0.5 arcseconds. The close proximity required to observe visual binaries combined with the potentially very low precision for the more distant systems limits their usefulness to studies of our local region of space.

A spectroscopic binary system is a system in which the motion of one or both components can be detected by periodic variations in the Doppler shift of the lines of the system's spectrum. The Doppler shift of a spectral feature is related to the star's radial velocity, v, by the equation:

$$v = \frac{\Delta\lambda}{\lambda} c , \tag{6}$$

where λ is the unshifted wavelength of the spectral feature, $\Delta\lambda$ is the Doppler shift in the feature's wavelength, and c is the speed of light. Plotting the star's radial velocity (RV) against time gives the *radial velocity curve* of the star (see Figure 2). Because RV curves are periodic, it is common to plot radial velocity against phase, φ, rather than time, t. The phase of an observation is calculated using:

$$\varphi = \frac{t - E_O}{P} - \text{int}\left(\frac{t - E_O}{P}\right) , \tag{7}$$
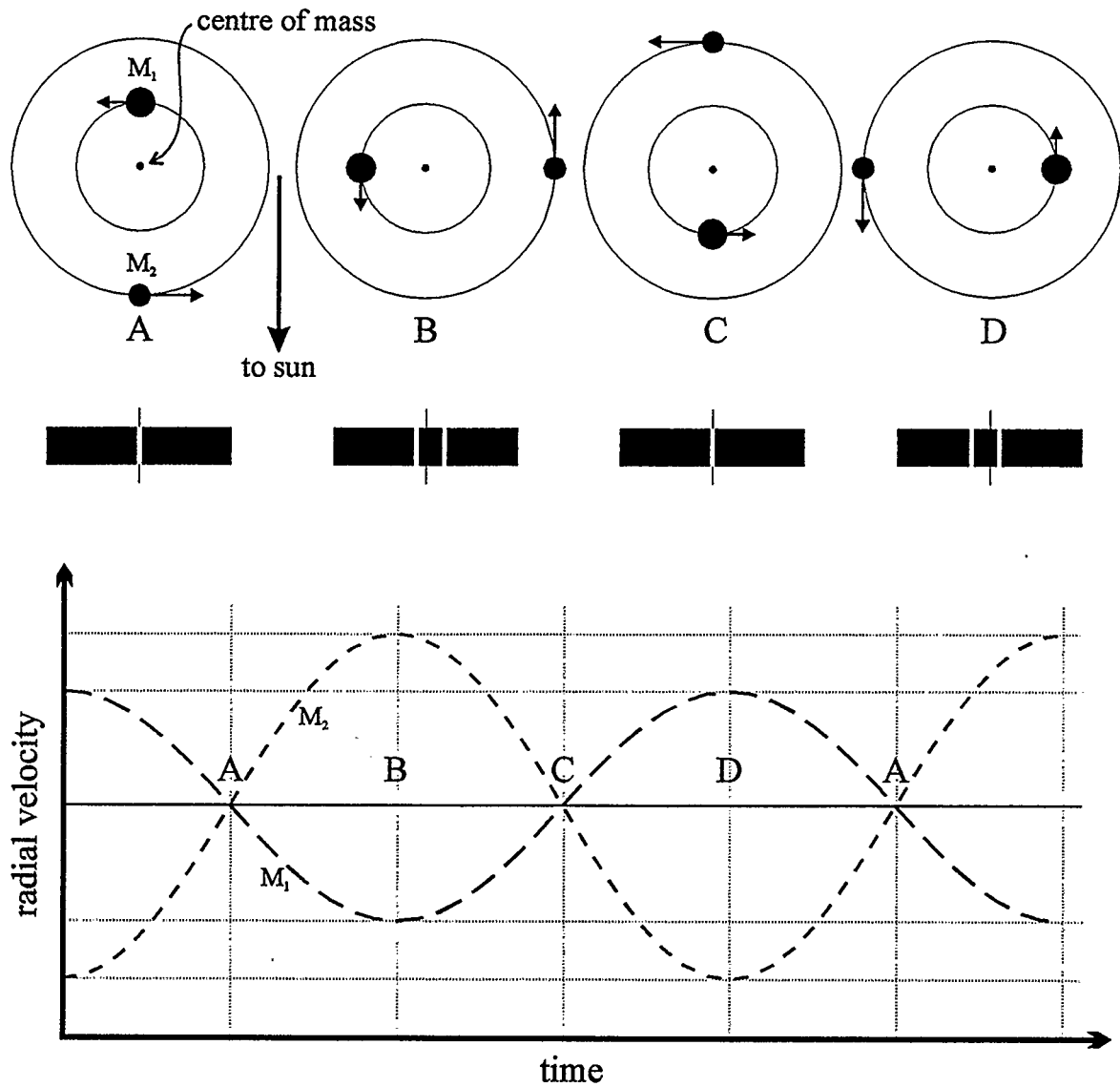
Figure 2 - A simplified radial velocity curve. The top of the figure shows the orbital configurations that correspond to the points A, B, C, and D in the radial velocity curve at the bottom of the figure. The middle portion illustrates the Doppler shifting of a spectral feature as the stars orbit.

where E_0 is the epoch of the system, a time that defines the zero-phase of the binary system. If one of the stars is considerably brighter than the other, it may not be possible to discern the second star's spectrum, in which case the system is a *single-line spectroscopic binary*. A *double-line spectroscopic binary* is one in which both stellar spectra are discernible, which is facilitated if the luminosities of the two stars are comparable and the spectral types are significantly different. This is because we depend on spectral lines to measure radial velocities, and distinct sets of lines moving in two separate groups aids in distinguishing the stars' contributions to the combined spectrum.

For a double-line spectroscopic binary the mass ratio of the components can be found from the ratio of the amplitudes of the radial velocity (RV) curves, V_i:

$$\frac{V_1}{V_2} = \frac{m_2}{m_1} = q.$$
(8)

The total mass can again be found using Kepler's third law if the semimajor axis is known. For circular orbits, the projected semimajor axis of the system's orbit can be found from the relative velocity—determined from the Doppler shift of the spectral lines—of one of stars and the period of the orbit using[2]:

---

[2] For a non-circular orbit, equation (9) becomes considerably more complicated for several reasons: the orbital velocity is not constant, so that an integration is required; the orbit is not circular, meaning the semimajor axis, a, is dependent on both the circumference, C, of the ellipse and its eccentricity, e, according to

$$a = \sqrt{\frac{C^2}{2\pi^2\left(2 - e^2\right)}} \; ;$$

and the relationship between the true semimajor axis and its tangential component, $a_\perp$, depends upon both the inclination i and the longitude of the periastron ω.

$$a_\perp = \frac{P v_{\text{relative}}}{2\pi}, \tag{9}$$

where $a_\perp$ is the projection of the semimajor axis onto a plane perpendicular to the plane of the sky:

$$a_\perp = a \cdot \sin i, \tag{10}$$

and

$$v_{\text{relative}} = |v_1| + |v_2|. \tag{11}$$

To find the true semimajor axis from the projected semimajor axis, again the inclination must be known. However, the inclination cannot be found from velocity curves alone; only the lower limit to the individual component masses of double-line spectroscopic binaries is determinable in general.

In the case of single-line spectroscopic binaries, the amplitude of only one velocity curve is observable so that considerably less information can be found. Combining equations (8), (9), (10) and (11) gives:

$$a \cdot \sin i = \frac{1}{2\pi} \left(\frac{m_1 + m_2}{m_2} \right) P v_1, \tag{12}$$

where v_1 is the observable radial velocity in the circular orbit case. Cubing this equation, combining it with equation (4) and manipulating the resulting equation gives

$$\frac{m_2^3 \sin^3 i}{(m_1 + m_2)^2} = \frac{P v_1^3}{2\pi G}. \tag{13}$$

The left hand side of this equation is the *mass function*, representing as much information as can be extracted from a single-line radial velocity curve. However, combined with the mass ratio, the mass function will allow the lower limit for the individual masses to be calculated, as was the case for a double-line spectroscopic binary.

The third type of binary star, the *eclipsing binary*, is a system in which the stars pass partially or totally in front of each other as viewed from earth as they orbit. This produces a periodic change in the brightness of the light from the system (see Figure 3). Plotting the brightness of the system against time gives the *light curve* of the eclipsing binary system. As is the case for RV curves, light curves are also often plotted using phase rather than time. The shape of a binary system's light curve is determined by the properties of the system, such as inclination of the orbit, temperatures of the stars, the size and shape of the stars, or the mass ratio, to name a few. For instance, W UMa-type binaries, which are characterized by continuously changing light levels and minima of similar depths, consist of two gravitationally distorted stars of nearly equal temperatures that are in contact or are nearly so. Algol-type binaries are characterized by light curves with nearly flat maxima and clearly delineated periods of eclipse. The stars of these systems are not in contact, although often one star is losing mass to its companion. Given all the factors that influence the shape of an eclipsing binary's light curve, there is potentially a great wealth of information to be found from studying eclipsing binary light curves (see Figures 4a through 4g for some samples). Among the parameters that are determinable is the inclination. To be an eclipsing binary star requires that the inclination be close to 90 degrees but a more precise determination of the inclination is possible by modelling the shape of the eclipses. The mass ratio can also be modelled, meaning that if a star is at once a spectroscopic binary and an eclipsing binary, individual masses, among other parameters, can be found. Other information such as size and physical dimensions, luminosity, temperature, and theoretically, even composition given a sufficiently high-quality light curve, can also be found.

However, some caution must be exercised before celebrating binary stars as a rich source of information. By definition, binary stars interact with each other. Therefore, it is
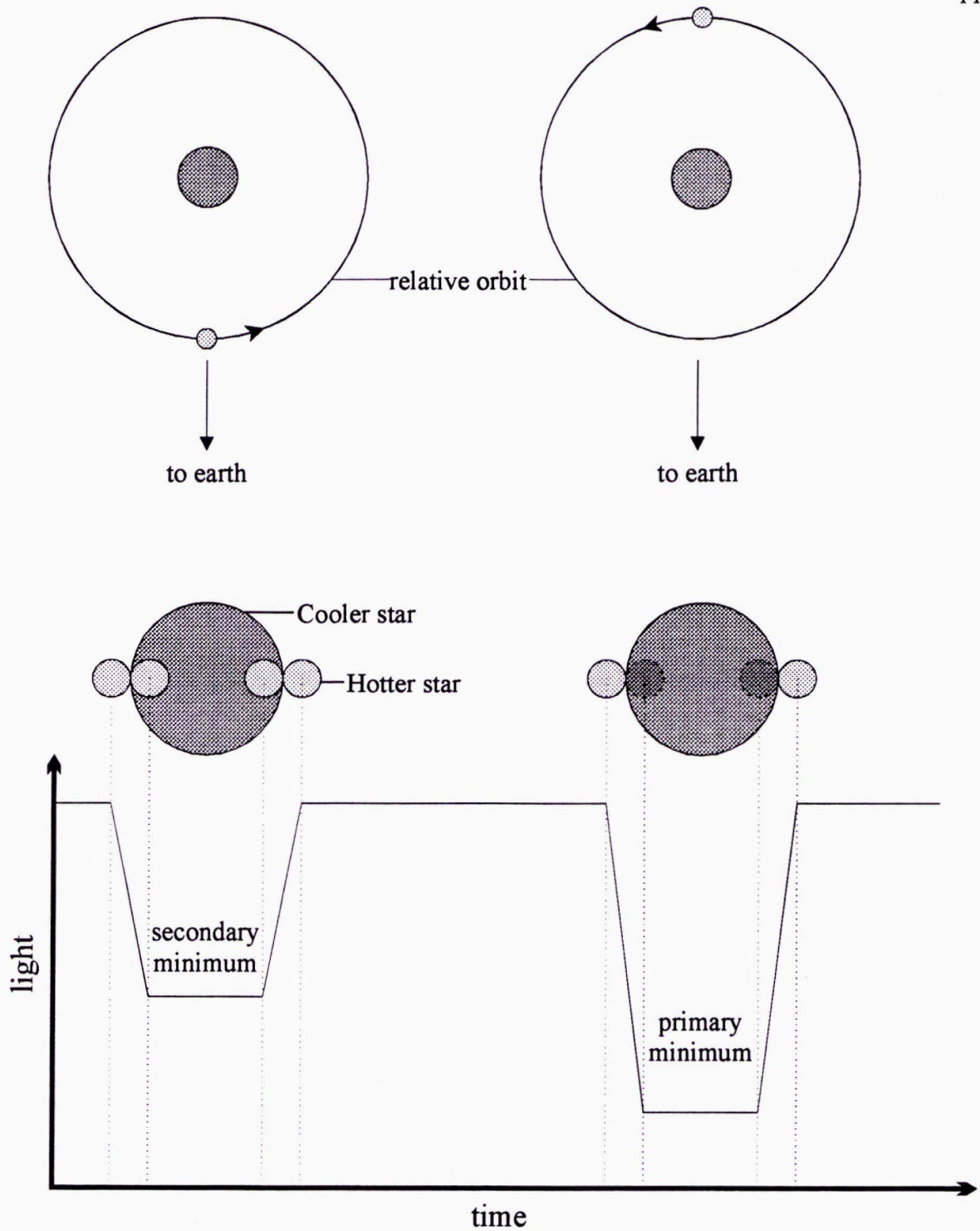
Figure 3 - A simplified light curve. When one star of an eclipsing binary system passes in front of the other as viewed from earth, the measured brightness of the system decreases. By modelling the shape of the light curve, information about the binary system can be found.
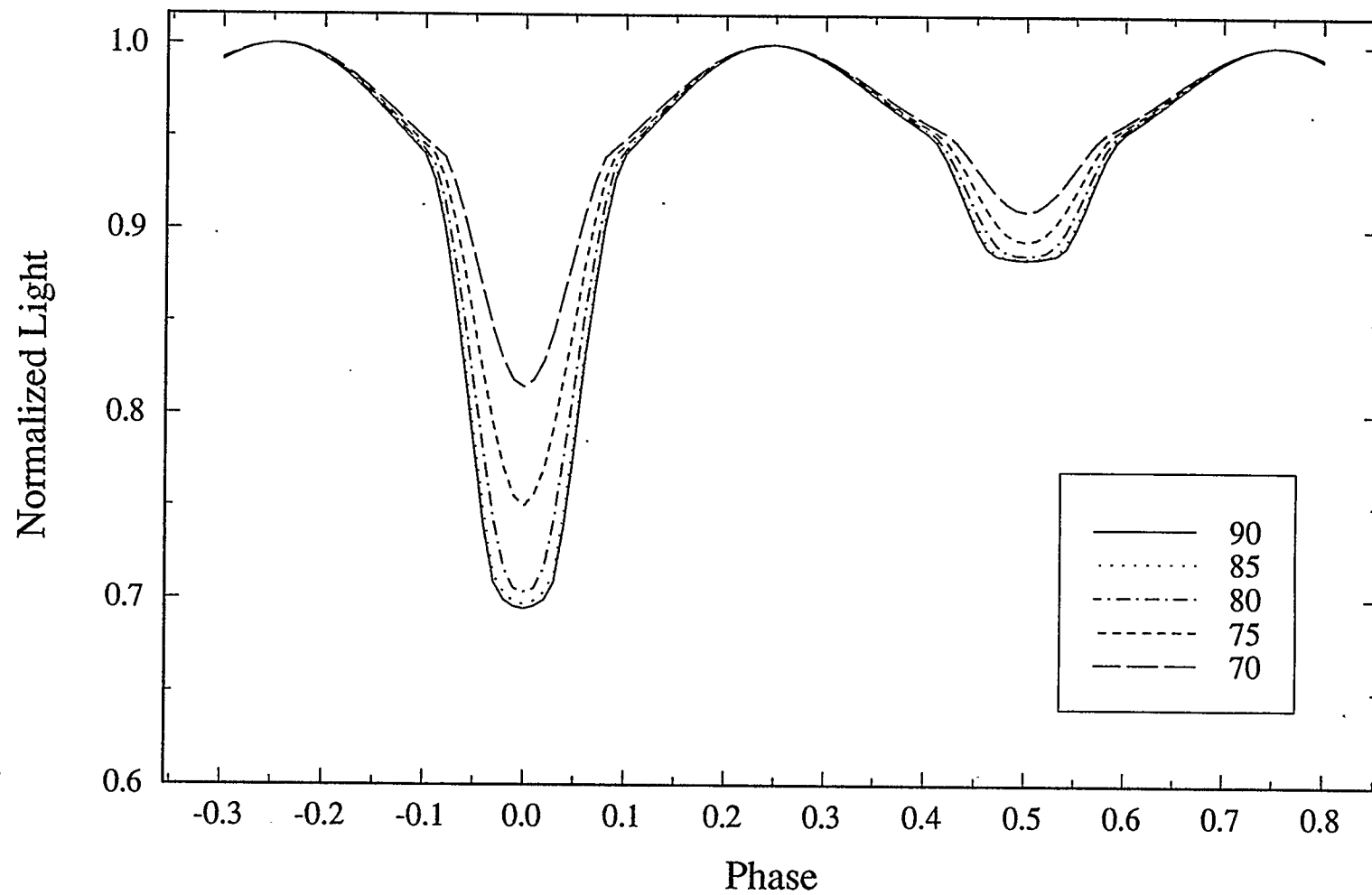
Figure 4a - The dependence of an eclipsing binary light curve on the orbital inclination is illustrated. The light curves were produced with the Wilson-Devinney light curve modeling code (see section 4.1) by varying *i* while holding all other parameters constant.
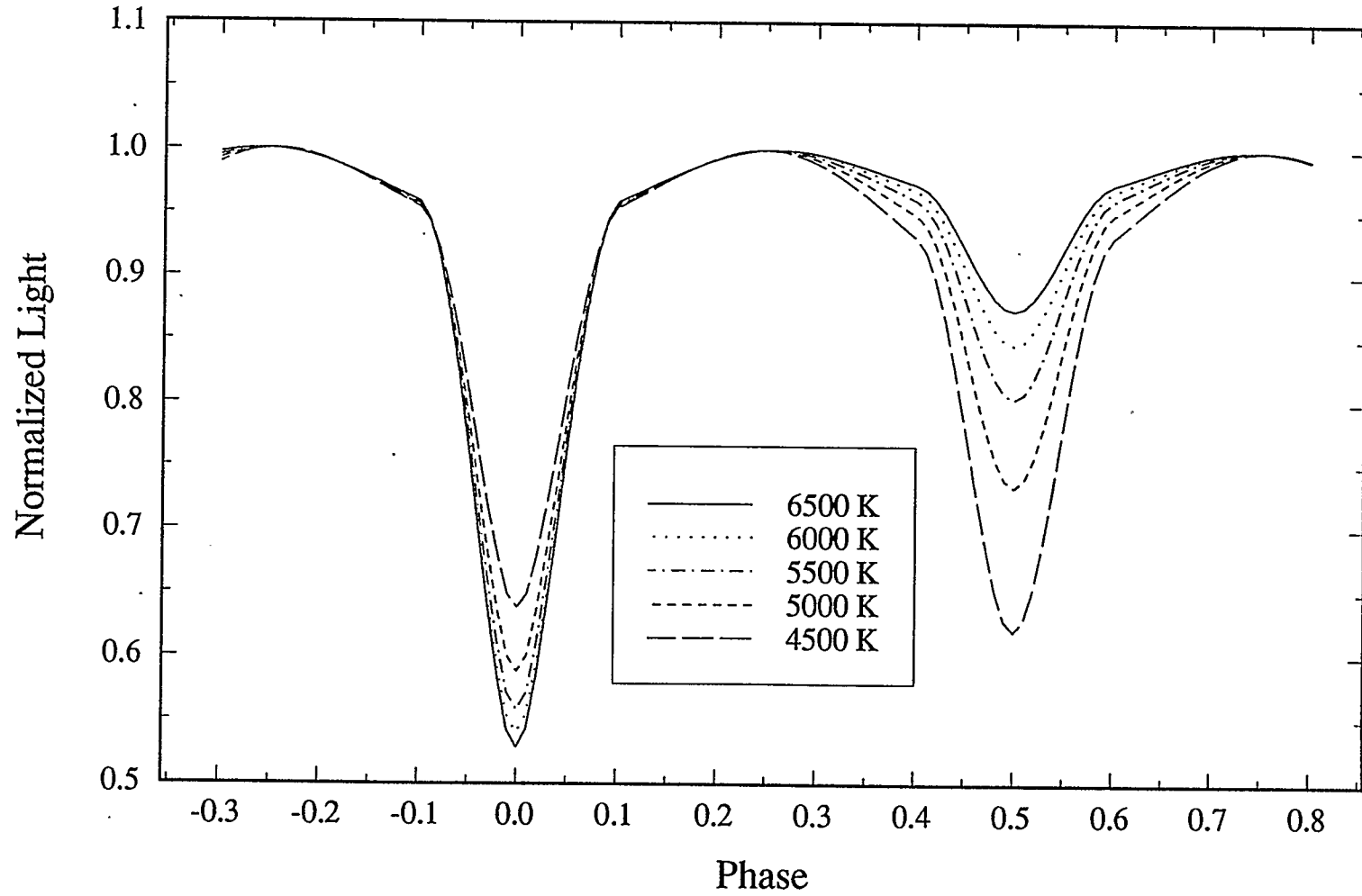
Figure 4b - The dependence of an eclipsing binary light curve on the temperature of the primary component is illustrated. The light curves were produced with the Wilson-Devinney light curve modeling code by varying T_1 while holding all other parameters constant.
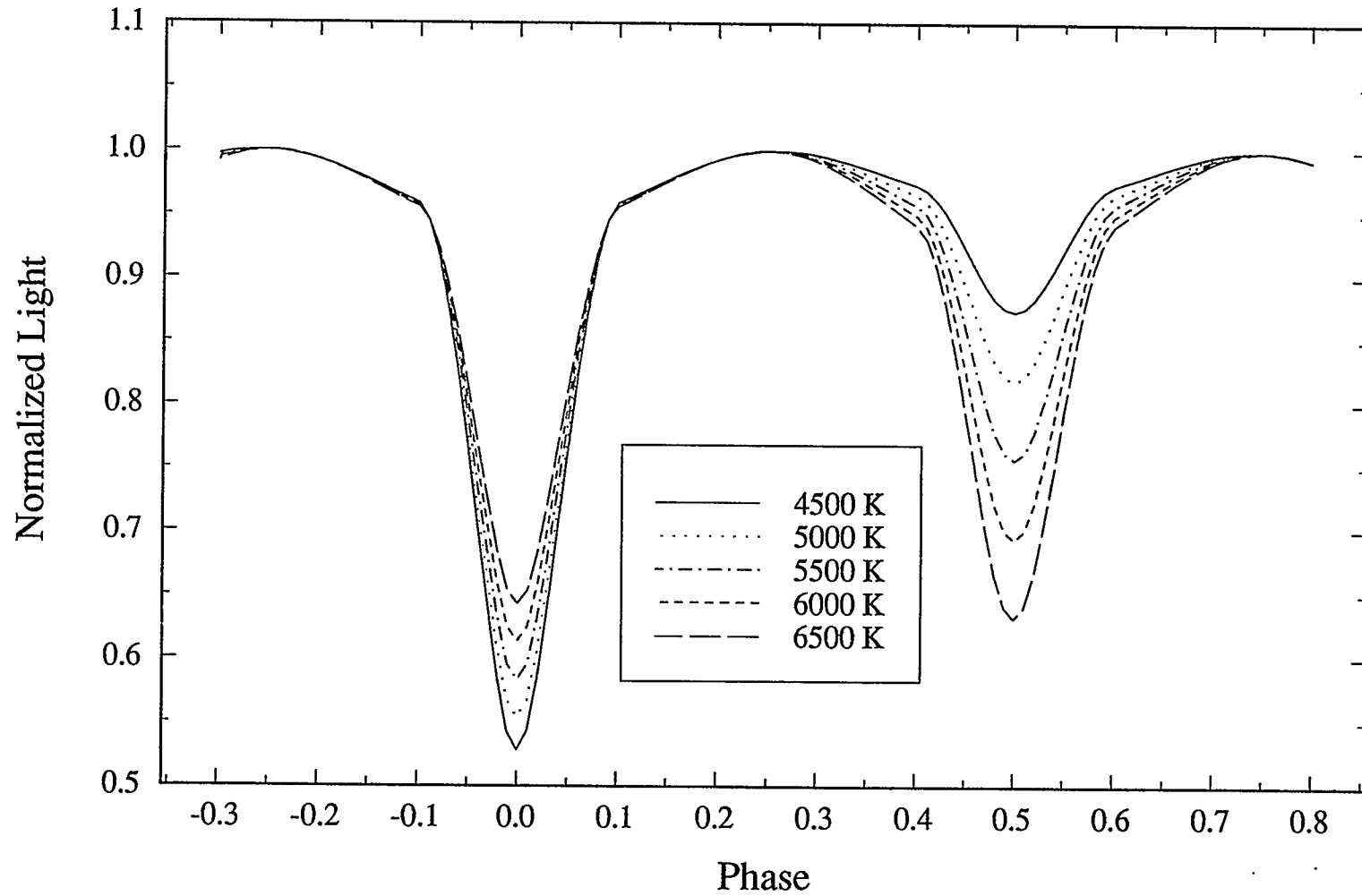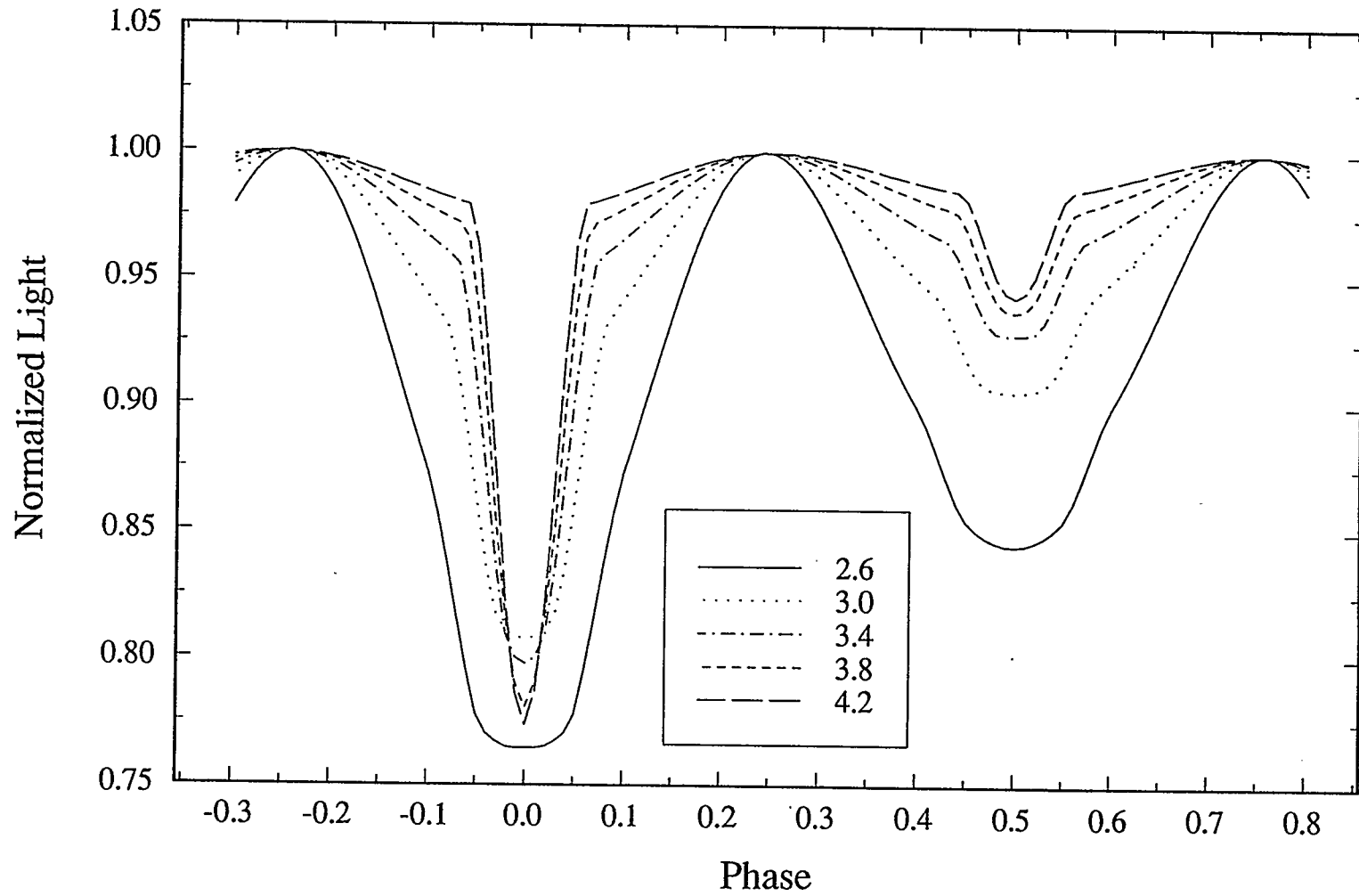
Figure 4c - The dependence of an eclipsing binary light curve on the temperature of the secondary component is illustrated. The light curves were produced with the Wilson-Devinney light curve modeling code by varying T_2 while holding all other parameters constant.
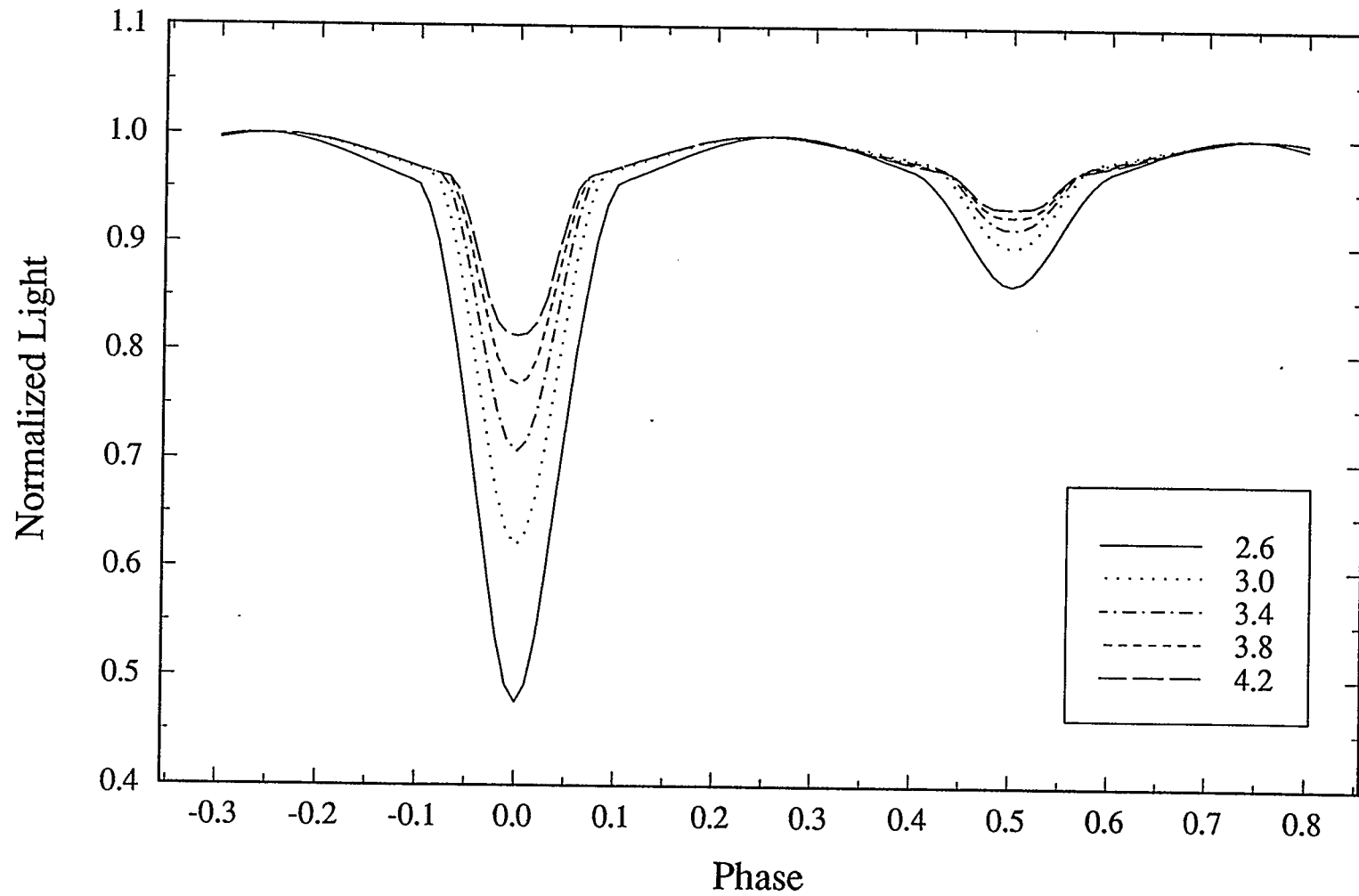
Figure 4d - The dependence of an eclipsing binary light curve on the potential of the primary component (which controls its size and shape—see section 1.3) is illustrated. The light curves were produced with the Wilson-Devinney light curve modeling code by varying Ω_1 while holding all other parameters constant.

Figure 4e - The dependence of an eclipsing binary light curve on the potential of the secondary component is illustrated. The light curves were produced with the Wilson-Devinney light curve modeling code by varying Ω_2 while holding all other parameters constant.
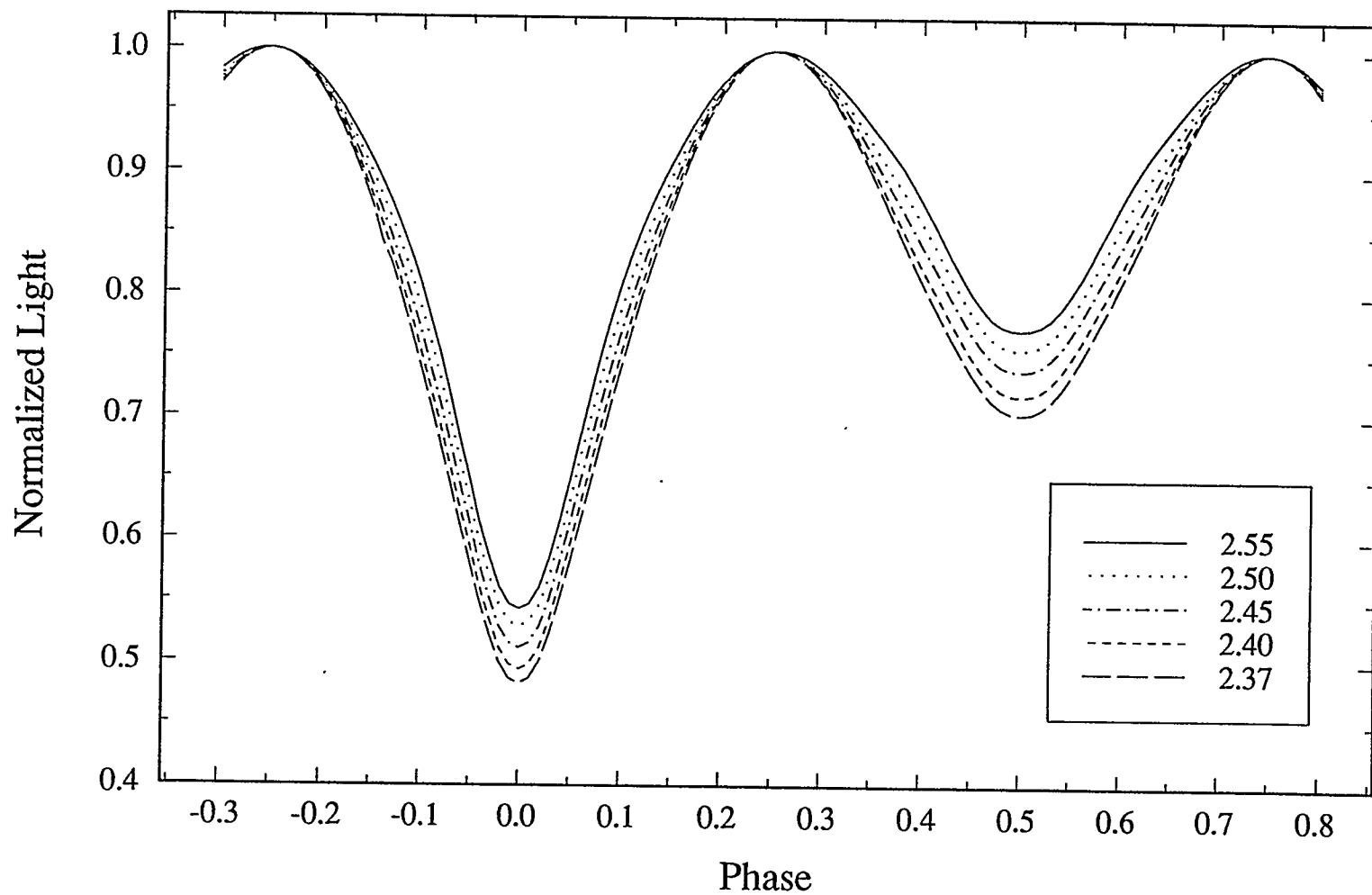
Figure 4f - The dependence of an eclipsing binary light curve on the potential of a contact system is illustrated. The light curves were produced with the Wilson-Devinney light curve modeling code by varying Ω while holding all other parameters constant.
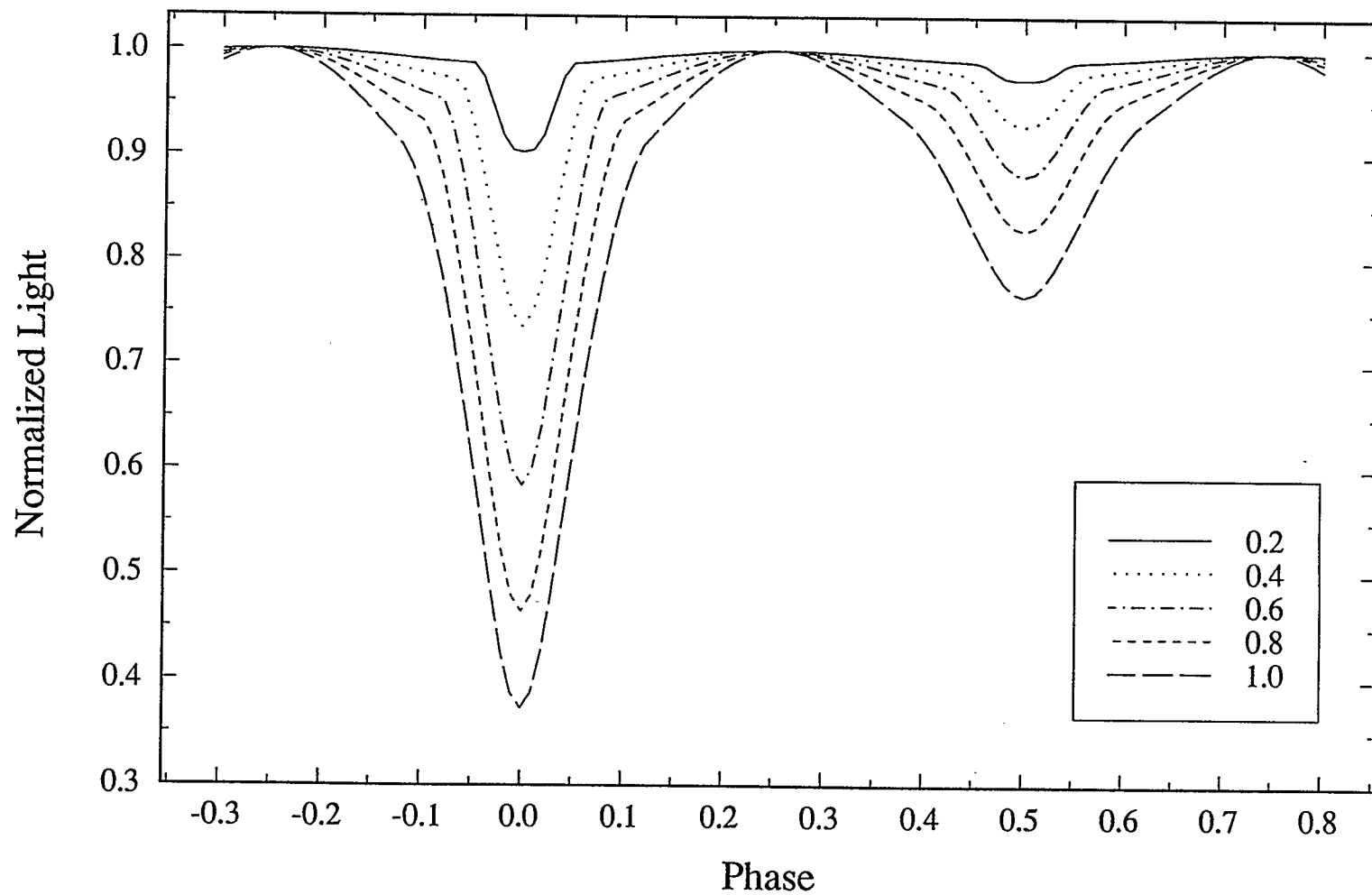
Figure 4g - The dependence of an eclipsing binary light curve on the mass ratio of the system is illustrated. The light curves were produced with the Wilson-Devinney light curve modeling code by varying q while holding all other parameters constant.

important to know how far this interaction extends. If it extends so far as to influence the evolution of each component, one cannot directly extrapolate the knowledge gained from the system to other systems. Perhaps the most obvious evolution-influencing interaction between binary components is mass exchange. Since mass is the most important property for the determination of the evolutionary course a star will take, it is reasonable to be concerned about evolutionary alteration through mass exchange.

1.3 Roche potentials and mass exchange

Mass exchange between binary components can result from a number of processes such as stellar wind and cataclysmic variation. Mass loss due to stellar wind can be quite significant for hot stars. Initially high mass stars (greater than approximately 60 solar masses) can lose all of their outer layers during main-sequence and early hydrogen-shell burning stages and expose their cores, preventing any evolution toward the red supergiant stage. Even less massive stars can be expected to lose quantities of mass significant enough to drastically alter their evolutionary paths (Chiosi & Maeder 1986). Huge quantities of mass can also obviously be lost due to cataclysmic variations such as novae or supernovae explosions. However, mass exchange resulting from Roche lobe filling is the most relevant to this discussion and will be described in more detail below.

Because of their rotation and mutual gravitational influence, binary components are not spherical, although sufficiently well separated stars may approach spherical shapes. The shape of the stars is defined by equipotential surfaces approximated by the equation

$$\Phi = -\frac{Gm_1}{\left(x^2 + y^2 + z^2\right)^{1/2}} - \frac{Gm_2}{\left(\left(x-a\right)^2 + y^2 + z^2\right)^{1/2}} - \tfrac{1}{2}\omega^2\left[\left(x - \frac{m_2 a}{m_1 + m_2}\right)^2 + y^2\right] \quad (14)$$

(Kopal 1978), where x, y, and z are Cartesian coordinates centred on the more massive star (star 1), with the z-axis lying along the axis of rotation and the centre of star 2 lying at the coordinates (a,0,0), and ω is the angular velocity

$$\omega = \frac{2\pi}{P} = \sqrt{\frac{G(m_1 + m_2)}{a^3}}. \tag{15}$$

Equation (14) assumes the orbit is circular, the stars rotate synchronously, and utilizes the Roche approximation, under which the mass of each star is centrally concentrated. These assumptions and approximations are quite reasonable in most cases. The first two terms are the gravitational components of the potential. The third term concerns the centrifugal flattening of the stars. By combining these equations and adopting m_1 as the unit of mass, a as the unit of distance, and the unit of time such that G=1, the potential Φ can be expressed in terms of spherical polar coordinates

$$\begin{aligned} x &= r\cos\phi\sin\theta = r\lambda, \\ y &= r\sin\phi\sin\theta = r\mu, \\ z &= r\cos\theta = r\nu, \end{aligned} \tag{16}$$

as

$$\Omega = \frac{1}{r} + q\left\{\frac{1}{\sqrt{1 - 2\lambda r + r^2}} - \lambda r\right\} + \frac{q+1}{2}r^2\left(1 - \nu^2\right), \tag{17}$$

where

$$\Omega \equiv -\frac{a\Phi}{Gm_1} - \frac{m_2^{\ 2}}{2m_1(m_1 + m_2)} \tag{18}$$

is the non-dimensional parameter used in the modelling software that was used for this work (see Chapter 4). Note that Ω should not be confused with $\mathit{\Omega}$, one of the orbital elements of a binary system discussed above. This potential, generalized to account for nonsynchronous rotation and eccentric orbits, is given by Wilson (1979):

$$\Omega = \frac{1}{r} + q\left\{\frac{1}{\sqrt{D^2 - 2\lambda rD + r^2}} - \frac{\lambda r}{D}\right\} + F^2 \frac{q+1}{2} r^2 \left(1 - v^2\right), \qquad (19)$$

where D is the instantaneous centre-to-centre separation in semimajor axis units and F is the ratio of the angular rotation rate to the synchronous rotation rate. Note that D is phase dependent while F is constant for the system.

Equipotential surfaces are nearly spherical near the centres of the stars but become increasingly distorted as they get larger. The potential at which two cusped volumes that touch at the inner Lagrangian point L_1 are enclosed is called the first (or inner) critical potential. These volumes are the Roche lobes of the two stars. Beyond the first critical potential, the two surfaces merge into one dumbbell shaped surface. At the second (or outer) critical potential, a cusp is formed at the outer Lagrangian point L_2. These Lagrangian points, as well as L_3, represent points at which the slope of the potential is zero:

$$\frac{\partial \Phi}{\partial x} = 0; \quad y = z = 0. \qquad (20)$$

As a star evolves and expands[3] it will fill successively larger equipotential surfaces until its Roche lobe is filled, at which point material will spill through the inner Lagrangian point into the Roche lobe of its companion. The exchange of mass that takes place can be of such a magnitude that the more evolved star can end up as the less massive of the pair.

---

[3] The expansion of the stellar envelope is due to an imbalance between the outward pushing radiation and gas pressure and the inward pulling gravitational force. The imbalance is due to an increase in core luminosity (and hence radiation pressure felt by the envelope) or shell luminosity in the case of stars undergoing shell burning. The increase can be due to the ignition of a new fuel or increasing core or shell temperature due to contraction when a fuel has been exhausted.

When one star overflows its Roche lobe, the system is a *semi-detached binary*. When both stars overflow their Roche lobes, the system is a *contact binary*. The envelopes of the stars then merge into a common, dumbbell-shaped envelope that can continue to expand up until its surface reaches the outer critical surface, at which point matter will leak through the outer Lagrangian point L_2 and be lost from the system. See Figures 5a through 5c for illustrations of detached, semi-detached, and contact systems.

The degree to which the stars fill their Roche lobes can be quantified with a *contact parameter* defined as

$$f = \frac{\Omega_{inner} - \Omega}{\Omega_{inner} - \Omega_{outer}}. \tag{21}$$

This parameter, sometimes referred to as the *fill-out factor*, indicates the degree of filling of the contact envelope. A value larger than one implies that the stars overflow the outer critical surface. A value of zero implies that the stars are barely in contact, as they just fill the inner critical surface. If the stars are not in contact, they do not have to be constrained by the same value of Ω and, hence, the two components will each have their own negative value for f.

Clearly it is important to know whether mass exchange or loss has taken place before drawing too many conclusions from the information gathered about a binary system. If the modelling results point to a semi-detached or contact system, then clearly evolutionary contamination has taken place, but even if the model describes a detached system, it remains possible that mass exchange could have occurred in the past. The probability of this can be estimated if the age of the system is known because, given the mass of the components, the approximate age at which evolution off the main-sequence occurs can be found from evolutionary models.
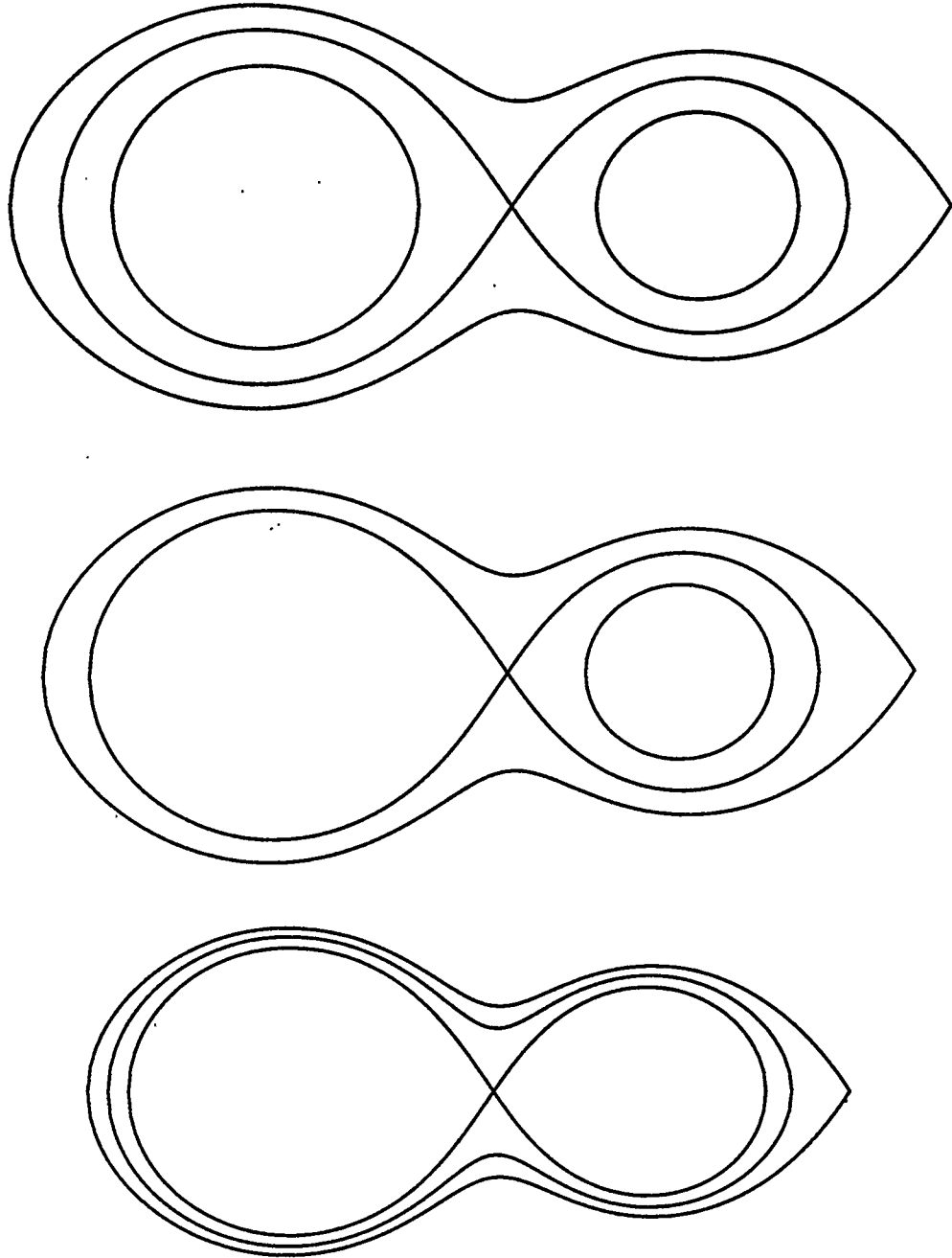
Figure 5a - The Roche lobe configurations of detached, semi-detached, and contact systems in the x-y plane. The less massive star is on the right. The inner critical surfaces (figure-8 shaped line) and outer critical surfaces (outer dumbbell) are shown with the surfaces of the components. In the detached system (top), both stars are smaller than the inner critical surface. In the semi-detached system (middle), one stellar surface is coincident with its Roche lobe. In the contact system (bottom), the components share a common surface that falls between the critical surfaces. These illustrations were produced with D. H. Bradstreet's *Binary Maker II*.
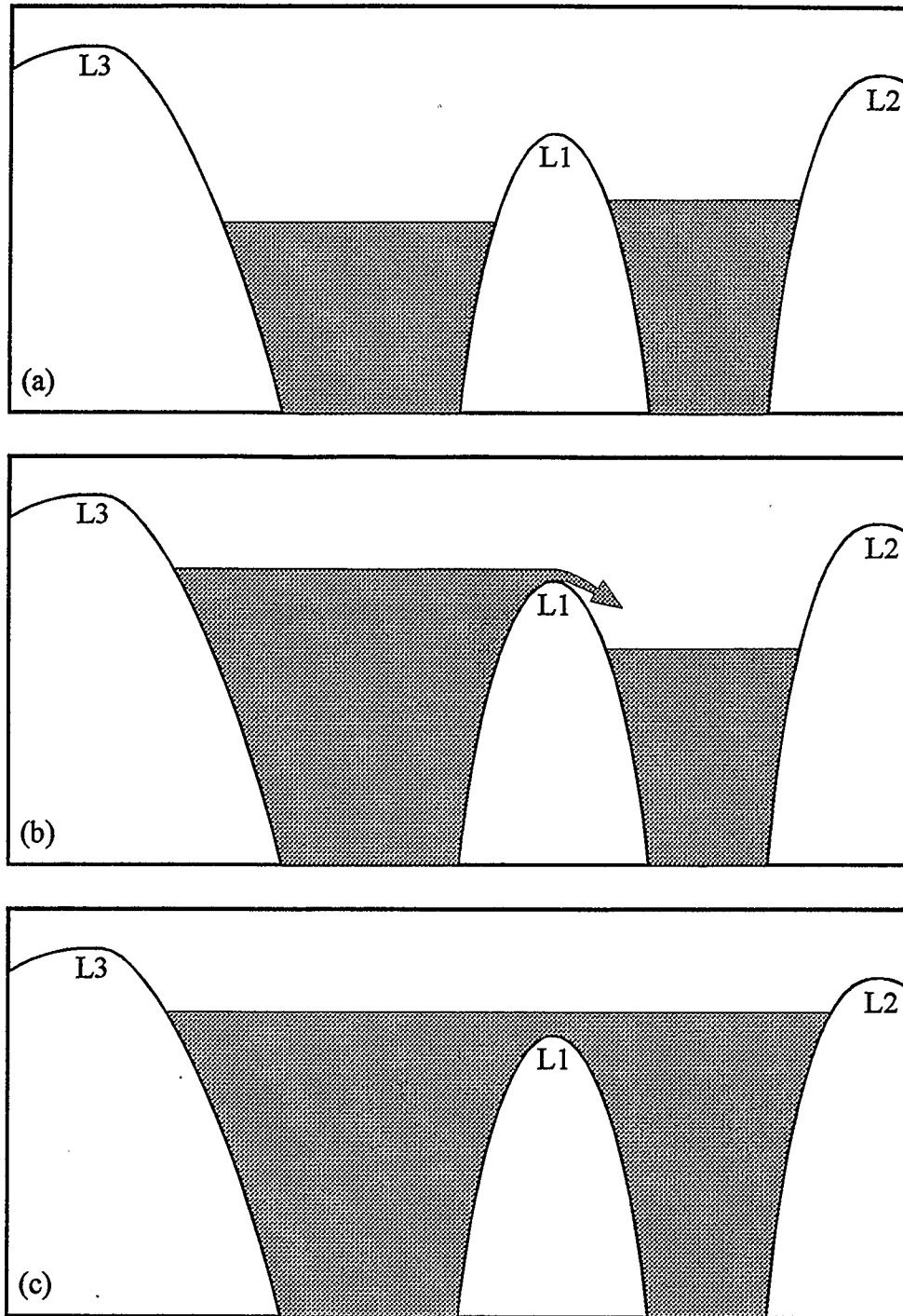
Figure 5b - The potential wells of a (a) detached system, (b) semi-detached system, and (c) contact system. In (a) there is no sharing of stellar material. In (b) the star on the left has expanded beyond its potential well and material spills into the potential well of the other star through the first Lagrangian point L1. In (c) both stars have expanded to a point that their now merged surface has a potential higher than that of L1. If they expand to a potential beyond L2, material will be lost from the system.

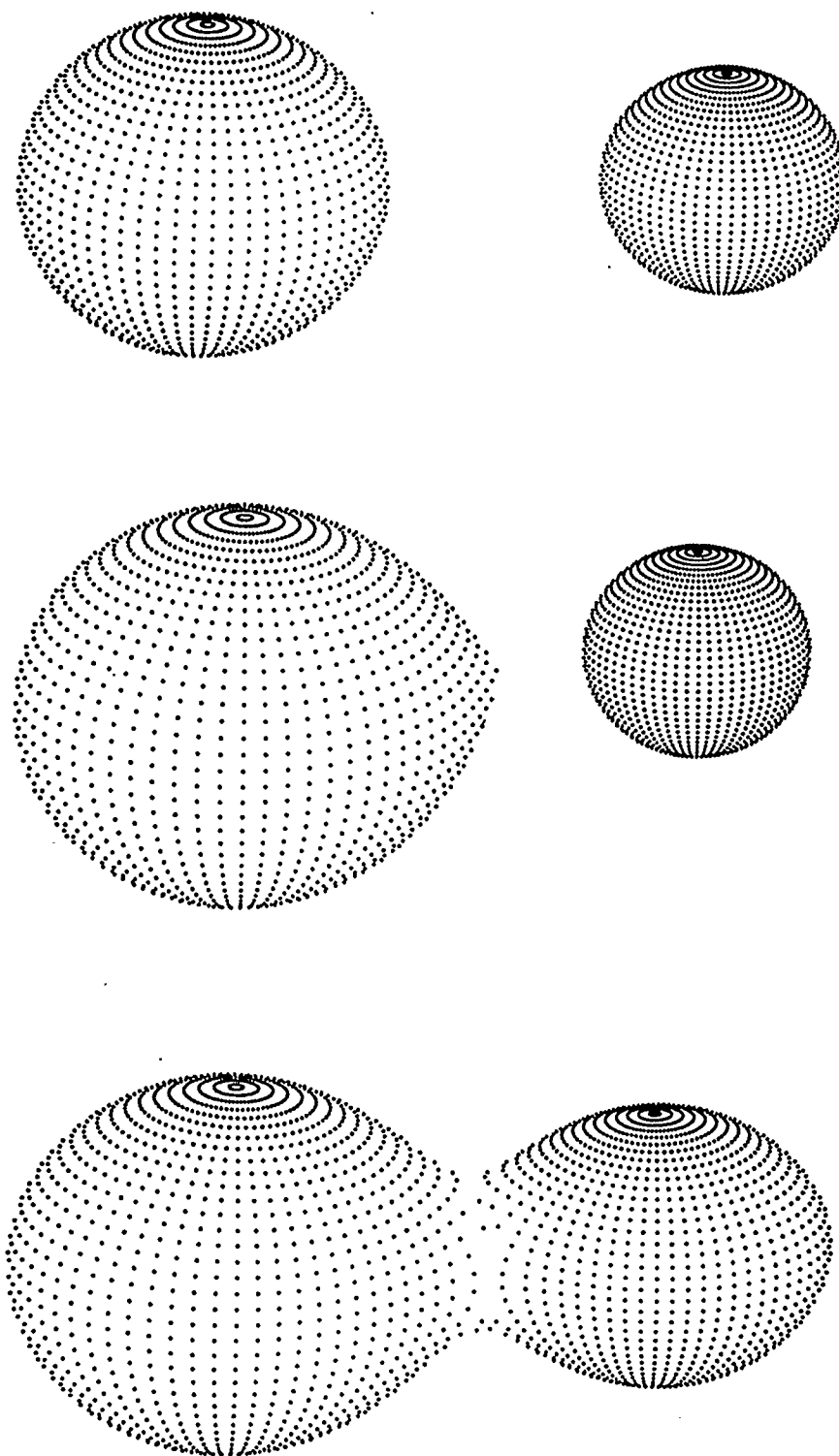**Figure 5c** - Three-dimensional representations of detached, semi-detached, and contact systems (from top to bottom) produced with D. H. Bradstreet's *Binary Maker II*.

1.4 The importance of binary stars in clusters

If the binary star is a member of a cluster, then its age can be assumed to be the same as the age of the cluster, which can be estimated by fitting theoretical isochrones to the colour magnitude diagram (hereafter, CMD) of the cluster (see Figure 6 for an example of a CMD—that of the open cluster NGC 752 from Milone *et al.* (1994)). To avoid a circular argument, some caution should be exercised here, as it is ultimately these same isochrones that are to be tested using the binary system data. The size of a star of a given mass can also be plotted against age using theoretical models. With the age and mass of each binary component known, it is possible to determine if the stars have filled their Roche lobes in the past. Again, the same caution applies to this procedure. This should at least give an approximate probability of whether the binary's components have exchanged mass. If it is concluded that they have not exchanged mass, then one has a set of very important checks for the evolutionary models that are used to determine cluster ages because knowing the masses of two stars of known position on the CMD allows a direct comparison of observation and theory. For an example of this procedure, see Schiller & Milone 1988, in which the components of the detached system DS Andromedae are placed on the CMD of the open cluster NGC 752 (indicated with '+' symbols in Figure 6).

If the components have exchanged mass, then one still potentially has a system of well known current mass, age, temperature, luminosity, etc., which is important for studying the evolution of interacting binary stars.

These tests are necessary because the prevalence of use of evolutionary models is very great and yet there are very few tests that can be made of their accuracy. Given that
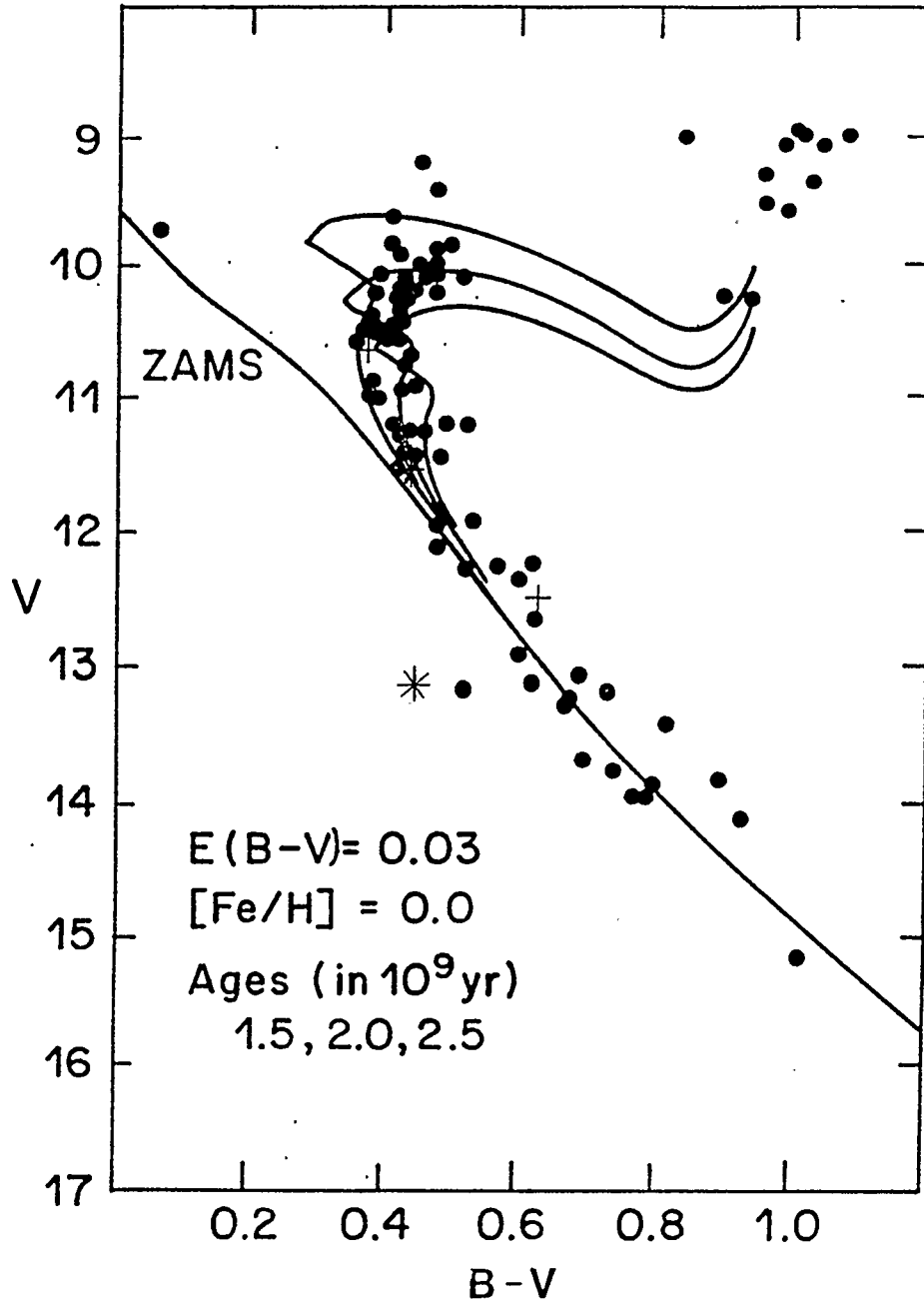
Figure 6 - The colour magnitude diagram of the open cluster NGC 752. The + symbols represent the components of DS And, a detached eclipsing binary. The ✳ symbols represent the components of H235, a contact binary system. The lines indicate the isochrones of VandenBerg (1985).

certain models have set the age of some clusters greater than some estimates of the age of the universe, testing is obviously required.

The study of binary stars in globular clusters is also important for another reason. The presence of binary stars can fundamentally influence the dynamical evolution of the globular cluster. In the absence of counterbalancing forces, a globular cluster will inevitably experience *core collapse*, in which the central portion of the cluster collapses towards infinite density and temperature while the outer regions expand. However, attempts to model the dynamical evolution of clusters have shown that the presence of binary systems, whether primordial or formed during the cluster's collapse, will change the evolution of the cluster before the collapse is complete.

Interactions between binaries and other stars release binary star orbital energy, which serves to "heat" the cluster. This heating effect will slow down the collapse and ultimately cause cluster re-expansion. The precise nature of the heating depends on the type of binaries considered. The binaries can be broadly grouped into three classes, each with a qualitatively different heating mechanism: three-body binaries, tidal capture binaries, and primordial binaries. The former are binaries formed through three-body encounters. They are expected to be few in number and located preferentially in the densest cluster regions. Tidal capture binaries are binaries that pass close enough to each other (about three stellar radii (McMillan 1991)) that they become tidally bound due to energy transfer from the orbit to stellar oscillations. Primordial binaries are binaries that formed at the time of the cluster formation. It is difficult to say which of these types of binary is the most important to cluster heating because most attempts at simulation give differing results depending on the technique used and the assumptions made. Nevertheless, McMillan (1991) argues that if a cluster contains a substantial population of primordial binaries, they can come to dominate the cluster dynamics and terminate core

collapse well before three-body or tidal binaries can form. Thus far, binaries in clusters have been relatively hard to find but the results of Heggie & Aarseth (1992) indicate that a primordial binary frequency as low as 3 percent can fundamentally change the cluster evolution.

Yet another reason for interest in binary systems in globular clusters is their relation to the long standing puzzle of the origin of *blue stragglers* (BSs). Blue stragglers are stars that lie above and blueward of the main-sequence turn-off region of CMDs. If these stars had been normal single stars, they would have evolved away from the main sequence with the rest of the stars that at one point had similar luminosities. Hence, they seem to *straggle* behind their companions in the evolutionary process. In the first modern study of M71, Arp & Hartwick (1971) pointed to the work of others (Hoyle 1964, McCrea 1964, Cannon 1968, Strom & Strom 1970), who suggested that BSs were the result of close binary evolution, to possibly explain M71's BS population. This explanation continues to be very popular. One theory that has been directly supported by observations (Mateo *et al.* 1990) suggests that BSs have increased their main-sequence lifetimes by gaining material through mass transfer from a binary companion. Another theory suggests that BSs are actually the product of mergers with a binary companion. The merger would require angular momentum loss, possibly through tidal coupling, gravitational radiation, or magnetic stellar winds. Binary stars also play a role in the collisional theory of BSs because star-binary and binary-binary interactions are much more likely than single star collisions (Leonard & Fahlman 1991). Even if these interactions do not result in immediate mergers, they can result in the *hardening* of binary systems (*i.e.*, the period of the system is reduced) which will accelerate the merger process through other means (Hills 1984, 1990). For recent reviews of BS theories see Stryker (1993), and Livio (1993).

2.0 THE GLOBULAR CLUSTER M71

M71 (NGC 6838) is a small, relatively sparse, metal-rich globular cluster near the galactic plane. Because of its proximity and moderate reddening, M71 is important as it can provide an accurate colour-magnitude diagram (CMD) to act as a comparison for other metal-rich clusters, about which relatively little is known concerning their early evolution and age dispersion. See Table 1 for a list of cluster properties.

It has been argued (Zinn 1985) that there are two populations of globular clusters, which are distinguished at least in part by metallicity. The *halo* population is largely metal-poor while the *intermediate* population is comparatively metal-rich ([Fe/H]>-0.8). The cluster M71 falls into the latter category. Reviews of the metallicity of M71 by Zinn & West (1984) and Burstein *et al.* (1986) conclude that [Fe/H]=-0.58±0.08 and ~-0.6 respectively. More recent estimates for [Fe/H] range from -0.2 (Buser & Kurucz 1992) to -0.79 (Sneden *et al.* 1994). Allen & Martos (1988) have shown by numerically integrating the cluster's orbit backwards, that M71 has a very similar orbit to the open cluster M67. This is also consistent with M71 being a member of the comparatively disk-like intermediate population. M71 is also grouped with the galactic clusters rather than the globular clusters in Allen & Martos' sample when metal abundance is plotted against apocentric distance, pericentric distance, and orbital eccentricity. Some caution is necessary, however, because the proper motions they used, derived by Cudworth (1985), are uncertain at nearly the 50% level. If true, these kinematics results, coupled with the relative richness, would tend to suggest that M71 is comparatively young among the globular cluster population.

Arp & Hartwick (1971) conducted the first modern study of M71 and noted the scarcity of subgiant sequence stars, complicating the age determination for M71, which is

TABLE 1
M71 Properties

Property	Value	Reference
Right ascension, α_{1950}	$19^h51^m33^s$	A
Declination, δ_{1950}	$18°38'47''$	A
Galactic longitude, l	$56°.7$	B
Galactic latitude, b	$-4°.5$	B
Galactocentric distance, R_{GC}	7.6 kpc, 7.4 kpc	B, C
Galactic plane distance, Z_{GP}	0.3 kpc	C
Distance, d	3.6(5) kpc	A
Uncorrected distance modulus, DM_{uc}	$13^m.70$	D
Reddening, $E_{(B-V)}$	$0^m.28$	D
$E_{(V-I)}$	$0^m.34$	E
$E_{(U-V)}$	$0^m.48$	D
Integrated absolute magnitude, M_V	$-5^m.60, -6^m.4, -5^m.76$	B, C, F
Radial velocity, v_{rad}	-19.3(9) km/s	G
	-22.1(8) km/s	H
Velocity Dispersion, μ_{int}	2.8(8) km/s	H
Age	7.6(+3.1, -2.3) Gyr	I
	$\approx\tau_{47\,Tuc}$	J
	~3 Gyr $> \tau_{47\,Tuc}$	K
Metallicity, [Fe/H]	-0.2	L
	-0.3(2)	I
	-0.58(8)	M
	~-0.6	N
	-0.79(1)	O
Central density, ρ_c	630 solar masses/pc^3	P
Angular core radius, r_c	$45''$	C
Angular tidal radius, r_t	$23'.5$	C
Concentration, $c\equiv\log(r_t/r_c)$	1.5, 1.1, 1.3	C, F, P

A=Cudworth (1985), B=Harris & Racine (1979), C=Chernoff & Fahlman (1988), D=Richer & Fahlman (1988), E=Yan & Mateo (1994), F=Richer & Fahlman (1989), G=Webbink (1981), H=Peterson & Lantham (1986), I=Arp & Hartwick (1971), J=Hodder *et al.* (1992), K=Heasley & Christian (1991), L=Buser & Kurucz (1992), M=Zinn & West (1984), N=Burstein *et al.* (1986), O=Sneden *et al.* (1994), P=Djorgovski (1993)
Numbers in parentheses indicate uncertainties in the least significant digits.

still a matter of some controversy. They estimated the age to be 7.6 (+3.1, -2.3) Gyr on the basis of their derived turn-off luminosity. The sparse subgiant sequence has led others to attempt relative age estimates by comparing M71 with 47 Tuc, a similar, but well-studied cluster with an age estimated to be 13.5±2 Gyr (Hesser *et al.* 1987). Hodder *et al.* (1992) concluded that M71 and 47 Tuc had similar ages while Heasley & Christian (1991) found M71 to be roughly 3 Gyr older than 47 Tuc. Davidge & Simons (1994) estimated an age of 16 Gyr based on their near-infrared CMD but caution that their conclusions should be considered tentative given uncertainties in metallicity and the current level of stellar physics knowledge.

The existence of blue stragglers in M71 was noted by Arp & Hartwick (1971). They observed a fairly well-defined extension to the main sequence and were surprised to discover that BSs were about as numerous as members of the subgiant sequence. To explain this, they noted M71's resemblance to the disk population and the suggestion of Abt & Levy (1969) that disk populations may contain a higher percentage of binaries. Therefore, they postulate that the BSs may be the result of close-binary evolution. More recently, Richer & Fahlman (1988) identified over 50 BSs using deep CCD photometry of 6′ × 4′ area (as well as a sequence of white dwarf candidates). They also found that the binary frequency in the cluster centre is low, which would seem to contradict the hypothesis of Arp & Hartwick. On the other hand, the centrally flat surface density profile and high degree of mass segregation which Richer & Fahlman (1989) found were not explainable by Druker *et al.* (1992) using dynamical models in which core reexpansion is driven solely by three-body binaries. They suggest that additional physics such as the effects of primordial binaries may be required.

Four variable stars in M71 were identified by Sawyer Hogg (1973); one of these was an eclipsing binary. The latter, however, was shown to be a field star by Liller &

Tokarz (1981) by virtue of its radial velocity. Cudworth (1985) found two additional variables which, in addition to Sawyer Hogg's cluster variables, lie near the end of the red giant branch. Hodder *et al.* (1992) found four other variables with varying probabilities of membership based on CMD position. None of these systems have radial velocity measurements. One star (H3) may be a W UMa binary and a second (H4) was suggested to be an eclipsing binary of a non-W UMa type which so far have proved to be very rare in globular clusters. The light curves of both of these stars suffer from incomplete phase coverage, however, making their classifications tentative. Three of the five binaries, the analysis of which is the topic of this thesis, were discovered by Yan & Mateo (1994). The other two (V3 and V4) coincide with Hodder *et al.*'s suspected binaries and confirm their tentative classifications. The issue of cluster membership for all the binaries is not definitively settled, but Yan & Mateo conclude that the five binaries are all probable members based on three tests. The first test calculates how many contact and Algol-type binaries are expected in the line of sight out to a distance of 20 kpc. They find the total number of expected binaries to be 0.11 and 0.04 for contact and Algol binaries respectively. Their second test consists of calculating the luminosities of the systems (using radii calculated from Roche criterion and effective temperatures) and hence finding their distance moduli. In all cases, they found the distances to be consistent with cluster membership. The final test utilized Rucinski's (1994) calibration of absolute magnitude of contact binaries. Again, the results are consistent with cluster membership. The results of the current work, presented in Chapter 5, tend to confirm their conclusions, with the exception of V3, which appears to be closer than the other four variables.

3.0 DATA ACQUISITION AND REDUCTION

3.1 Acquisition

The data reduction discussed in this chapter was applied to data obtained at the Mount Laguna Observatory 1m telescope jointly operated by the San Diego State University and the University of Illinois Astronomy Departments[4]. Although much time was spent on the reduction of these *charged coupled device* (CCD) data, accurate results proved more difficult to extract than originally anticipated due to poor seeing and guiding conditions, the extreme faintness of the stars, and the crowding in the field. While these numerous, 5-colour data continue to be analyzed and will provide important additional information, higher precision 2-colour light curve data from the 1.5m Palomar telescope were made available by Lin Yan and Mario Mateo in advance of their own publication (Yan & Mateo, 1994). Their data come from 328 Johnson V and Gunn i CCD images, covering a 6.3'×6.3' field, taken during 4 nights in 1991 and 11 nights in 1993. Tables 2a and 2b show the positions and basic properties of the five eclipsing binaries that were found using these images. Figures 7a through 7j show the light curves of these binaries. A more detailed description of the data and reduction procedure can be found in Yan & Mateo, 1994. However, the procedure is similar to that performed on the larger Mt. Laguna set.

---

[4] The Mt. Laguna CCD has the following properties: 800 × 800, 15 μm × 15 μm pixels; conversion gain, 1.7 electrons/adu (analog to digital unit); read noise, 7 adu; and linearity to 32,000 adu.

Period = 0.3489 days

Figure 7a - The Yan & Mateo Johnson V light curve of M71-V1 with photometric errors.

Figure 7b - The Yan & Mateo Cousins I light curve of M71-V1 with photometric errors.
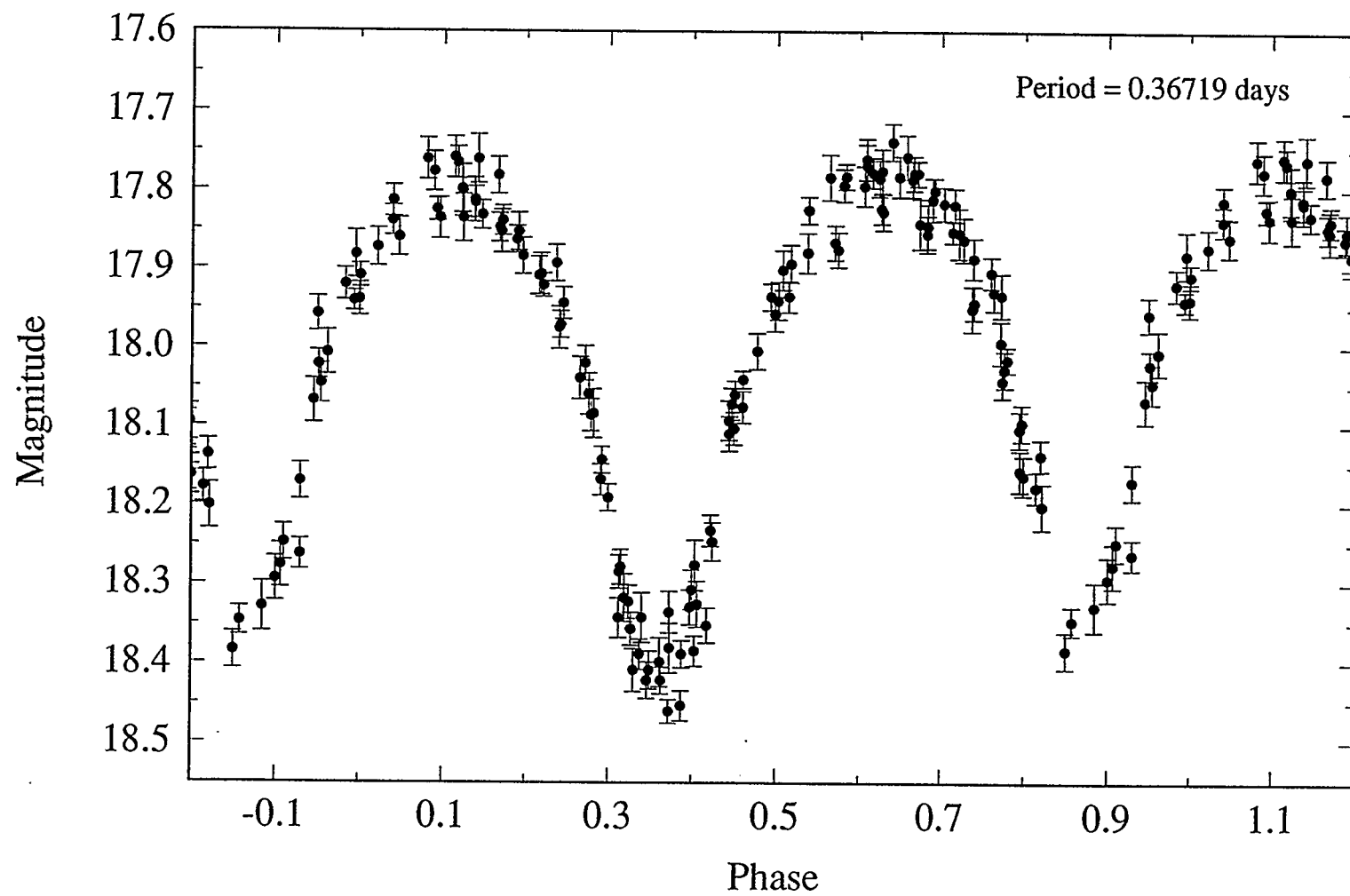
Figure 7c - The Yan & Mateo Johnson V light curve of M71-V2 with photometric errors.
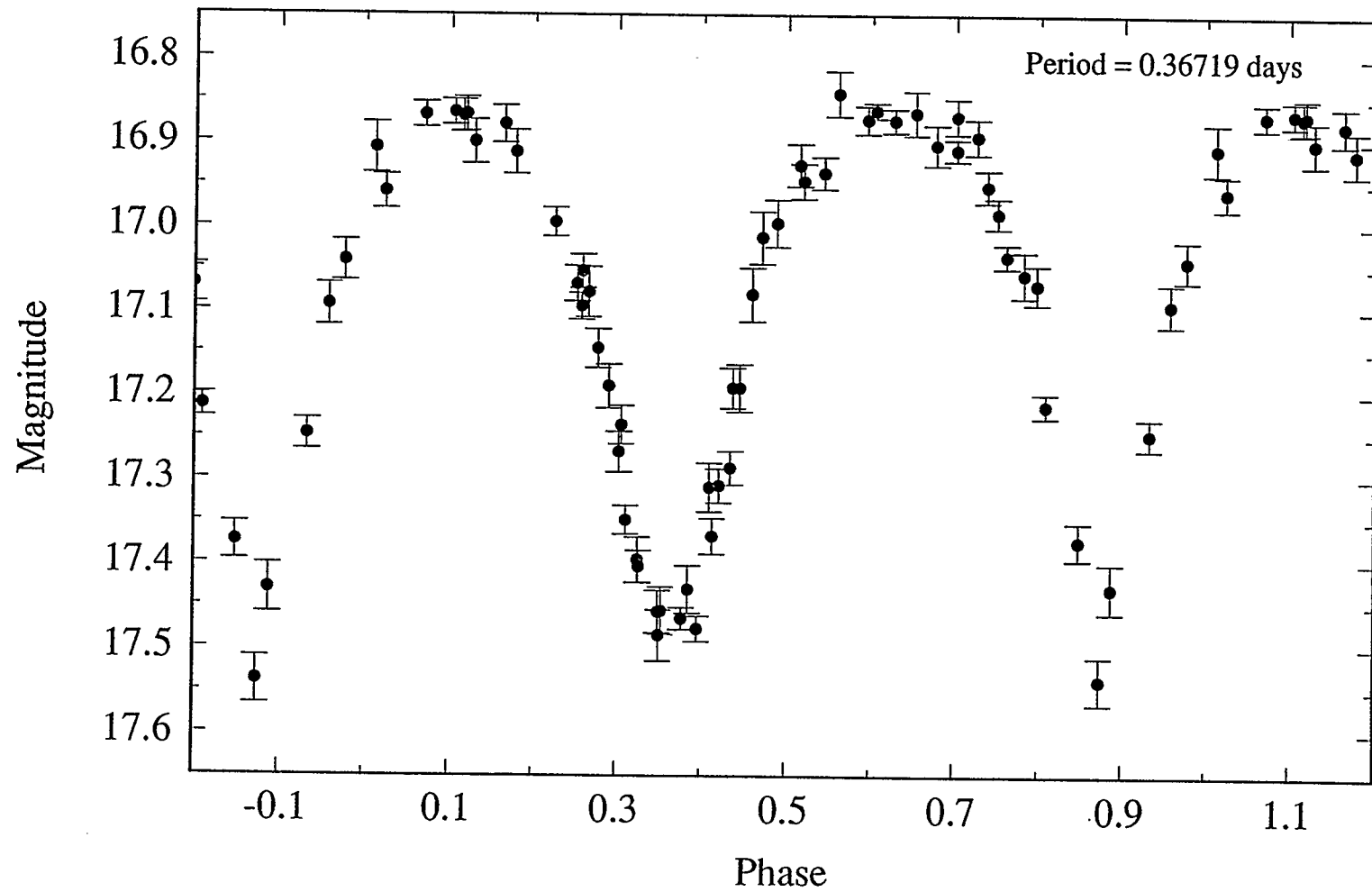
Figure 7d - The Yan & Mateo Cousins I light curve of M71-V2 with photometric errors.

Figure 7e - The Yan & Mateo Johnson V light curve of M71-V3 with photometric errors.
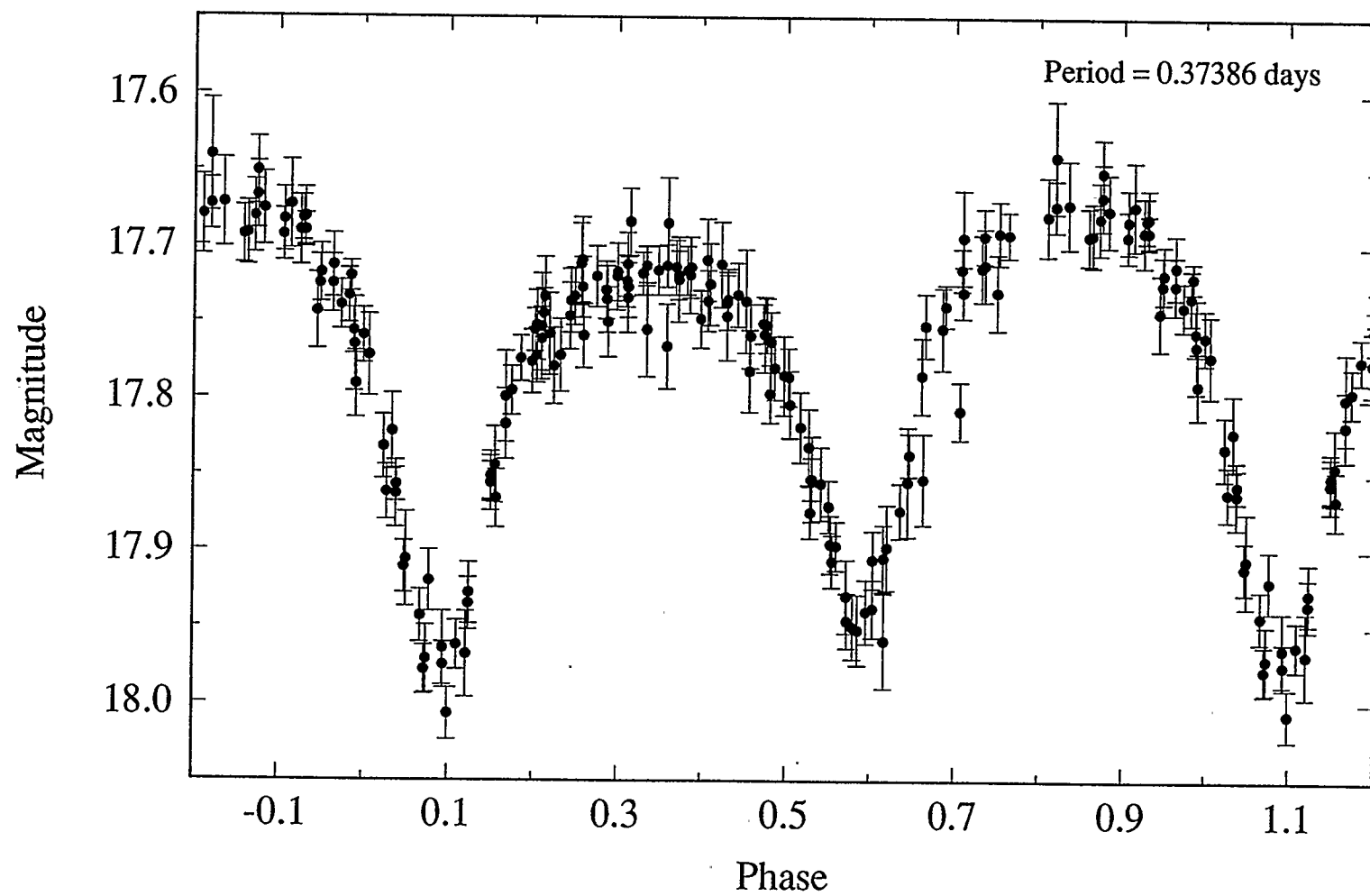
Figure 7f - The Yan & Mateo Cousins I light curve of M71-V3 with photometric errors.

Period = 0.55616 days
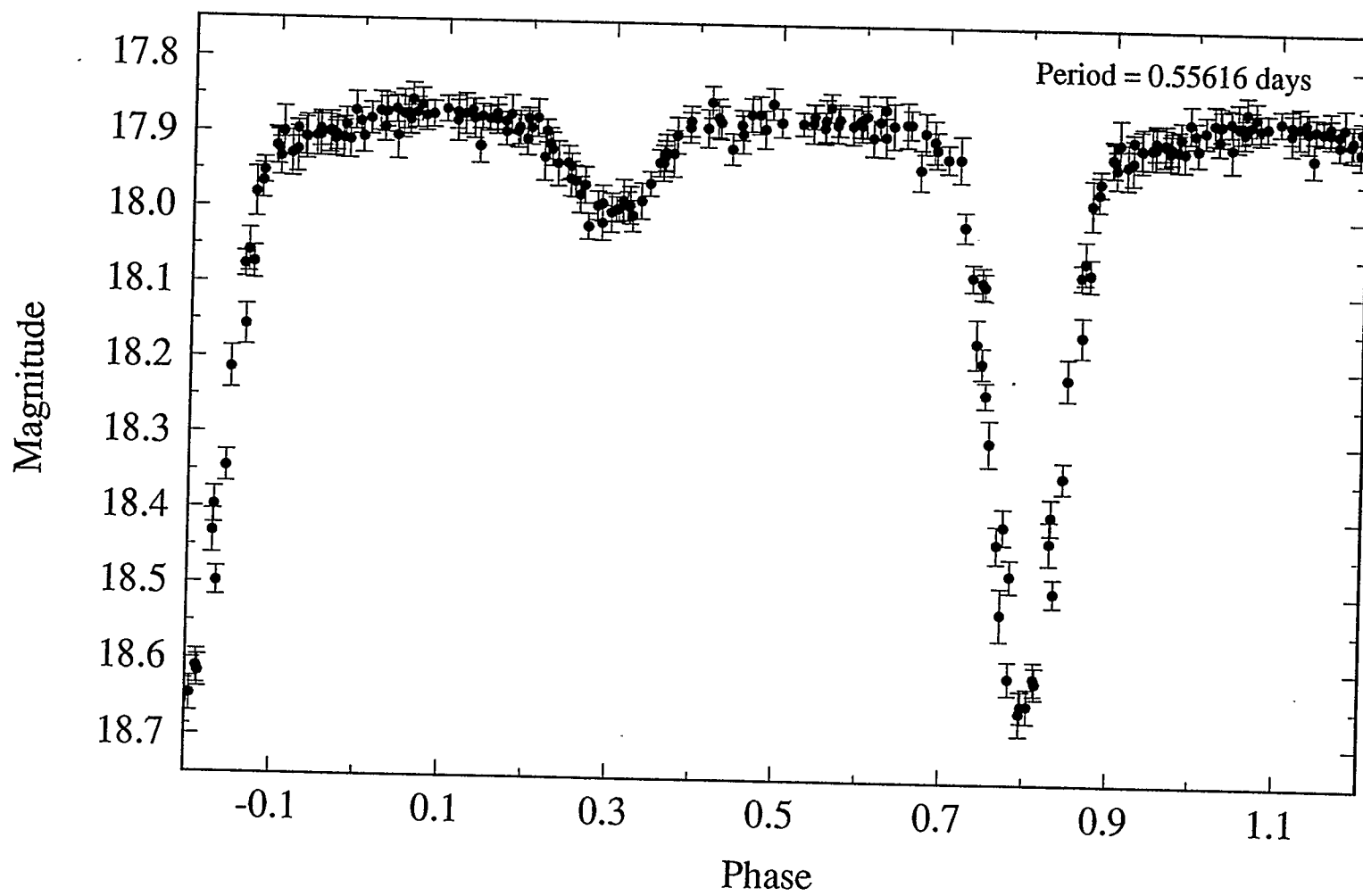
Figure 7g - The Yan & Mateo Johnson V light curve of M71-V4 with photometric errors.
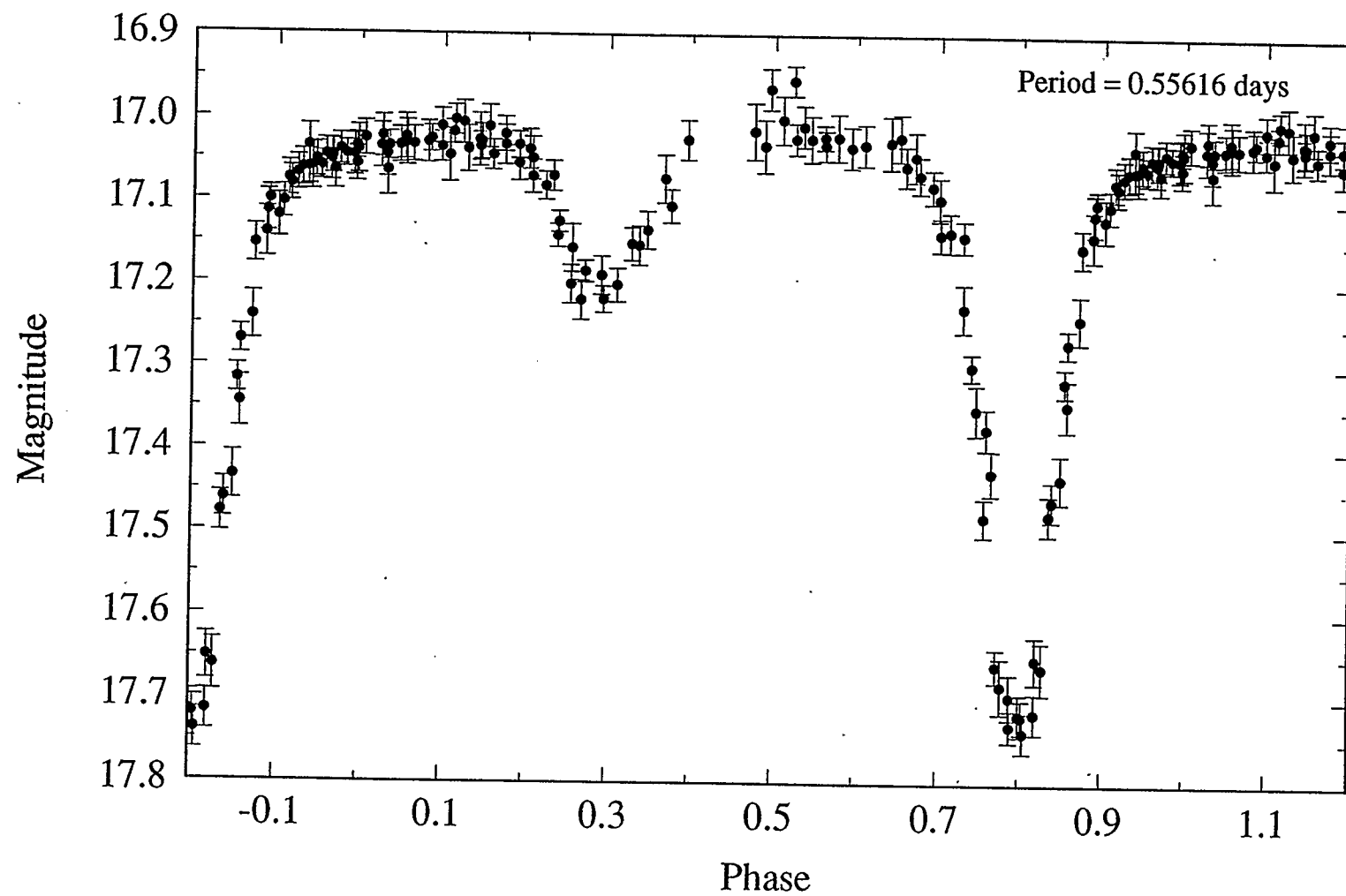
Figure 7h - The Yan & Mateo Cousins I light curve of M71-V4 with photometric errors.
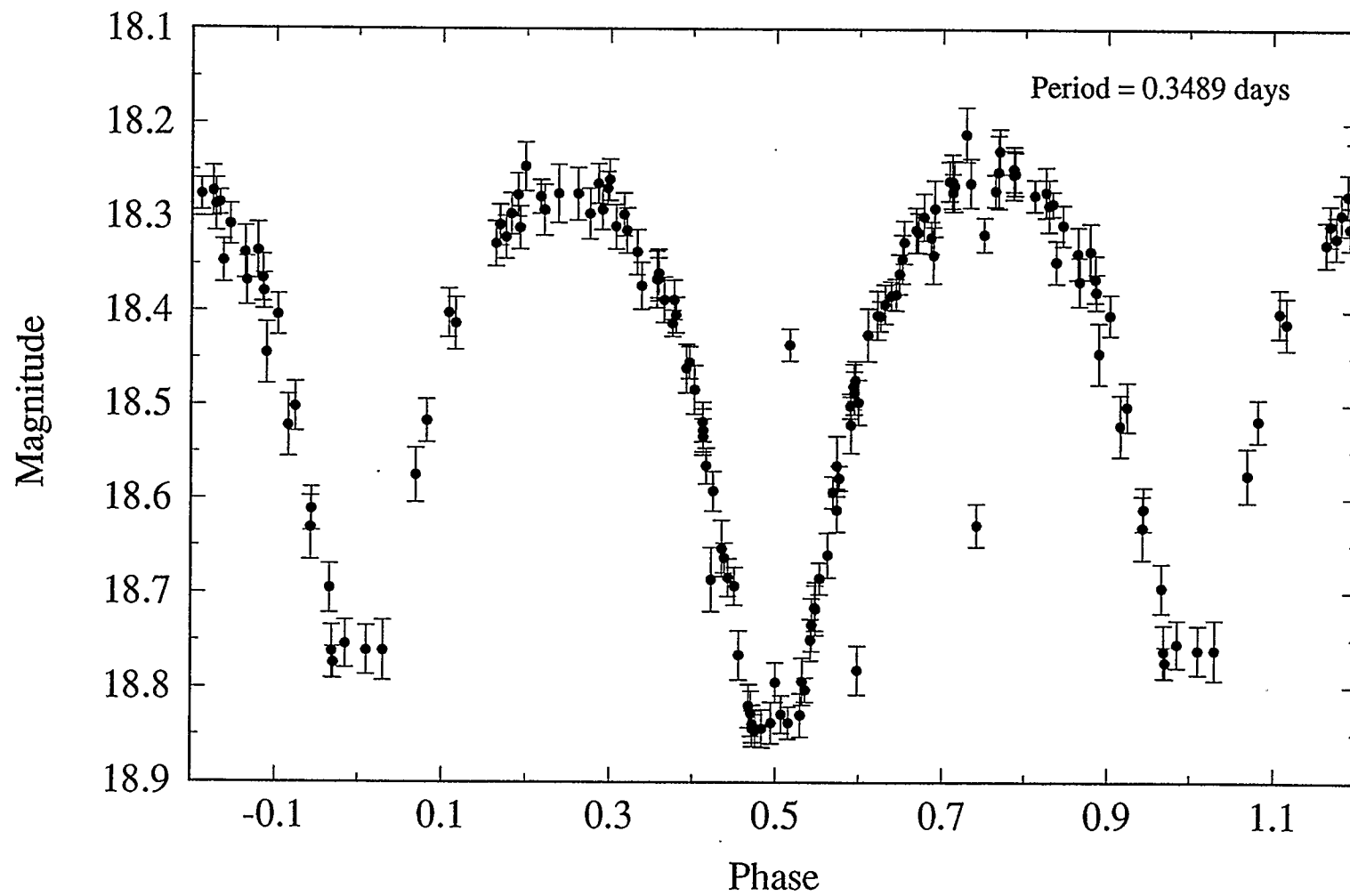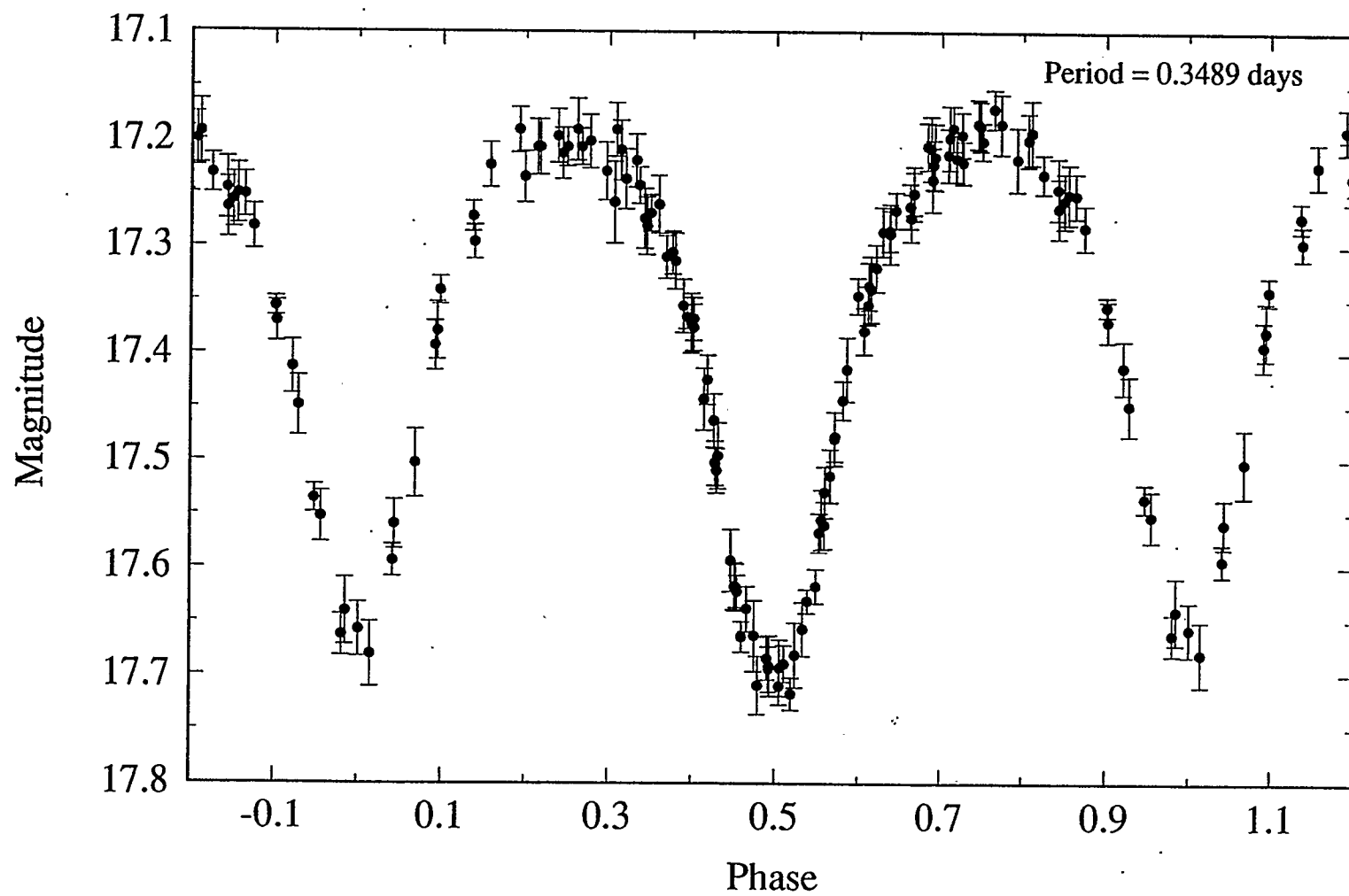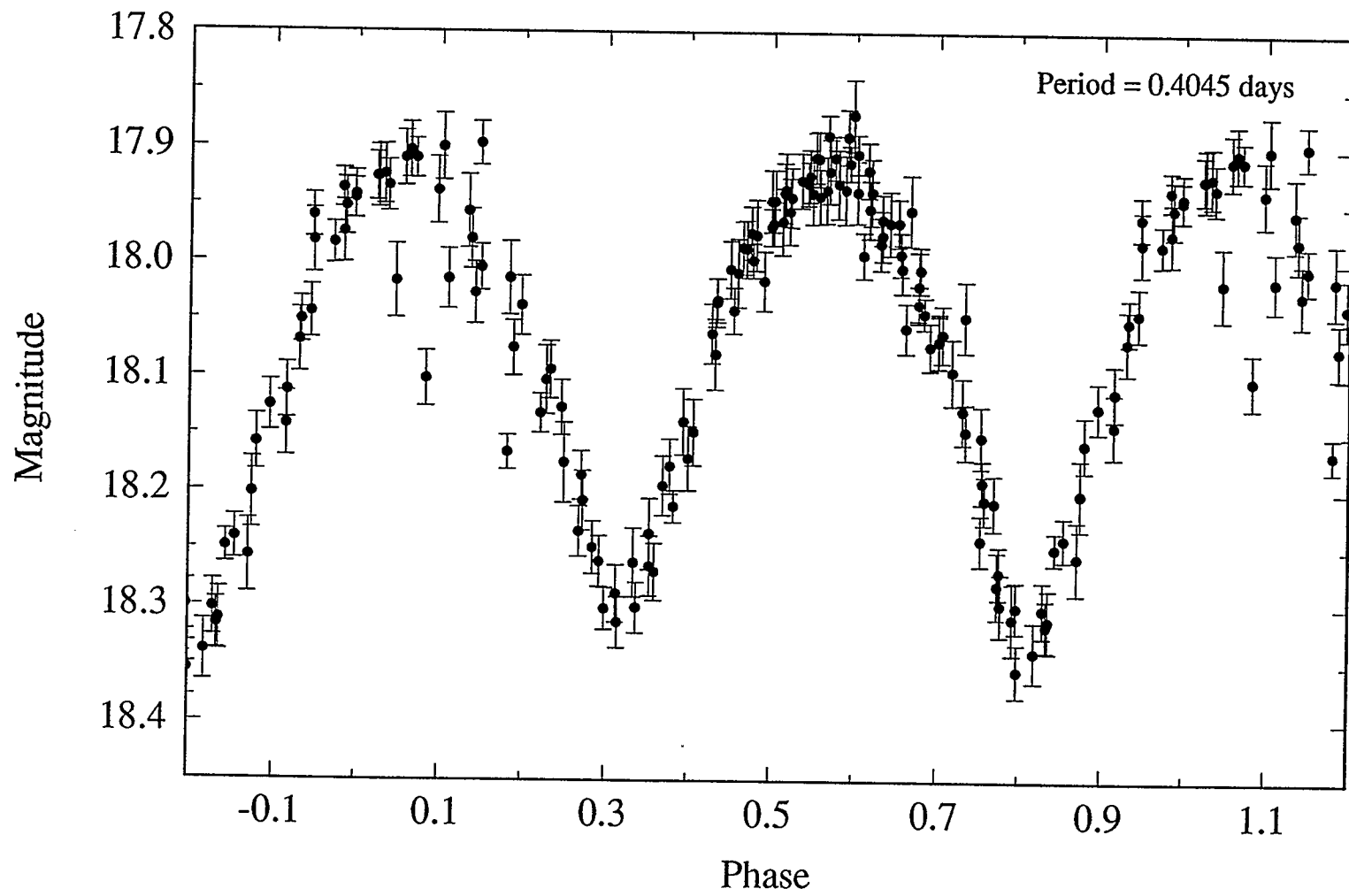
Figure 7i - The Yan & Mateo Johnson V light curve of M71-V5 with photometric errors.
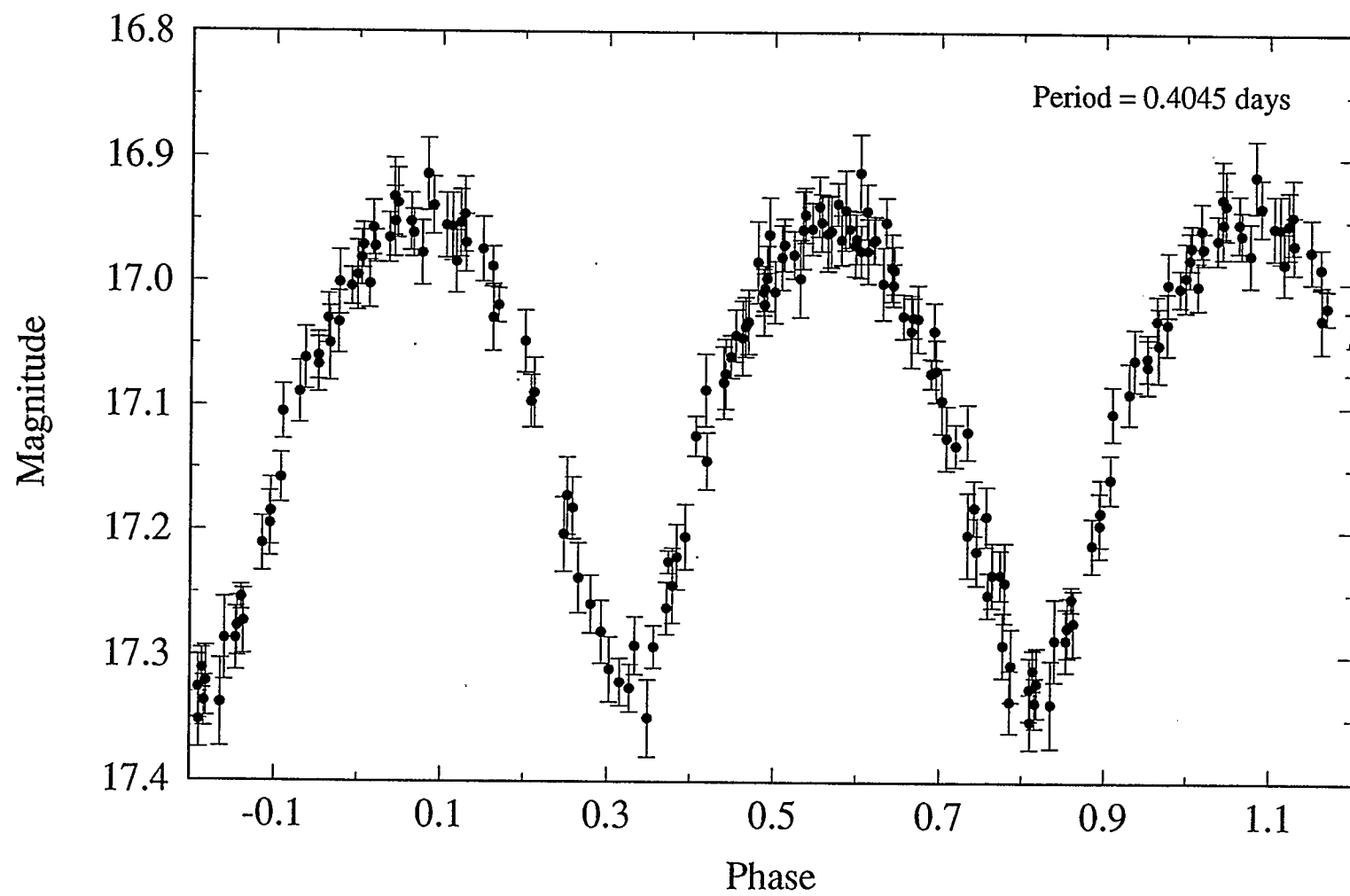
Figure 7j - The Yan & Mateo Cousins I light curve of M71-V5 with photometric errors.
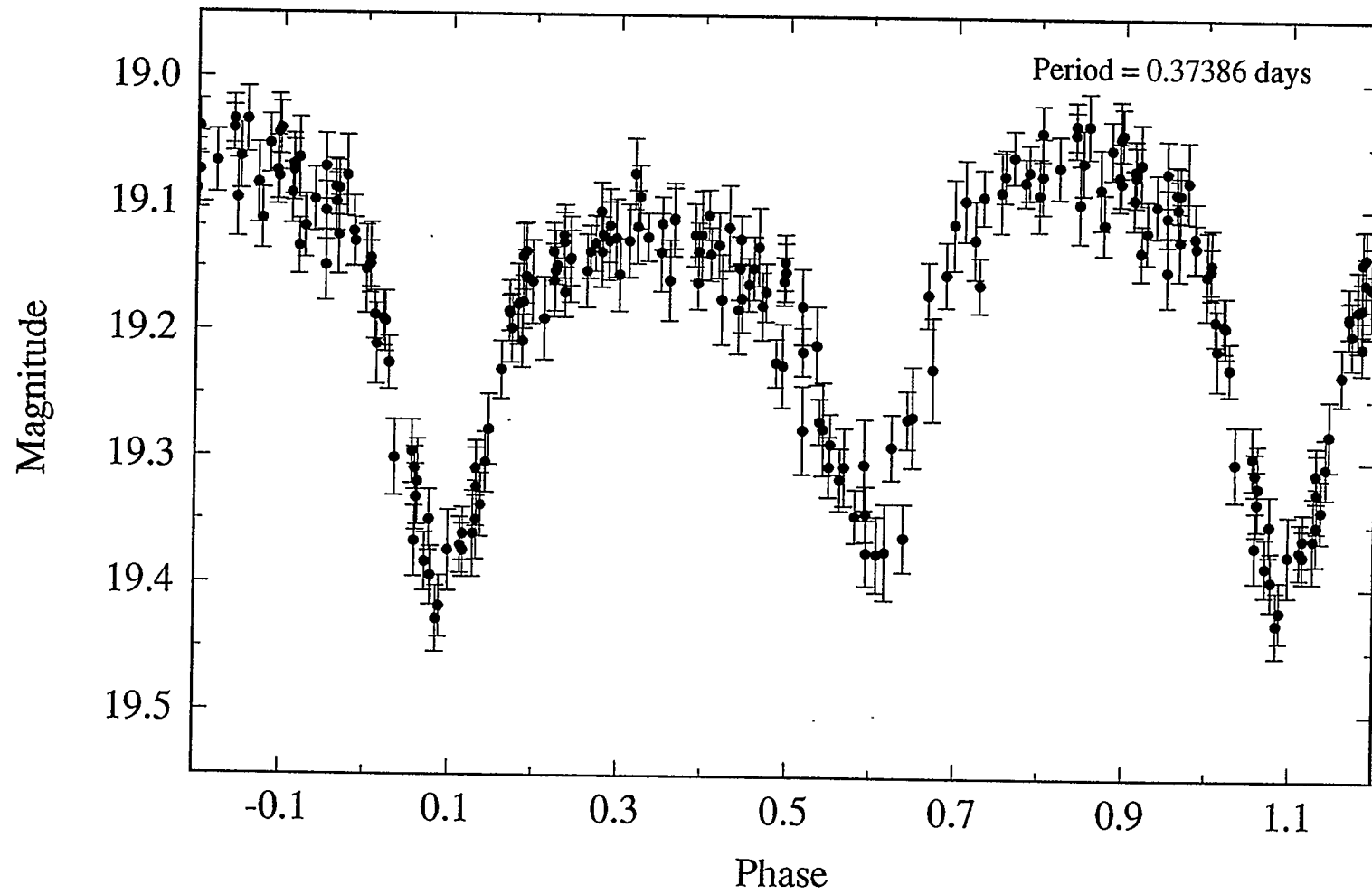
Because the reduction of CCD data is essential to the quality of the resulting light curves, and because the success of the analyses depends on that quality, the reduction process will be discussed in detail here.

TABLE 2a
Positions of the Yan & Mateo Binaries

Name	α_{1950}	δ_{1950}	Central Distance
V1	$19^h51^m43^s.31$	$18°40'35''.1$	$247''.3$
V2	$19^h51^m43^s.14$	$18°39'38''.2$	$166''.3$
V3	$19^h51^m36^s.99$	$18°41'12''.4$	$99''.2$
V4	$19^h51^m35^s.14$	$18°41'00''.9$	$81''.6$
V5	$19^h51^m20^s.17$	$18°40'51''.7$	$225''.8$

TABLE 2b
Basic properties of the Yan & Mateo Eclipsing Binaries

Name	Type	Period	HJD$_0$	I_{amp}	I_{max}	(V-I)	$I_{max, o}$	(V-I)$_o$
V1	W UMa	0.34890^d	2448415.482	$0^m.50$	$17^m.20$	$1^m.09$	$16^m.83$	$0^m.754$
V2	W UMa	0.36719^d	2448415.730	$0^m.65$	$16^m.87$	$0^m.94$	$16^m.52$	$0^m.604$
V3	W UMa	0.37386^d	2448415.669	$0^m.35$	$17^m.67$	$1^m.40$	$17^m.24$	$1^m.064$
V4	Algol	0.55615^d	2448415.713	$0^m.75$	$17^m.02$	$0^m.85$	$16^m.58$	$0^m.541$
V5	W UMa	0.40450^d	2448487.441	$0^m.45$	16^m96	$0^m.98$	$16^m.56$	$0^m.644$

3.2 Reduction

The reduction of, and magnitude determination from, CCD images is a difficult process and some discussion is illuminating. The process required to go from raw CCD images to usable stellar magnitudes can be divided into three stages. The first stage is the image reduction in preparation for stellar magnitude determinations by removing noise, defects and anomalous count source signatures. The second stage is the determination of magnitudes by one of several methods. The third stage is the correction of the magnitudes for atmospheric extinction and conversion from a local system to a standard system.

CCD photometry has many advantages over single-channel photoelectric photometry (PEP): simultaneous observation of several sources; spatial resolution for extended objects; simultaneous sky background measurement; and the ability to recover individual images from superimposed images. But with those advantages come significant disadvantages. The most important is a decrease in the signal-to-noise ratio per pixel. A second potentially important disadvantage is the much larger memory storage space required for data acquisition and processing and a corresponding increase in time required for reduction. A moderately successful CCD photometry observing run can often yield gigabytes of data and take months to reduce whereas even a long PEP observing run will often yield less than a single megabyte of data and can be reduced in a single day. The reasons for this are: (1) a CCD image contains the equivalent of n PEP observations in a two dimension array (where n is the number of pixels); and (2) the reduction procedure requires a great number of extra images in order to reduce the influence of noise and sensitivity variation across the CCD. Since typically $n \approx 512^2$ or 800^2, and light curves usually require ~200 points per passband, the requirement for gigabytes of storage space is obvious. However, much of the information contained in a CCD image is ultimately not needed, at least in the case of CCD photometry.

Before discussing the reduction procedure in depth, it is informative to briefly mention the topic of noise. There are potentially many contributors to the uncertainty in a CCD measurement, the three most common of which are discussed here. A more detailed description of these and other noise sources can be found in Gilliland (1992). One very fundamental source of noise is the statistical variation in the number of detected counts. The uncertainty associated with photon counting is Poissonian in nature. Photons from a constant source do not arrive at a uniform rate. They are instead randomly clumped so the number of photons detected in any given time interval will vary. In addition, detectors

only register a certain fraction of the photons that strike them (this fraction is called the *quantum efficiency* and it varies with wavelength and from CCD to CCD). Shot noise is a measure of the width of Poissonian distribution expected if the same measurement was taken repeatedly. Any measurement will have a root mean square (rms) variation of at least the square root of the number of recorded photons. Therefore, if the number of electrons that represents the brightness of a star is given by C_{star}, the rms noise level can never be less than $C_{star}^{1/2}$. A second noise source is the shot noise associated with the background contribution to the measurement. If this contribution is given by C_{sky}, the associated noise will be $C_{sky}^{1/2}$. The importance of this quantity clearly depends on the brightness of the sky, but it also depends on the size of the stellar image. The sky contributes signal to each pixel of the CCD frame so the amount of signal contributed to a small stellar image will be less than that contributed to a large stellar image. The final noise contribution to be discussed is created in the process of electronically measuring the charge level of each CCD pixel. When the signal generated by light falling on a CCD is collected, amplified, and digitized, noise is introduced. This is known as *read-out noise, R*. It is a per-pixel quantity and is typically a few electrons to a few tens of electrons (root mean square variation), depending on the CCD. Again, the significance of read-out noise for CCD photometry depends on the size of the stellar image since it is a per-pixel quantity. Each of these noise contributions add in quadrature so the signal-to-noise ratio of a measurement is expressed as

$$S/N = \frac{C_{star}}{\sqrt{C_{star} + N_{pix} \cdot \left(c_{sky} + R^2\right)}}, \qquad (22)$$

where N_{pix} is the number of pixels occupied by the stellar image and c_{sky} is the number of background counts per pixel in the region of the stellar image. When the noise is dominated by the sky contribution—as might be the case when observing under a bright

moonlit sky or when observing near an urban centre—the data are said to be sky-limited. When the noise is dominated by read-out noise, the data are said to be read-noise-limited.

There are three common types of images required for the preparation stage, usually referred to as *bias frames, dark frames,* and *flats.* Bias frames are zero second, or as close to zero second as possible, closed-shutter exposures. They are intended to measure any spatial pattern in the zero point of the CCD images. This pattern, if it exists and does not change with time, is referred to as the *bias structure.* The amplitude of the bias structure is generally expected to be quite low, and is sometimes exceeded by read-out noise. The frames will often have a large (several thousand electrons per pixel) zero point offset that is not spatially dependent, however. This offset can be subtracted off and does not contribute Poissonian (shot) noise to the image. If the bias frames are dominated by read-out noise, they can be used to determine the read-out noise, if it is not already known, by forming a histogram of the number of pixels versus count level. This will yield a Gaussian distribution with a standard deviation equal to the read-out noise.

Dark frames are also closed-shutter exposures but they are of durations typical of normal exposures. Their purpose is to measure any dark current that might exist, which is expected to be position dependent. To this end, ideally one would take a dark frame of equal duration for every program frame. However, this is impractical when rapid time-variations are to be investigated. Alternatively, one can obtain many dark frames, sampling a wide range of exposure times for each night of the observing run when conditions (such as clouds or daylight) preclude observations of program or calibration objects. Fortunately, such time-consuming procedures are not usually necessary because the dark current exhibited by most CCDs is not important provided the temperature of the chip is low. Furthermore, many CCD systems have an unexposed strip along one side

which effectively measures the dark current offset if not the detailed structure. This is the case for the Mt. Laguna chip.

Flats are intended to measure the variation on the gain of the CCD from pixel to pixel and are produced by observing a uniform source. The best uniform source to use for this purpose is the source of much controversy. The most common types of flats are *dome flats, twilight sky flats* and *dark sky flats*. Dome flats are produced by observing an illuminated screen inside the dome. Often the light source illuminating the screen is changed for each filter for which observations are taken. Twilight sky flats are produced by observing the sky in twilight, hopefully when the sky is bright enough that stellar contributions are negligible but not so bright that the CCD saturates. Dome flats have the advantage of not needing constantly changing exposure lengths as the sky brightness changes, not to mention the fact that they can be done during the day (provided the dome is light tight against daylight) or during weather not suitable for observing program objects. However, some observers prefer sky flats because the sky is closer in colour to certain program objects (such as the metal-poor stars of globular clusters) than are the projector lamps used to illuminate dome flats. Other observers feel that the wavelength dependence of the CCD sensitivity requires that flats be taken under precisely the same conditions as the program frames, *i.e.*, with the night sky itself. Such dark sky flats are produced by observing a "blank" region of sky, one in which there are relatively few stars. Acquiring several of any type of frame is always an advantage because statistics can be improved and cosmic rays can be medianed out (using several offset frames), but it is especially important for dark sky flats because regions that appear blank may actually contain unnoticed faint stars which must be medianed out if the flats are to be of any use. A very important disadvantage of dark sky flats is that extremely long exposures are required to acquire significant signals, particularly in shorter wavelength passbands. If

long exposures are not used, any advantage gained by using this method will almost certainly be lost due to large Poissonian error.

Although many software packages are available, the Mount Laguna images discussed here were all reduced with the aid of the widely used Image Reduction and Analysis Facility (IRAF), developed at the Kitt Peak National Observatory, Tucson, Arizona.

Before anything can be done with these frames or with the program images, each must have its zero-point offset and large scale *bias structure* removed. The IRAF package COLBIAS (for 'column bias'; a 'row bias' task is also available) is extremely useful for this purpose. The package fits one of four functions to the bias region of the frame (the region that is not exposed), subtracts the bias level from the entire CCD, and trims the bias region from the image.

Once this has been done, the smaller scale bias structure is determined. To this end, the bias frames should be averaged using the task IMCOMBINE (for 'image combine'). If there is no significant change in bias frames as the night progresses or from night to night, all bias frames can be used to produce a single averaged frame. A median average is best because it will remove any one-time occurrences such as cosmic ray hits and random noise that are not representative of the bias structure. This requires at least three bias frames but considering that they require little time to produce, a considerably larger sample is preferable. This method of cosmic ray removal and statistics improvement is extremely fast and effective and so is used whenever at least three identical frames are available.

The median COLBIASed bias structure can be used next to prepare the flats, once their DC offset has been removed with COLBIAS. The bias structure can then be simply subtracted using the task IMARITH (for 'image arithmetic'). The flats are then averaged.

Again, a median is the preferred statistic but this requires at least three images per filter. Because the flats measure the multiplicative gain variation from pixel to pixel, it is desirable to scale the images by their respective modes before the median is performed in order to make their ranges roughly similar[5]. To account for images with varying counts having differing shot errors, the images should also be weighted by their respective modes. This scaling and weighting can be done in one step using IMCOMBINE. The final step is to divide the median flat for each filter by its mean using IMARITH. This normalizes the flat and is done in order to avoid drastically changing the level of the program images when the sensitivity structure is divided out.

The program images can now be reduced. Once again, the zero-point offset and large scale bias structure is subtracted off with the use of COLBIAS and the median residual bias structure is subtracted off using IMARITH. The sensitivity structure is then divided out with the use of IMARITH by dividing the program image by the normalized median flat(the pixel values of which are of the order of unity) for the appropriate filter. It is important to properly remove the zero-point offset before dividing by the flat because failure to do so may produce an image that is worse (less flat) than the program image that has not been divided by the flat. Another possible reason for a non-flat resultant image is the variation of some element in the telescope-CCD system (see Figure 8). However, as long as the program objects appear many times brighter than the background fluctuation, the magnitude determination should not be drastically affected.

---

[5] It would be more intuitive to scale the images by their exposure times but this would produce meaningless results unless the source was identical from image to image. This is clearly not the case for sky flats and might not be the case for dome flats unless precautions to ensure uniformity are taken, so it is easier and safer to scale by the mode.
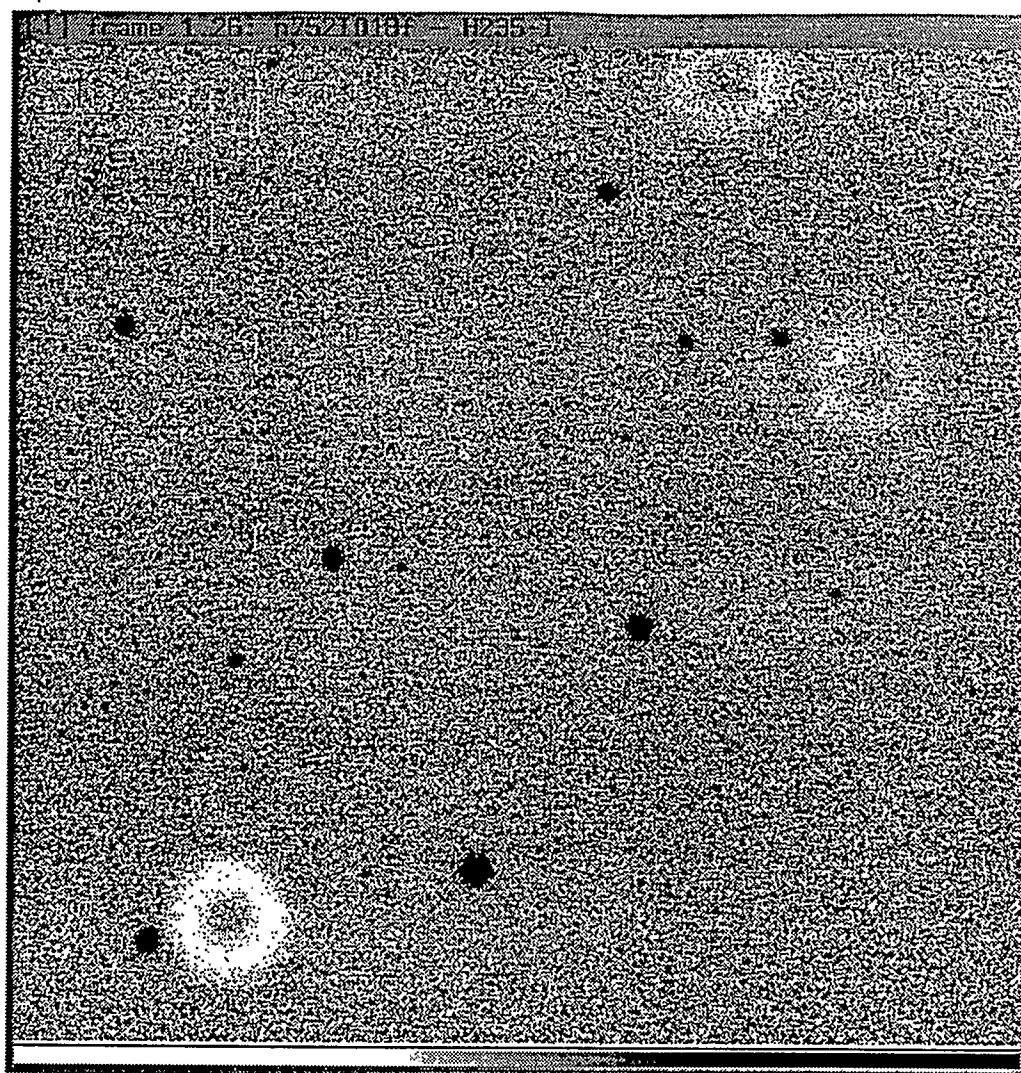
Figure 8 - An example of imperfect flat-fielding. The large rings are most likely a result of dust settling in the telescope-CCD system.

Up to this point, the effects of cosmic rays have not been discussed because they are removed when several images are medianed together. However, one usually does not have several identical program images that can be combined. In fact, if one did not have at least three biases or flats which could be combined, the following procedure would need to have been used in the earlier reduction stages. Inspection and editing of cosmic ray signatures in each frame is the most accurate method of cosmic ray removal but is excessively tedious. The scanning of several hundred 800x800 CD images and manual smoothing of cosmic ray spike regions is not practical. However, this process can be automated through software. The IRAF task COSMICRAYS scans the image for the characteristic signature of a cosmic ray hit: one or a few pixels that stand out well above the surrounding pixels. The task COSMICRAYS smoothes out pixels that exceed the mean of the surrounding pixels by a user-defined threshold (typically 5σ) and also have a ratio of the mean neighbouring pixel level to the candidate pixel level less than a second user-defined threshold (typically 2 to 10 percent). If the first threshold is not set properly, either cosmic rays will go undetected or spurious spikes will be mistaken for cosmic rays, unnecessarily slowing the reduction process. If the second threshold is set too low, again, many cosmic rays will not be found, and if it is set too high, stellar images can be mistaken for cosmic rays. The latter possibility is especially important to consider if the image scale and seeing is such that a stellar image occupies only a few pixels.

3.3 Magnitude extraction

Once the images are reduced to the stage that one can be confident that the number of counts in any given image pixel is linearly related to true intensities and that this

relationship does not vary significantly from pixel to pixel, the process of measuring the brightness of the program objects can begin.

There are many ways that this can be done and the most appropriate strategy will depend on the nature of the image under consideration. In the case of the fairly sparse standard star fields, simple aperture photometry was deemed sufficient. This process involves the counting of photons within a set of concentric apertures and 'sky' annuli of specified size centred on each star image. This was carried out using the IRAF task APPHOT (for aperture photometry). Several aperture sizes were selected and then each star was manually selected by visual inspection. The task's automatic centroiding option was used to avoid inadvertent errors in aperture positioning.

In the case of the Mount Laguna M71 images, the field was extremely crowded and so it was decided that *point spread function* (PSF) magnitudes would be preferable to aperture magnitudes. Peter Stetson's DAOPHOT II (a 1993 upgrade to the earlier DAOPHOT) program, and its ancillary programs, were used for this purpose. The less well-known program DoPHOT (Mateo & Schecter 1989) was also considered but difficulties in adapting this package to our workstations and other considerations made the more familiar DAOPHOT II a better choice. A comparison between these packages was carried out by Janes & Heasley (1993), who concluded that the programs, along with their own software, all produce comparable results, such that ease-of-use issues of one package over another tend to be the limiting consideration.

DAOPHOT requires certain information:

- the approximate size or full-width at half-maximum (FWHM) of the objects in the frame
- the number of photons corresponding to an analog-to-digital unit (ADU)
- the readout noise per pixel

- the saturation level, beyond which the detector no longer operates linearly

Knowing this information, DAOPHOT will, with variable levels of interaction, locate star-like objects in the frame above a certain threshold detection level; perform aperture photometry for these objects with a range of concentric apertures, estimating a local sky brightness for each object; and obtain a PSF for the frame by averaging several stars. At this point the auxiliary program ALLSTAR II can be used. ALLSTAR computes precise positions and magnitudes by fitting the PSF to each object. It then subtracts the fitted images from the real images to allow for the location and measurement of previously undetected objects.

3.4 Extinction and transformation

Almost all empirical information in astrophysics is obtained by studying the electromagnetic radiation received from astrophysical objects. Aside from the direction from which the radiation comes, the most obvious measurement that can be made is its brightness, more specifically, its brightness at various wavelengths. If anything is to be learned from these measurements, the relationship between the amount of radiation received and the amount emitted at the source, and how this light has been changed, must be understood. There are many factors that influence this relationship, including the distance of the source, interstellar extinction, the speed at which the source is moving, *etc*. However, before most of these factors can be taken into account accurately, usually one must consider other quite local problems. Every observatory on earth is affected, and affected differently, by: (1) the path length through the earth's atmosphere; and (2) the equipment used to measure the radiation. Therefore, one of the first steps in interpreting astrophysical data for earth-bound observers is to measure, understand and minimize these locally caused effects. There are two parts to this problem in the case of magnitude

measurements: correction for the atmospheric extinction; and the transformation of the corrected magnitudes from the instrument's system to a standard system. Although these two steps are largely necessitated by different effects, the procedures for extinction correction and transformation are linked: both involve transformations. What follows is a quick derivation of the extinction and transformation equations. For an in-depth discussion of these equations, see Hardie (1962).

Light traveling through any material will lose a certain amount of intensity. This loss of intensity, dI, is related to the incident intensity, I, the amount of material it transverses, dx, and the absorption/scattering coefficient of the material, κ, by:

$$dI = -I \cdot \kappa \cdot dx. \tag{23}$$

Integrating this expression through the entire path length, x, gives:

$$\log I_\mathrm{f} = \log I_o - \kappa x, \tag{24}$$

where I_f and I_o are the final and initial intensities. In magnitudes, this equation becomes

$$m_o = m - 2.5\kappa x = m - kX, \tag{25}$$

where m_o is the magnitude outside the atmosphere, m is the observed magnitude, k is the extinction coefficient in units of magnitude per airmass, and X is the airmass. Airmass is essentially a measure of the path length of atmosphere through which the light passes. It is expressed in units of the zenith thickness of the atmosphere at the location of the observer. It can be expressed, to a first approximation, as

$$X = \sec z, \tag{26}$$

where z is the zenith distance, the angle of separation between the zenith and the object of interest. This equation is based on the approximation of a plane parallel atmosphere and is accurate to 0.01 of an airmass at zenith distances up to 65 degrees. For more accurate calculations at larger zenith angles, the equation

$$X = \sec z - A(\sec z - 1) - B(\sec z - 1)^2 - C(\sec z - 1)^3$$
$$A = 0.0018167$$
$$B = 0.0028750 \tag{27}$$
$$C = 0.0008083$$

can be used (Hardie 1962).

The colour of an object is also affected by the amount of atmosphere through which its light must travel. An equation similar to (25) can be used for colour indices:

$$c_o = c - k_c X, \tag{28}$$

where c is a colour index and the subscript o denotes outside atmosphere values. The extinction coefficients k and k_c are actually functions of the object's light distribution and so it is more accurate to write:

$$m_o = m - k'X - k''cX \tag{29}$$

$$c_o = c - k_c'X - k_c''cX \tag{30}$$

where k', k_c' and k'', k_c'' are the principal and second-order extinction coefficients. The second-order coefficients are found to be fairly constant, even though, in principle, the coefficients can vary significantly.

There are several methods of determining extinction coefficients which require differing amounts of time and sky conditions. The Hardie method, described here, requires a generally uniform sky but is also quite quick to perform, leaving most of the night for observing program objects.

If two known stars are observed, one of which is observed through a low airmass and the other through a high airmass, equations (29) and (30) can be re-expressed differentially:

$$\Delta m_o = \Delta m - k'\Delta X - k''\Delta(cX) \tag{31}$$

$$\Delta c_o = \Delta c - k_c'\Delta X - k_c''\Delta(cX). \tag{32}$$

If approximate values are assumed for the second-order coefficients, which in general are fairly constant, then these equations are easily solved for the principal coefficients. The effect of inaccurate second-order coefficients can be minimized by selecting stars that are closely matched in colour indices. For increased accuracy, several sets of high-low stars can be observed and the principal coefficients can be found with a least-squares method. Observing three sets of stars usually yields principal coefficients accurate to 2 or 3 percent.

Unfortunately, the fact that equations (31) and (32) contain outside-atmosphere magnitudes and colour indices complicates matters considerably. Unless the telescope used is very close to a standard system, these values will not be known. For simplicity, all further discussion will use notation specific to the UBVI system used for the Mount Laguna data. This does not, however, affect the generality of the method described. Using the equations:

$$V = v_o + \mu_V(B-V) + \zeta_V \qquad (33)$$

$$C = \mu_c c_o + \zeta_c, \qquad (34)$$

which are usually adequate to transform from one system to another provided the systems are reasonably similar and extremely high wavelengths and stellar temperatures are avoided, the outside-atmosphere magnitudes can be found. Here, all upper case letters refer to the standard system—the colour indices C are (B-V), (U-B), (V-R), and (V-I)—and μ and ζ are the transformation coefficients and zero-point respectively. Differentially, these equations are:

$$\Delta V = \Delta v_o + \mu_V \Delta(B-V) \qquad (35)$$

$$\Delta C = \mu_c \Delta c_o. \qquad (36)$$

The zero point has been eliminated but if the transformation coefficients are not known, an iterative procedure of successive approximation must be used to calculate μ, ζ, and k' simultaneously. By combining equations (31) and (35) and equations (32) and (36), the equations used for the iterative procedure are obtained:

$$k'_V \Delta X = \Delta v - k''_V \Delta[(b-v)X] + \mu_V \Delta(B-V) - \Delta V \tag{37}$$

$$k'_c \Delta X = \Delta c - k''_c \Delta(cX) + \Delta C \mu_c^{-1}. \tag{38}$$

To iterate, the equations are solved for one unknown, k'_V for instance, and an enlightened guess is used for the second unknown ($\mu_V=0$, $\mu_c=1$ for example). The resulting value for k'_V is then used to calculate μ_V, which in turn is used to find an improved value for k'_V and so on.

Once the extinction and transformation coefficients are known, the program object magnitudes can be corrected for extinction and transformed to the standard system of magnitudes so that comparisons with the work of others or the work from other telescopes are meaningful.

4.0 LIGHT CURVE MODELLING

4.1 The modified Wilson-Devinney modelling code

The light curve modelling program that forms the bulk of the code used for this work was written by Robert E. Wilson and Edward Devinney and was first described in 1971 (Wilson & Devinney, 1971). Since then, numerous additions and improvements have been made (Wilson 1979, Milone *et al.* 1992, Stagg & Milone 1993, Stagg *et al.* 1994) to arrive at the version used for this work. Some of the more important new features are: the handling of eccentric orbits, the ability to include and adjust star spots, the use of Kurucz's modern stellar atmospheres (Milone, 1993) integrated over appropriate passbands, several modes of operation depending on the type of binary system (i.e., contact, semi-detached, detached, x-ray binaries), and a dramatic increase in speed thanks to more efficient code. The usage of the Wilson-Devinney code has grown considerably since its introduction—being used in roughly 50 percent of the light curve solutions carried out between 1987 and 1990 (Wilson 1990). Thus this program is the one of choice, especially in the exploration of properties of binary systems involving non-solar compositions. A discussion of light curve modelling software and comparisons between existing programs may be found in Milone (1993).

The University of Calgary version of the Wilson-Devinney modelling program (hereafter, WD) joins the light curve calculation program (LC) and the differential corrections program (DC) but the two still remain essentially independent. The two subprograms have different purposes but both are an integral part of the modelling process. The appropriate subprogram to be used is signaled by an initial control integer in the input file.

LC, as previously mentioned, is used to calculate light and radial velocity curves based on the parameters supplied within the input file. This is accomplished by dividing the surface of the stars, as described by a Roche equipotential model, into a grid. In the case of light curves, it is then determined which grid points will contribute light to the calculated light level for each phase point: parts of the surface of a star that are occulted by the other star or by another part of the same star cannot contribute except for light reflected off the other star. The grid points that are visible to the observer contribute to the total light level for the current phase of the light curve according to temperature, limb darkening, gravity darkening, and the amount of light from the other star that is reflected in the direction of the observer. Radial velocity curves are calculated in essentially the same manner. However, for the current work, no velocity data were available so the synthetic RV curves are primarily useful only for predicting RV curves for observation planning and for testing the model against subsequent RV data.

An example of an LC input file is given in Appendix B. The input file is identical to the standard LC input file, a full description of which can be found in the WD manual (Wilson 1992), with the exception of the first few lines. The lines up to and including the first occurrence of "END", the first five lines in the example given, are related to the University of Calgary enhancements to the WD code. Rather than having two separate programs (LC and DC) containing redundant subroutines, a single program is used. The first line of the input file contains a 1-digit integer and indicates whether LC or DC is to be run (1 for LC, 2 for DC). The second line contains the logarithm of the surface gravity (in CGS units) for each component. The third and fourth lines contain the names of the files containing the ratios of the integrated passband fluxes to the monochromatic blackbody fluxes for a range of temperatures and surface gravities. These files correspond to the synthetic light curves requested later in the input file. An example of a flux file is given in

Appendix C. The flux ratios are based on the 1993 model atmospheres of Kurucz and are specific to the passband in question and metallicity. The use of modern model atmospheres addresses what has long been a weakness of the WD code. In the example given, two files are listed, one for each synthetic light curve requested later in the file (Johnson V [Fe/H]=-0.3 and Cousins I [Fe/H]=-0.3). If more light and velocity curves are present, there must be a corresponding number of flux files listed, and they must appear in the same order as the curves appear in the file. The fifth line in this example signifies the end of the flux ratio file list. The surface gravities and temperatures (contained in the standard part of the LC and DC input files) are used to interpolate among the Kurucz models in the flux files for the appropriate ratio of atmospheric to blackbody fluxes.

The DC subprogram is for determining differential corrections to the modelled parameters. The corrections to the adjusted parameters are obtained from a least squares analysis, the equation of condition for which is

$$\Delta L = \frac{\partial L}{\partial x_1}\Delta x_1 + \frac{\partial L}{\partial x_2}\Delta x_2 + \frac{\partial L}{\partial x_3}\Delta x_3 + ..., \tag{39}$$

where x_i are the adjusted parameters. The process requires the generation of at least m+1 synthetic light curves for each wavelength, where m is the number of adjusted parameters. Asymmetric partial derivatives require m+1 synthetic light curves and are calculated according to

$$\frac{\partial L}{\partial x} = \frac{L(x+\Delta x) - L(x)}{\Delta x}, \tag{40}$$

where Δx is a controllable step size. Symmetric partial derivatives can also be used but they require 2m+1 synthetic light curves and are calculated according to

$$\frac{\partial L}{\partial x} = \frac{L\left(x+\frac{\Delta x}{2}\right) - L\left(x-\frac{\Delta x}{2}\right)}{\Delta x}. \tag{41}$$

This method of finding light curve solutions has its limitations, as was noted in some detail by Kallrath & Linnell (1987). In particular, many of the adjusted parameters are often strongly correlated which may lead to the failure of the differential corrections to converge on a solution. To avoid this, DC allows the calculation of corrections for subsets of uncorrelated parameters. Since the partial derivatives are already calculated for the main parameter set, the subsets require little extra time. However, having multiple subsets of uncorrelated or weakly correlated corrections rapidly leads to numerous possible search branches, the exploration of which can be tedious. One might have some faith that all of the search branches would eventually lead to the same minimum in parameter space since all corrections should in theory point downhill, even if they do not point in the steepest direction. However, it is often the case that uncorrelated correction sets yield worse fits than the initial parameter sets. In fact, even subsets with only one adjusted parameter, leaving no possibility of correlation, can give corrections that result in worse fits. This is probably due to limitations in the accuracy of the partial derivative calculations, particularly during final convergence. The WD code was originally written with these limitations in mind and automated iteration procedures were omitted intentionally for this reason. Careful subset selection and exploration will usually lead to a local minimum in parameter space but, without caution, convergence may take much longer than is necessary, or may not occur at all.

Unfortunately, finding a local minimum in no way ensures that a deeper minimum does not exist elsewhere in parameter space. This problem is traditional and persistent for DC because the program makes no effort to address it. Like a marble on an irregular surface, DC will always try to move to the nearest local minimum. If the initial set of parameters is not close to the best solution, as is very often the case, DC will have little hope of finding this solution. Of course it is possible to start DC in many locations in

parameter space and see where each search leads, but this requires a great deal of computer time and even more time and effort for the user. One stratagem that was used by Groisman (1989) and Milone *et al.* (1991) was to vary each parameter by ±10% in search of deeper minima. This method is useful, but changing one parameter at a time limits the search directions to the directions of the parameter axes and neglects the m-dimensional diagonals. Since many parameters are regularly correlated (T_2 and L_1 or Ω_i and q for instance), valleys along diagonal directions are to be expected.

An example of a modified DC input file is found in Appendix D. Again, the first five lines are recent additions to the standard DC input file. They are the same as described above, but here, the list of flux files must correspond with the observed light curves included in the standard portion of the DC input file rather than the requested synthetic light curves. The rest of the input file is the same as the standard DC input file; an illustration can again be found in the WD manual (Wilson 1992).

For all its limitations, WD, with the University of Calgary modifications, is the most powerful light curve analysis program available. The global minimum search can be met, at least to some degree, by an additional program.

4.2 The simplex search algorithm

The application of the simplex algorithm, as implemented by Kallrath & Linnell (1987), is an attempt to avoid many of the problems associated with the differential corrections method of optimization, which, for the most part, stem from the partial derivative calculations. Several *direct search methods*, which by definition do not require derivatives, are described by Murray (1972). Of these, the simplex algorithm as given by

Nelder & Mead (1965) becomes comparatively more efficient when more than two or three parameters are to be adjusted, as is the case for light curve modelling.

The simplex algorithm calculates an initial set of m+1 synthetic light curves, each representing a vertex of the simplex in m-dimensional parameter space. The size and location of the initial simplex is controlled by the user. The fit of each light curve, or point in parameter space, to the observed data is then determined. The simplex moves around in parameter space in search of the best solution according to four operations: *reflection*, wherein the worst of the m+1 vertices is reflected through the centre of the other m vertices to a new position; *expansion*, wherein the worst vertex moves away from by a controllable amount; *contraction*, wherein the worst vertex moves toward the centre of the other m vertices by a controllable amount; and *shrinkage*, wherein all the vertices move toward the best vertex by a controllable amount. Figure 9 is a flow chart which illustrates when each of these operations is used. A more detailed explanation of the simplex algorithm is given by Kallrath & Linnell (1987). In this fashion, the simplex "walks" about in an ordered but flexible manner until it converges to a minimum. Again, it cannot be guaranteed that the absolute minimum has been found but the simplex algorithm is much more far reaching than gradient dependent searches and due to its convenience of use, many searches can be started and left to run with little intervention from the user. A set of constraints on the variation of each parameter precludes non-physical results. The constraint conditions, and the circumstance that the best vertex is always retained, assures a sensible result. This compares favorably with automatic iteration with DC, were that program to be modified to permit automatic iteration. The gradient-free search method is also faster since each step usually requires a single new synthetic light curve calculation for the new vertex instead of the m+1 or more light curve calculations required by DC. By using the relevant parts of the WD code to generate the required synthetic light curves,

START

$S^{(0)}=(x_I^{(0)},f_I),l$

$S^{(k)}$=the kth simplex
f=the fit of a given vertex
σ_f=standard deviation of the fits of the vertices

h=worst vertex   α=reflection operator
s=second worst vertex   β=contraction operator
l=best vertex   γ=expansion operator
c=centre of simplex   δ=shrinkage operator

$x_c,h,x_\alpha(x_h),f_\alpha$

$f_\alpha<f_l$ NO $f_\alpha>f_s$ YES $f_\alpha>f_h$

YES   NO

YES NO

$x_\gamma(x_\alpha),f_\gamma$

$x_\beta(x_h),f_\beta$ $x_\beta(x_\alpha),f_\beta$

$f_\gamma<f_\alpha$ NO

YES

NO $f_\beta>f_h$ YES

$x_l=x_\delta(x_l),f_l$

$S^{(k+1)}=\gamma(S^{(k)})$ $S^{(k+1)}=\alpha(S^{(k)})$ $S^{(k+1)}=\beta(S^{(k)})$ $S^{(k+1)}=\delta(S^{(k)})$

$\langle f\rangle, \sigma_f$

NO $\sigma_f<\sigma_{ext}$ or $k>k_{max}$ YES **STOP**

Figure 9 - A flow chart demonstrating the operation selection process for the simplex algorithm. Adapted from Figure 9 of Kallrath & Linnell (1987).

the results of the simplex parameter space searches are expected to be in agreement with the WD program. In practice, the simplex and WD programs are not in complete agreement but in the examples reported by Stagg & Milone (1993), the results agree within the uncertainties.

It should be noted that DC and other derivative dependent procedures, while suffering in overall efficiency (*i.e.*, efficiency from the user's perspective), due to the difficulty and number of calculations required, are actually more efficient in terms of convergence effectiveness because they use a directed search (*i.e.*, the number of steps required to reach convergence is expected to be smaller, even though the time required may be longer). It is often desirable, therefore, to switch from simplex to WD once the search has come close to the solution. Also, WD allows the determination of probable errors and the identification of poorly constrained parameters.

There are several files required to run simplex besides the main program. The input file, which generally has a 'dci' extension, is exactly the same as a modified DC input file, described above, with no subsets, since subsets have no meaning in the context of the simplex algorithm. The use of a DC input file is deliberate to facilitate comparisons between WD and simplex. The flux files specified in the dci file are also required. A second file containing the limits beyond which simplex will not allow parameters to move is called the constraint file, and generally has a 'con' extension. A third file, the information file, contains information such as the size of the initial simplex, coefficients for adjusting the way it moves and contracts, the parameters that are to be adjusted, and when the program is to stop (*i.e.*, after a certain number of iterations or when the simplex contracts to a certain size). This file generally has an 'inf' extension. Finally, the 'run' file is actually a small program that calls the main program and organizes the input and output files. All of these files except the DC input file are well organized and include some

explanatory text to avoid the formatting problems and confusion that are common with the somewhat cryptic DC input files. Examples of all these files are given in Appendix E.

4.3 Modelling procedure

The exact procedure used for modelling the light curves was dependent on the nature of the light curves and on how the modelling proceeded. The general procedure can be summed up as follows: (1) the calculation of initial parameter sets and preparation of input files; (2) the approximate location of the solution using simplex; (3) and the fine tuning of the solution using WD. These steps are discussed in detail for the present case below.

Of the five systems studied, four appear to be W UMa-type systems. Following the work of Rucinski (1973, 1974) the depth of the primary and secondary minima were measured and converted to normalized light units using

$$\frac{l_{1,2}}{l_{max}} = 10^{\left(\frac{m_{1,2}-m_{max}}{-2.5}\right)} \tag{42}$$

and

$$J_{1,2} = 1 - \frac{l_{1,2}}{l_{max}} \tag{43}$$

The difference in the depths

$$\Delta = J_1 - J_2 \tag{44}$$

and the depth J_1 of the primary were then used to find approximate values for inclination i and mass ratio q by linearly interpolating from Table 1 of Rucinski, 1974. For this interpolation, it was assumed that the fill-out parameter f_R, defined by Rucinski as

$$f_R = \frac{\Omega - \Omega_{outer}}{\Omega_{inner} - \Omega_{outer}},$$

(45)

was equal to 0.5. The total mass of each binary system was assumed to be 1.7 solar masses, roughly twice the turn-off mass of the M71 colour magnitude diagram according to the models of Bergbusch & VandenBerg (1992). An age of 14 Gyr and a metallicity of [Fe/H]=-0.78 were assumed as was suggested by Hodder et al. (1992). The use of this mass implies that each system consists of two main sequence stars near the current main sequence turn-off. There is little justification for this assumption but at the commencement of modelling, no other information was available. It will be argued in Chapter 5 that the use of this total mass is of no significant consequence for the usefulness of the final models, allowing more reasonable masses to be substituted later. With the total mass and periods for each system, the respective semimajor axes were then calculated using equation (4). Rough radii, R, were then calculated using Eggleton's (1983) approximation of effective Roche lobe radii:

$$\frac{R}{a} = \frac{0.49q^{-2/3}}{0.6q^{-2/3} + \ln(1 + q^{-1/3})}.$$

(46)

Note that this equation has been modified slightly in order to account for Eggleton's definition of q being the inverse of that used in the present work. Knowing the approximate radii, the surface gravities were estimated using

$$\log g = \log\left(G\frac{M_i}{R_i^2}\right).$$

(47)

The effective temperatures of the hotter star in each system, T_1 were estimated from the tables of Popper (1980) for Johnson (V-R) colour indices. These colour indices were determined from the Johnson V and Cousins I light curves supplied by Lin Yan (private communication) using the relationships:

$$(V - R)_{JC} = 0.505 \cdot (V - I)_{JC} + 0.707 \tag{48}$$

and

$$(V - R)_{JC} = -0.03206 + 0.71652 \cdot (V - R)_{J}. \tag{49}$$

Equation (48) was derived by fitting tabulated (V-R) colour indices against (V-I) values for the Landolt's (1983) standards (see Figure 10). Equation (49) was determined by Landolt (1983). Based on the differences between the temperatures derived in this manner and those derived by Yan & Mateo (1994), the uncertainty in T_1 was assumed to be 150 K. Further improvement in these values requires spectral classification but, given that the temperature difference between the primary and secondary overshadows the effects of small uncertainties in the absolute temperatures, later modelling attempts based on new temperatures are not expected to yield results greatly different from the present results. Once the effective temperatures and the surface gravities were estimated, bolometric, Johnson V, and Cousins I limb darkening coefficients (X_i^{bol}, X_i^{V}, and X_i^{I} respectively) were estimated by linearly interpolating from the tables of Van Hamme (1993). Values for the luminosities of the primary stars (normalized to 4π) were calculated assuming both stars had identical effective temperatures using

$$l_i = 4\pi R_i^2 \sigma T^4 \tag{50}$$

and

$$L_1 = 4\pi \frac{l_1}{l_1 + l_2}. \tag{51}$$

$$(V-R) = 0.505 \, (V-I) + 0.007$$
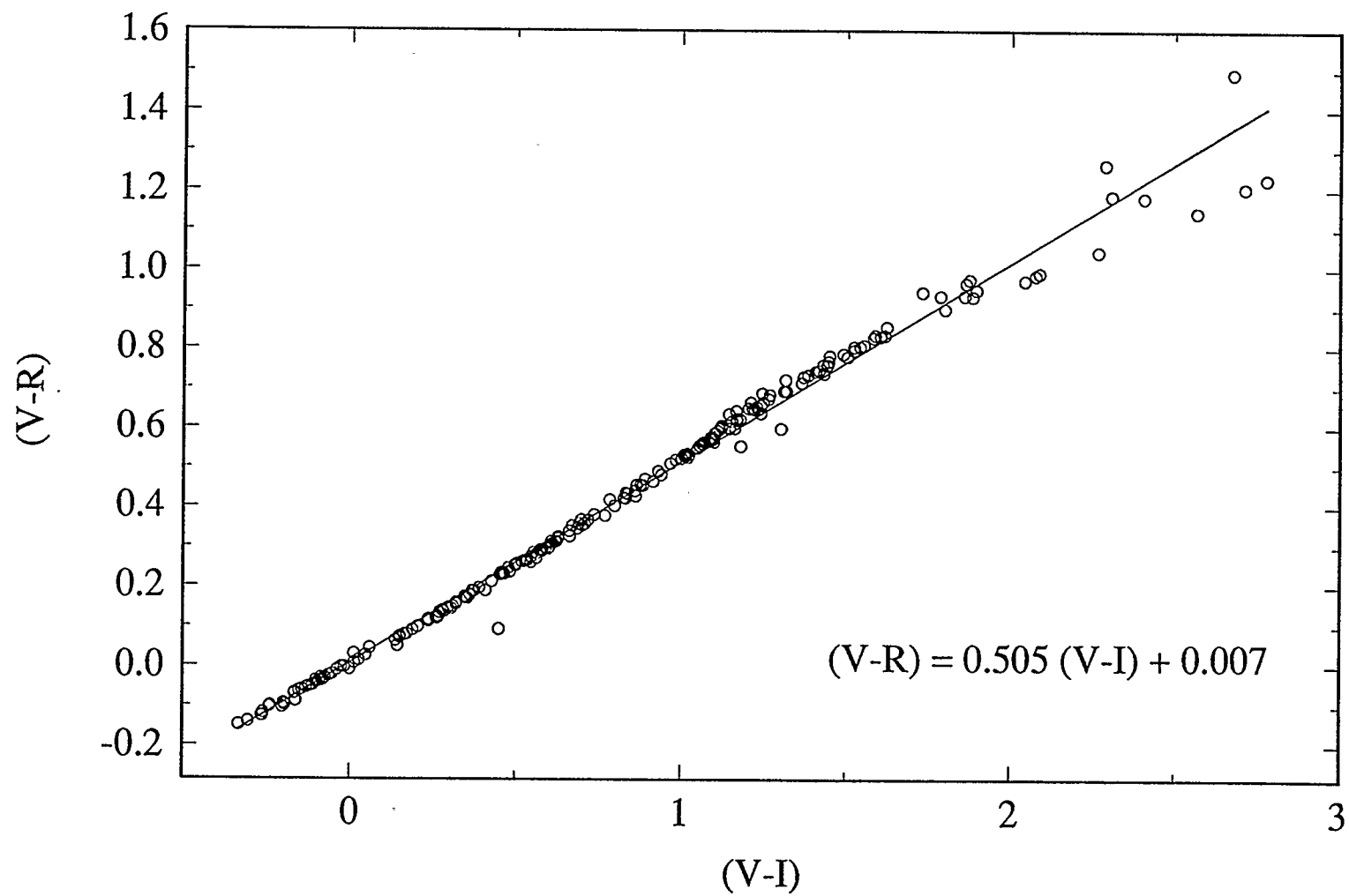
Figure 10 - The determination of the relationship between (V-R)$_J$ and (V-I)$_{JC}$.

If an initial difference between the V and I luminosities or between primary and secondary temperatures was used, it resulted from a guess as the models were expected to quickly move to reasonable values. The normalized luminosity of the secondary star is constrained in WD by the values of other parameters and hence is not determined directly by the user. The initial values for Ω were based on values from systems with similar light curves.

The modelling of the W UMa stars was well underway before the Algol-type system was attempted. By then, experience had demonstrated the efficiency of the simplex program such that the lack of detailed spectral information did not pose a great impediment. Rough guesses were made for most of the modelled parameters, except for the primary temperature and semimajor axis, which were estimated as per the contact systems. Convergence to reasonable and self-consistent values occurred after only a few simplex runs.

In all cases the eccentricity and the argument of the periastron were held at zero and 90 degrees, respectively, since no compelling evidence for non-circular orbits was seen. Since the data supplied by Lin Yan and Mario Mateo (private communication) were not phased, the phase shift, $\Delta\phi$, was modelled in all cases. Initial estimates for $\Delta\phi$ was visually estimated from the light curves. For effective temperatures above 6000 K, a radiative atmosphere was assumed and gravity darkening coefficients, g_i, were kept constant at 1.00. For effective temperatures below 6000 K, a convective atmosphere was assumed and gravity darkening coefficients were kept at 0.32 after Lucy (1967). Similarly, albedos, A_i, were held at 1.0 and 0.5 for radiative and convective atmospheres respectively. In some instances where modelled temperatures fluctuated around the 6000 K level, the 6000 K division was not rigidly adhered to until temperature convergence, at

which point the gravity darkening coefficients and albedos were changed appropriately. The initial estimates of all these parameters are summarized in Table 3.

TABLE 3
Initial Estimates for Model Parameters

Parameter	V1	V2	V3	V4	V5
$\log(g_1)$	4.40	4.38	4.31	4.4	4.32
$\log(g_2)$	4.36	4.35	4.23	4.3	4.29
a (R_{sun})	2.49	2.57	2.61	4.97	2.75
$\Delta\phi$	0.50	0.37	0.10	0.80	0.80
i	88°	81°	82°	80°	79°
g_1	0.32	1.00	0.32	1.00	0.32
g_2	0.32	0.32	0.32	0.32	0.32
T_1 (K)	5460	6050	4740	6500	5900
T_2 (K)	5300	6050	4700	5000	5900
A_1	0.50	1.00	0.50	1.00	0.50
A_2	0.50	0.50	0.50	0.50	0.50
Ω_1	2.4	2.6	1.9	3.5	2.5
Ω_2	n/a	n/a	n/a	2.8	n/a
q	0.35	0.44	0.17	0.40	0.42
L_1^V	9.03	8.52	10.45	11.00	8.66
L_1^I	9.06	8.52	10.45	10.50	8.70
X_1^{bol}	0.521	0.496	0.538	0.5	0.502
X_1^V	0.650	0.569	0.765	0.6	0.587
X_1^I	0.474	0.411	0.551	0.4	0.425
X_2^{bol}	0.521	0.496	0.538	0.5	0.502
X_2^V	0.650	0.569	0.765	0.6	0.587
X_2^I	0.473	0.411	0.550	0.4	0.425

Before the modelling could begin, the DC input files had to be constructed. There were several concerns. Firstly, the light curves must be converted from magnitudes to normalized light units. This was done using a spreadsheet program and the equation

$$L = \frac{l_i}{l_{max}} = 10^{\left(\frac{m_i - m_{max}}{-2.5}\right)}, \tag{52}$$

where m_{max} is the peak brightness (smallest magnitude) of the light curve. This was determined from the light curve plots by visual inspection. For systems with a clear O'Connell effect[6], the brighter of the two maxima was used.

Secondly, the weights for the data points and light curves had to be determined. Almost all data points were given weights (between 0 and 99) that were inversely proportional to their photometric errors. A few widely divergent points were given zero weight. If modelling with simplex made it clear that more weight was required for certain points to get an acceptable fit, their weight was increased. Usually it is sufficient to increase weights for this reason only temporarily in order to encourage the location of the best minimum—once the search closes in on the solution the weights for these data points can be restored to their normal values. However, it was discovered that the few points comprising the flat bottom of the secondary minimum of the V1 (Figures 7a and 7b) light curves had to be left at triple values or the programs would converge to light curves that were obviously too shallow in the secondary minimum. Normally it is desirable to avoid the arbitrary adjustment of data point weights, but in this instance, the under-sampling of a crucial part of the light curve hindered the determination of an accurate solution. The few points in the secondary minima (V and I curves) play an unusually important role in constraining the system's parameters, and hence required unusually high weights to obtain reasonable results. The light curves are also weighted, allowing higher quality light curves to play a more important role in determining parameters. For the light curves considered here, the qualities of the V and I light curves were approximately equal and so they were

---

[6] Eclipsing binary light curves which exhibit the O'Connell effect have maxima of differing brightnesses. This difference may be due to star spots being distributed unevenly over the stars' surfaces (Davidge & Milone, 1984).

given equal weight, except in the case of V2, which had far fewer points in the I light curve. For this reason, the I light curve was given less weight than the V curve.

Finally, there are several factors related to the operation of the programs. The increments applied to the parameters during partial derivative approximations in WD are set in the first three lines of the standard DC input file. They are also contained in the simplex input file but are obviously not used since simplex does not require partial derivatives. The values used were not changed. The number of grid points into which the model stars are divided is also adjustable. The *grid size integers* are specified for both high and low precision calculations, the latter applying to certain derivatives requiring less precision in order to save computation time. Specifically, these numbers determine the number of latitude rows per hemisphere. The number of longitude rows is scaled with the number of latitude rows and with the approximate sine of the latitude. The selected high and low precision grid size integers were 30 and 15, respectively, for both stars.

Once the input files were constructed, the modelling could begin. The general procedure was to perform several simplex runs starting at or near the region of parameter space suggested by the initial estimates. The final location for the converged simplex (*i.e.*, the average of the vertices of the final simplex) was then used as the starting place of a new run if the fit corresponding to that location in parameter space was comparable (within $\Delta\sigma \approx 0.015$) to the best runs up to that point. This process was repeated for each promising simplex location until the final location of the simplex did not migrate from run to run. Generally, no more that three runs were required to meet this condition. At this point, if more than one minimum had been found, it was clear which was the best and fine-tuning with WD could begin. To this end, several iterations of DC were applied until it became clear that either the best minimum had been found or that further searching was required. If convergence seemed to be not imminent in the WD fine-tuning, further

simplex runs were employed, often beginning with parameters suggested by the main WD correction set. This proved often to be a successful strategy. For parameters that generally are not strongly determined, such as inclination, several simplex runs were started with a range of values to search for better values that might not otherwise be found due to very shallow gradients along those axes in parameter space. Thus the simplex routine provided a useful tool both for establishing the current region of parameter space and for exploring alternative regions. In all, combined operations for all stars required over 100 simplex runs and well over 600 DC iterations.

5.0 RESULTS AND DISCUSSION

The best fit solutions for atmosphere flux ratios with [Fe/H]=-0.3, -0.5, and -1.0 were found for each of the binary systems. The two measures used to gauge the goodness-of-fit of the light curve data are the sum of the weighted residuals squared (Σwr^2) and the standard error of a single average weighted point (σ). The best fit (smallest Σwr^2 or σ) was usually obtained with the [Fe/H]=-0.3 models but the significance of this should not be overestimated. The modelling was initially done using [Fe/H]=-0.3 stellar atmospheres and once the solution had been found or nearly found, the other metallicities were tested. Usually only a few iterations were required to converge to an acceptable solution for the other metallicities, although in some cases further exploration was conducted. Therefore, the [Fe/H]=-0.5 and -1.0 models may not be as optimized as the first model attempted. The best-fit model light curves are shown with the observed light curves (in normalized light units) in Figures 11a through 11j. The small differences in the final solutions due to different metallicities is not large enough to produce discernibly different light curves and so only one set of V and I curves per system is shown. The predicted radial velocity curves are also included (Figures 12a through 12e) as an aid to, and test of, future observations. Using the modelling results, the absolute parameters of each system were calculated as follows.

While the semi-major axes are listed as model parameters, they in fact play a very small role in models of systems for which radial velocity data are not available. All parameters that are dependent on the scale of the system, such as the radii, are expressed in units of the semi-major axis. Consequently, any change to the semi-major axis of a model will affect the light curves only by virtue of slight changes in the limb darkening coefficients and model atmosphere flux, which are surface gravity dependent. It is
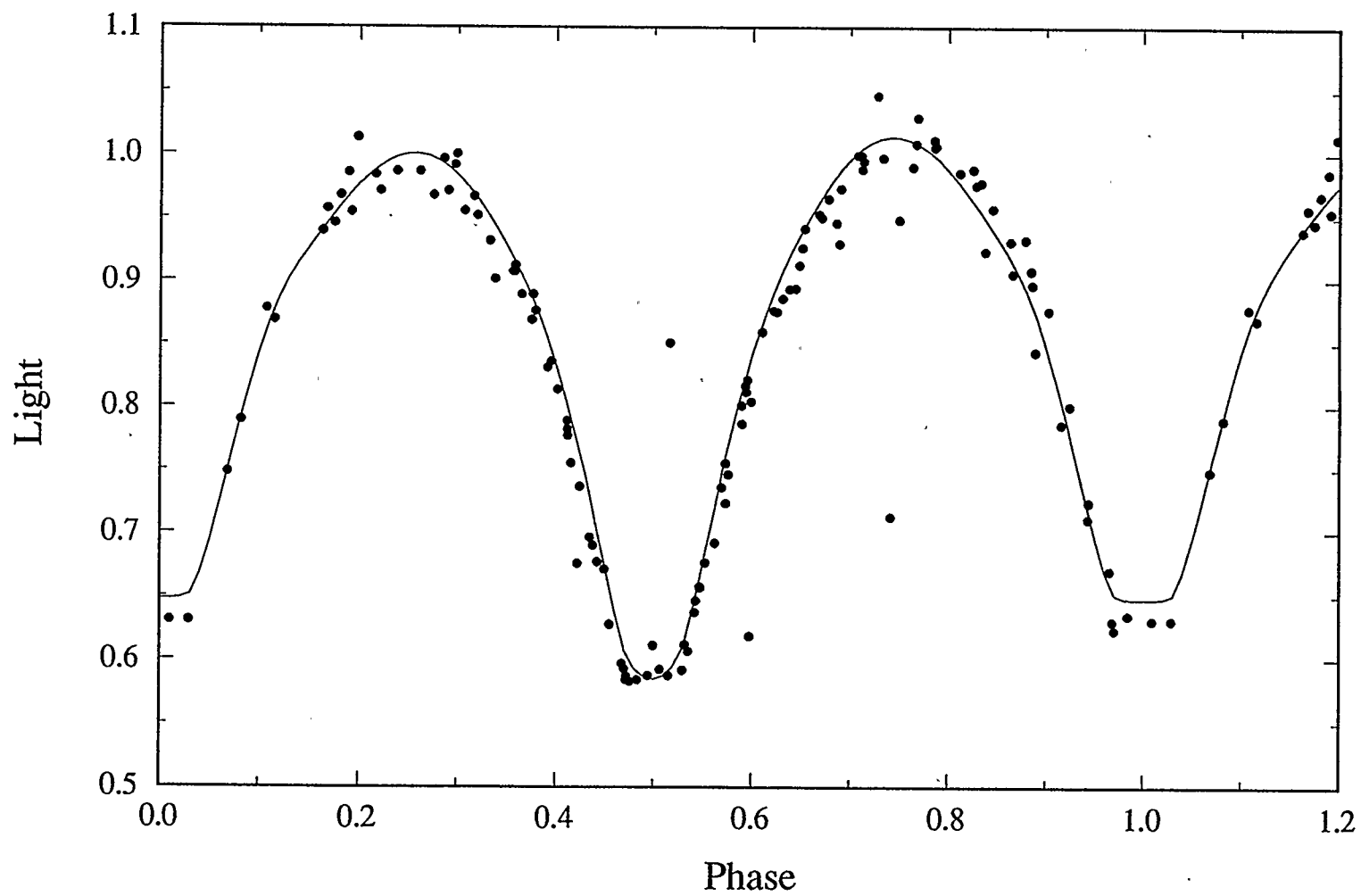
Figure 11a - The observed and model light curves for V1 in the Johnson V passband.
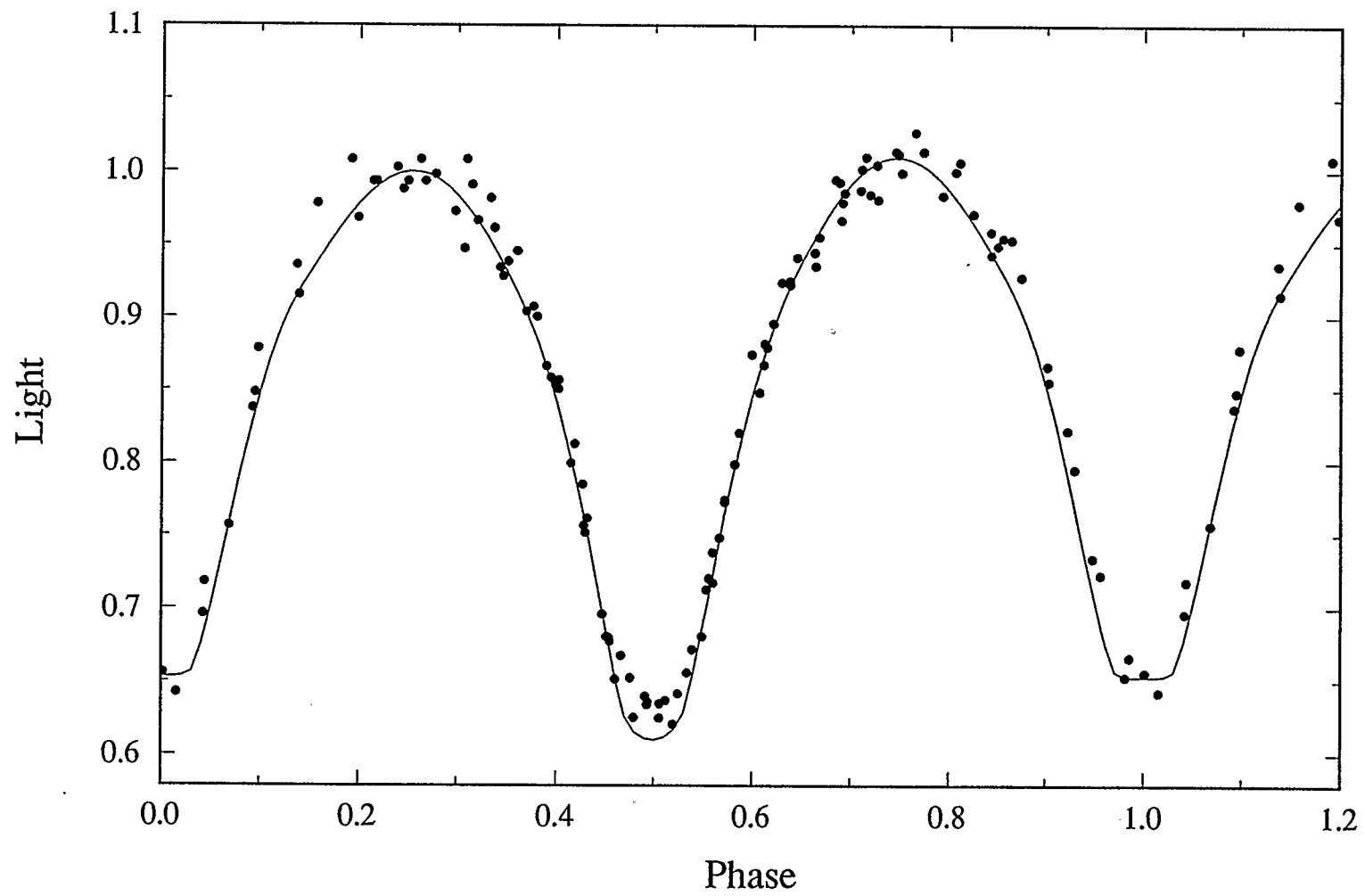
Figure 11b - The observed and model light curves for V1 in the Cousins I passband.
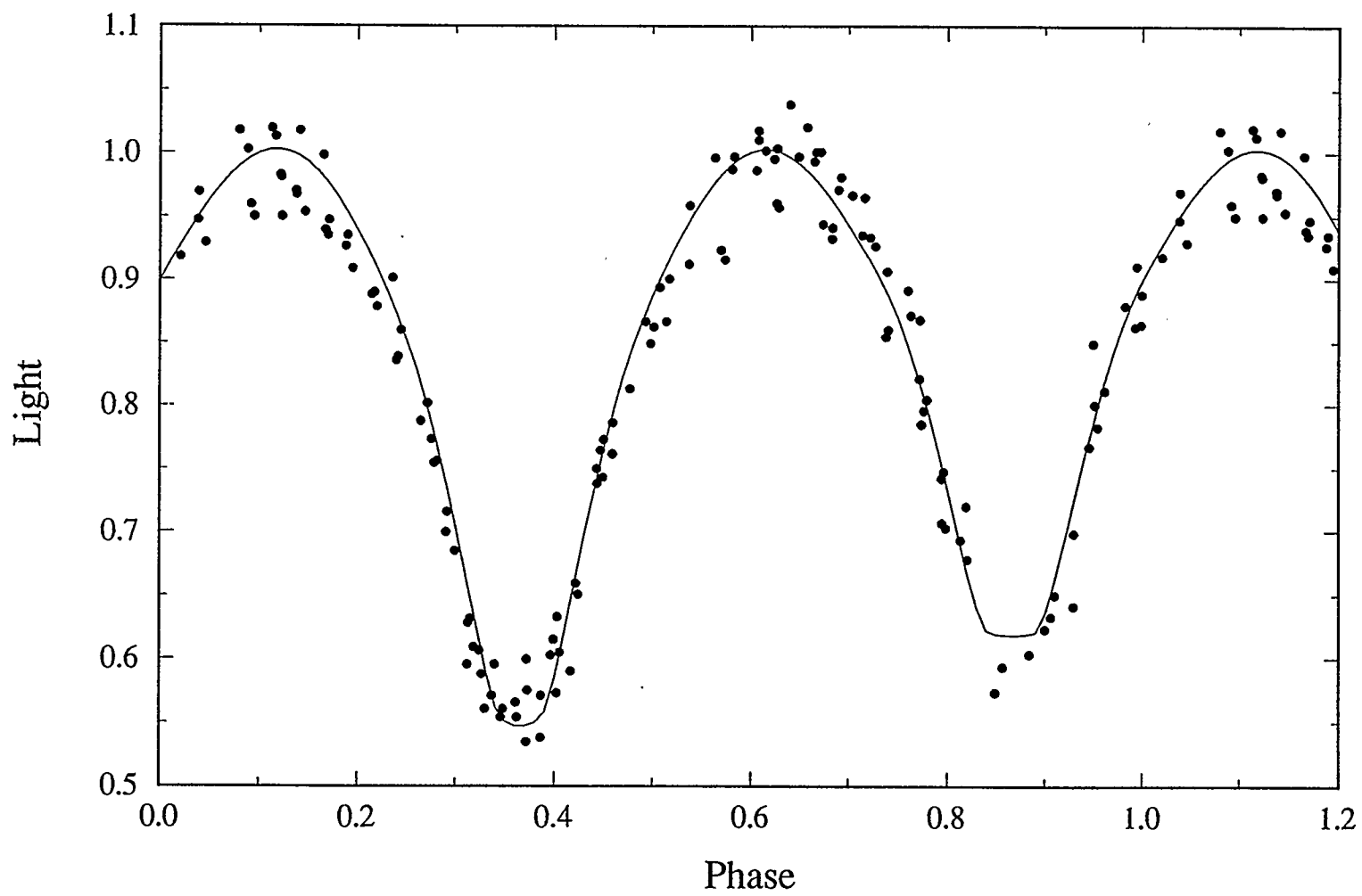
Figure 11c - The observed and model light curves for V2 in the Johnson V passband.
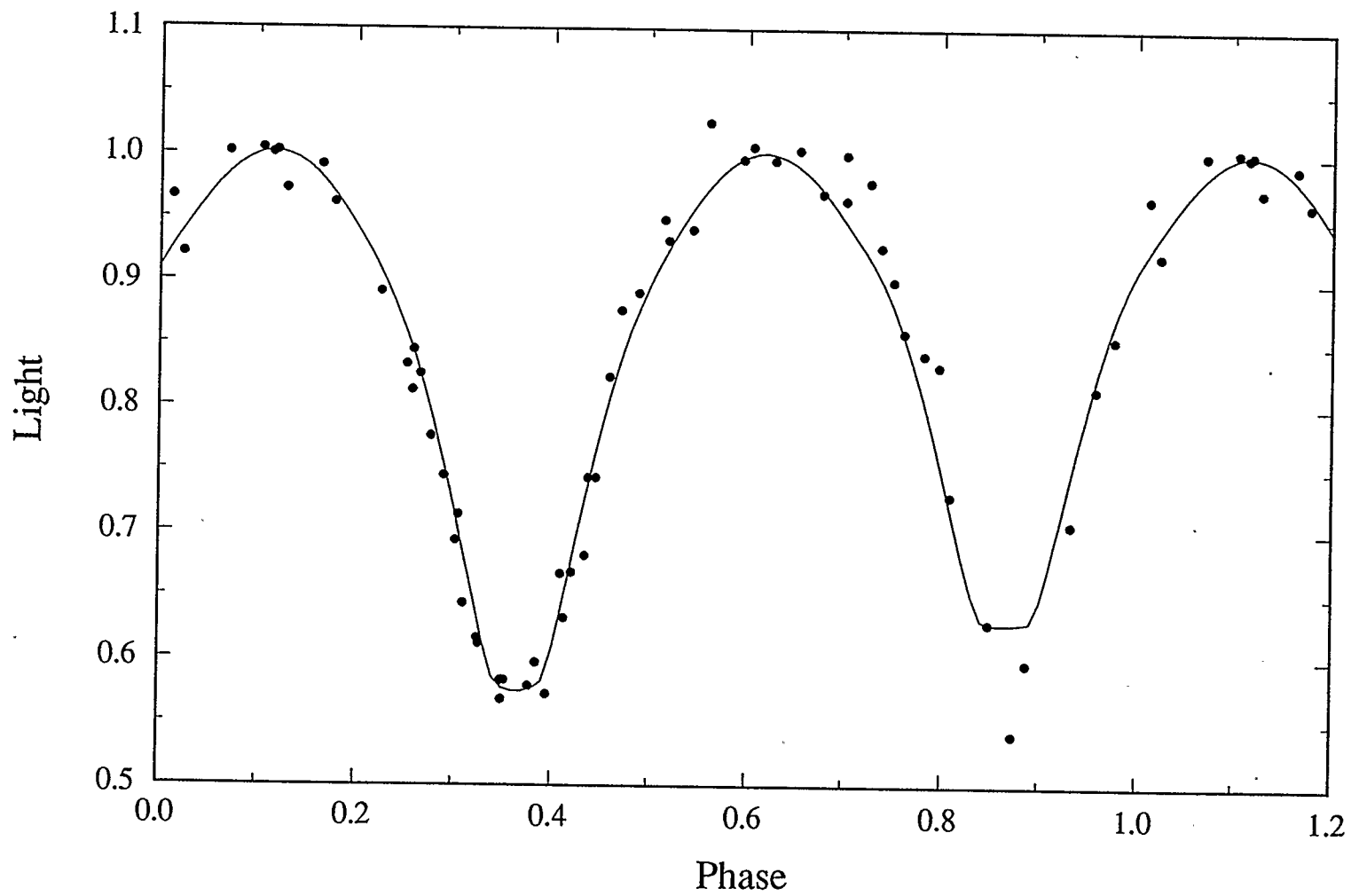
Figure 11d - The observed and model light curves for V2 in the Cousins I passband.
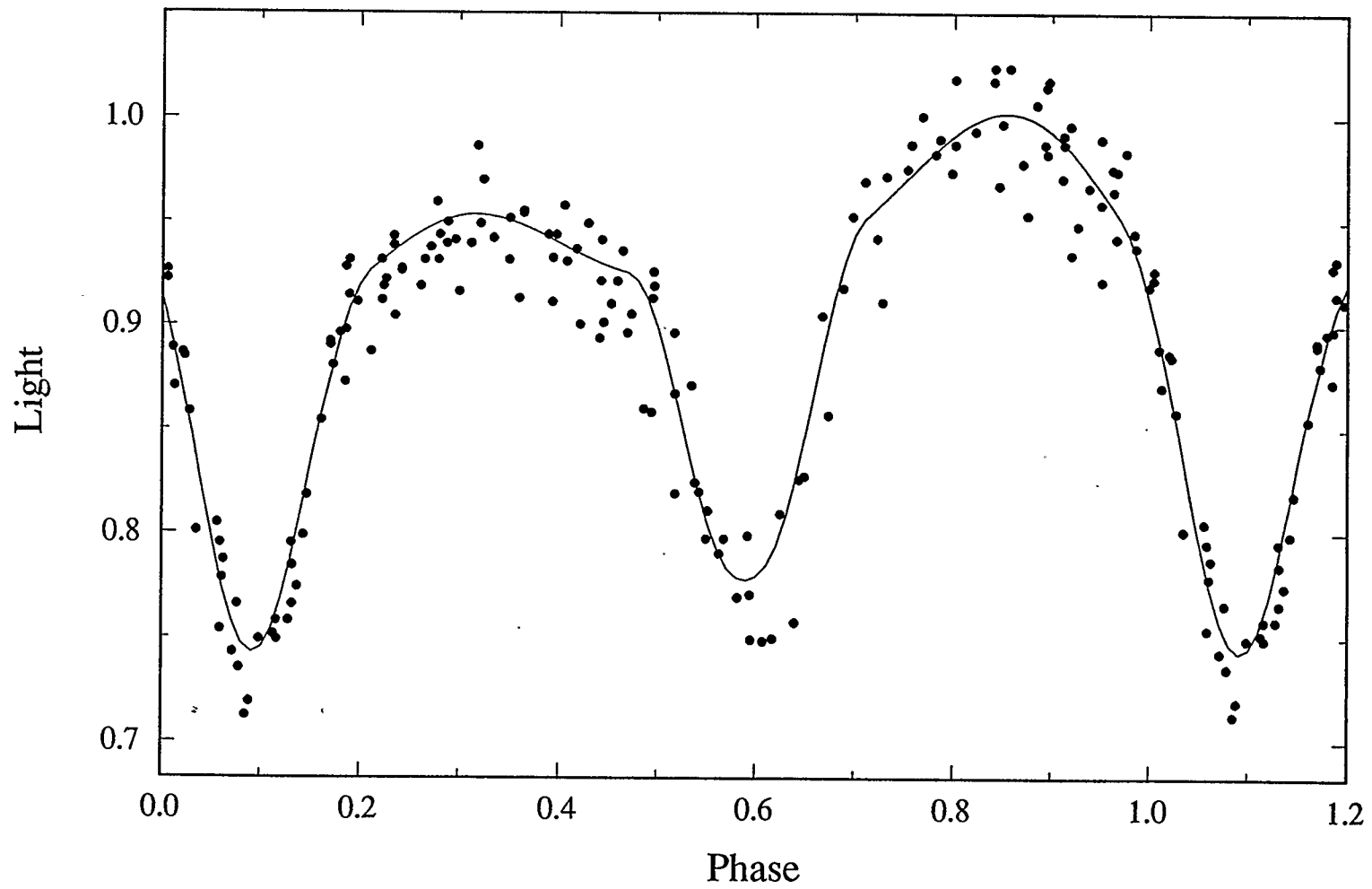
Figure 11e - The observed and model light curves for V3 in the Johnson V passband.
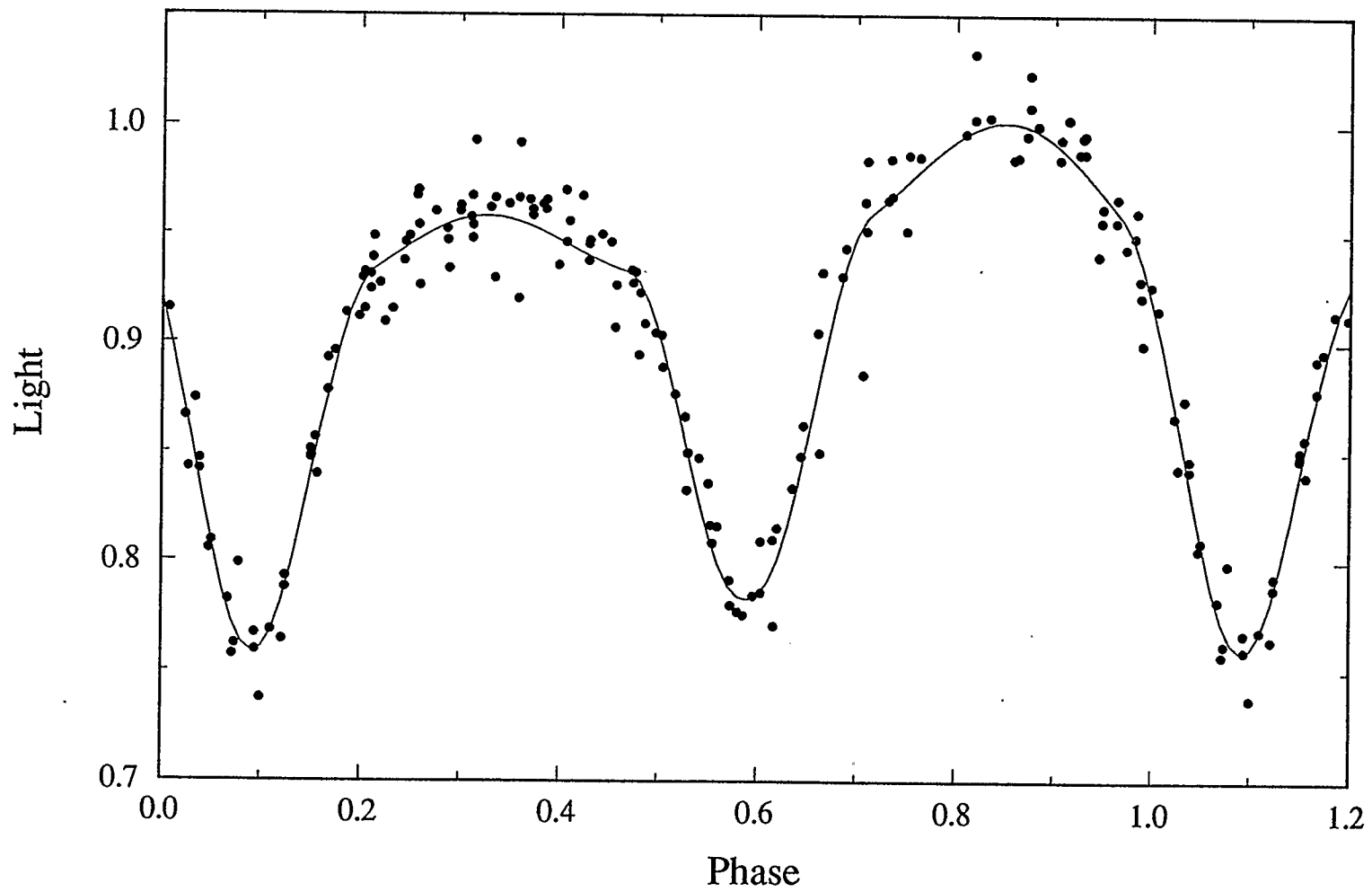
Figure 11f - The observed and model light curves for V3 in the Cousins I passband.
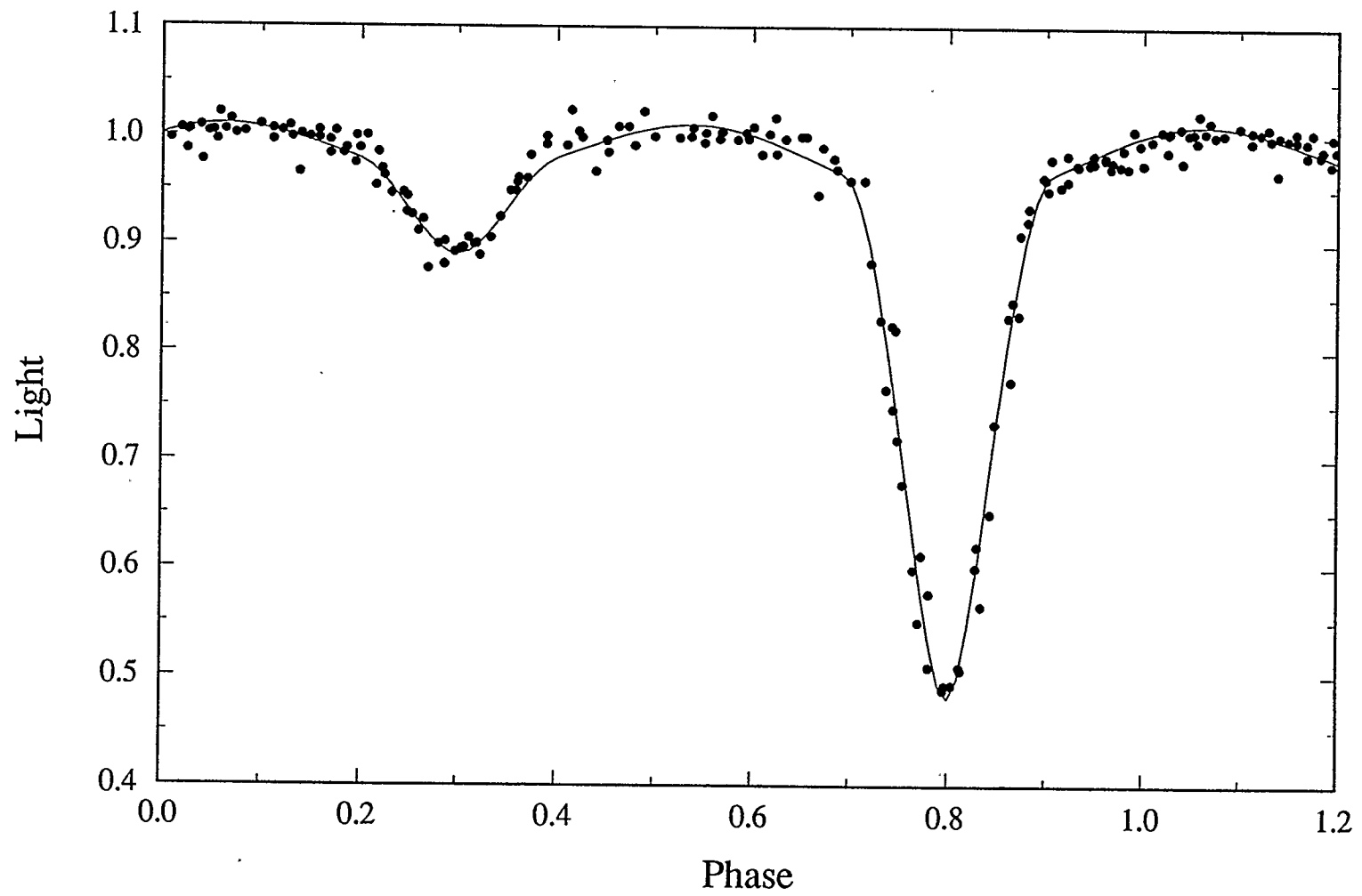
Figure 11g - The observed and model light curves for V4 in the Johnson V passband.
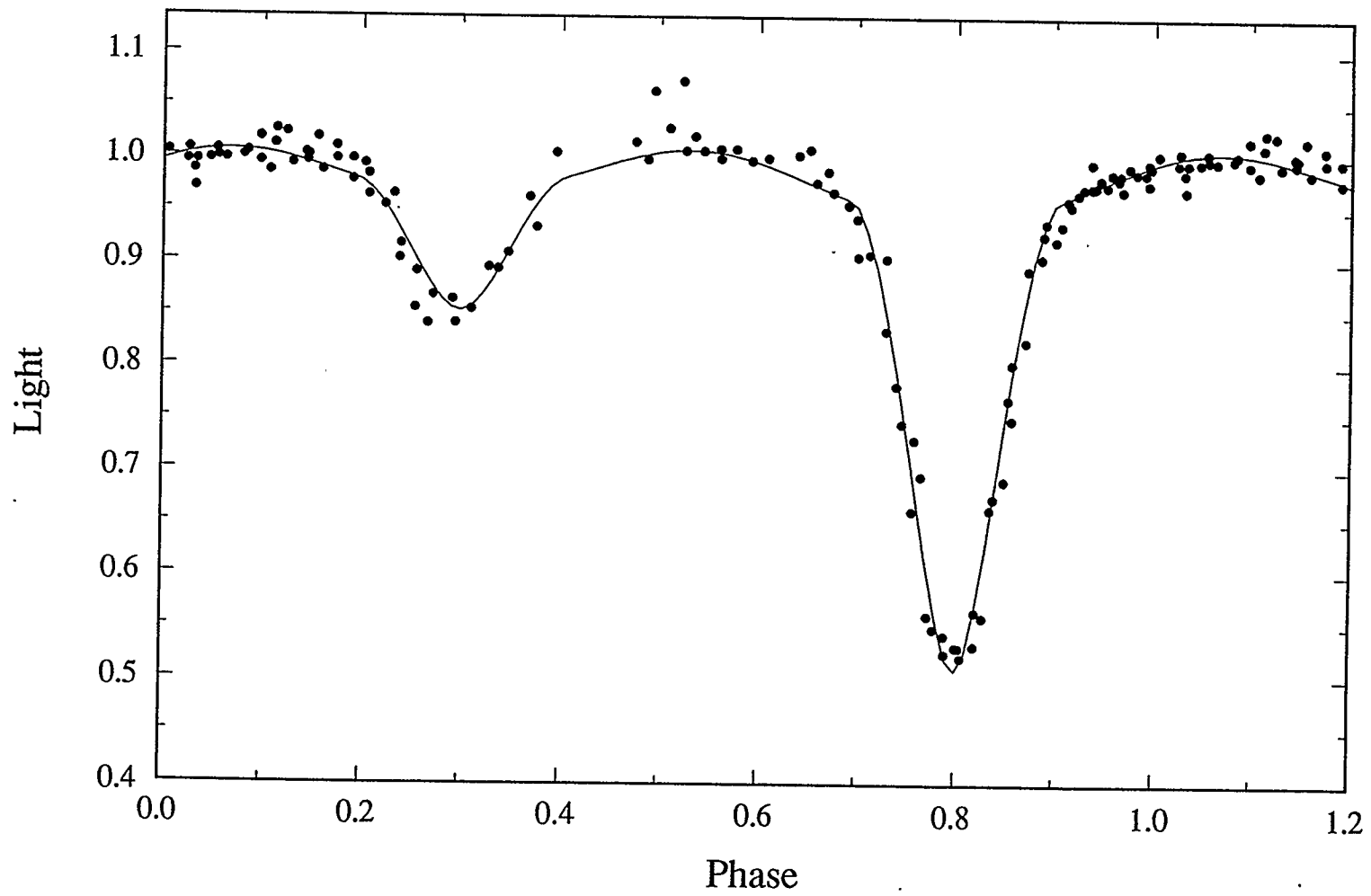
Figure 11h - The observed and model light curves for V4 in the Cousins I passband.
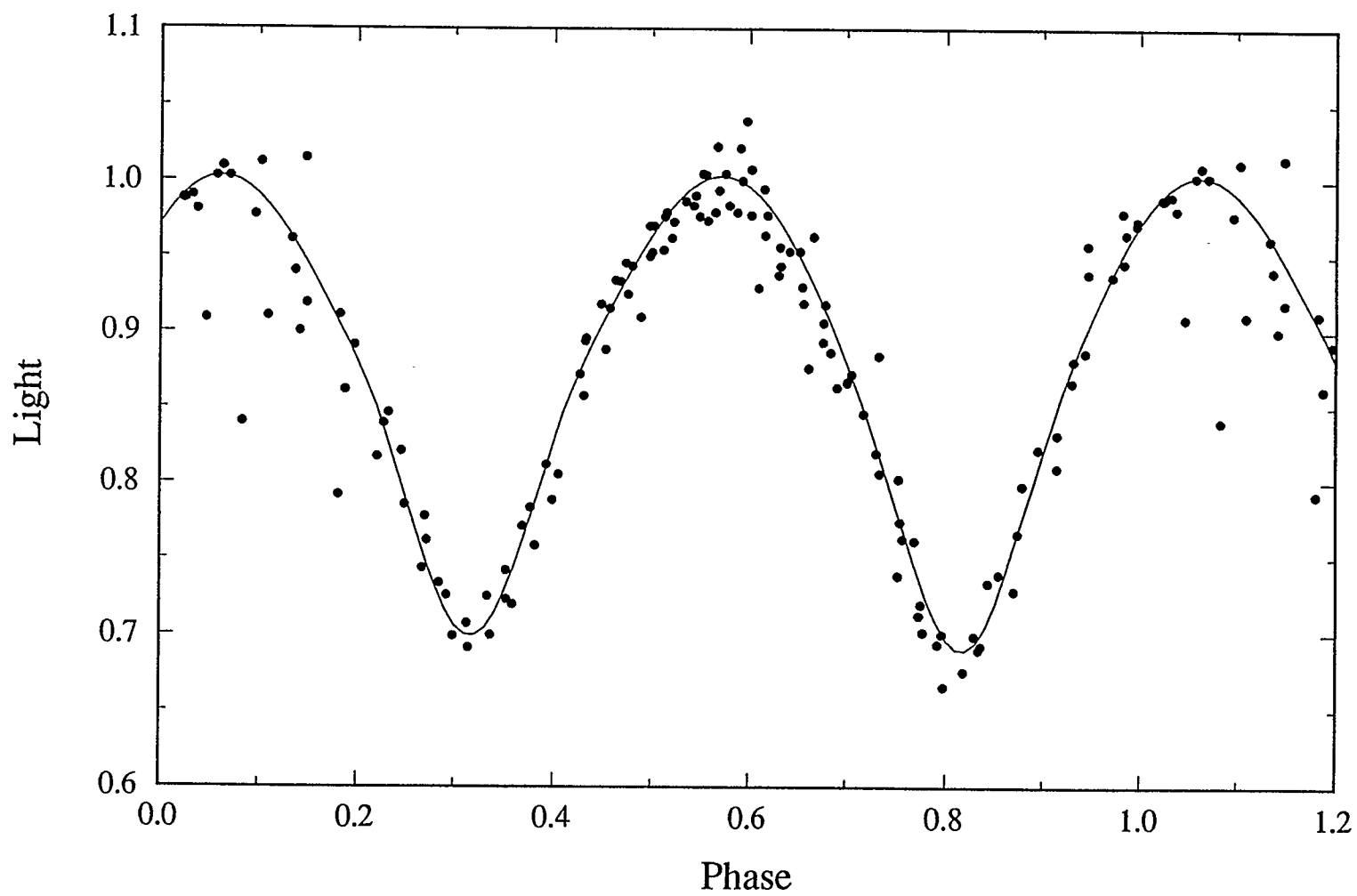
Figure 11i - The observed and model light curves for V5 in the Johnson V passband.
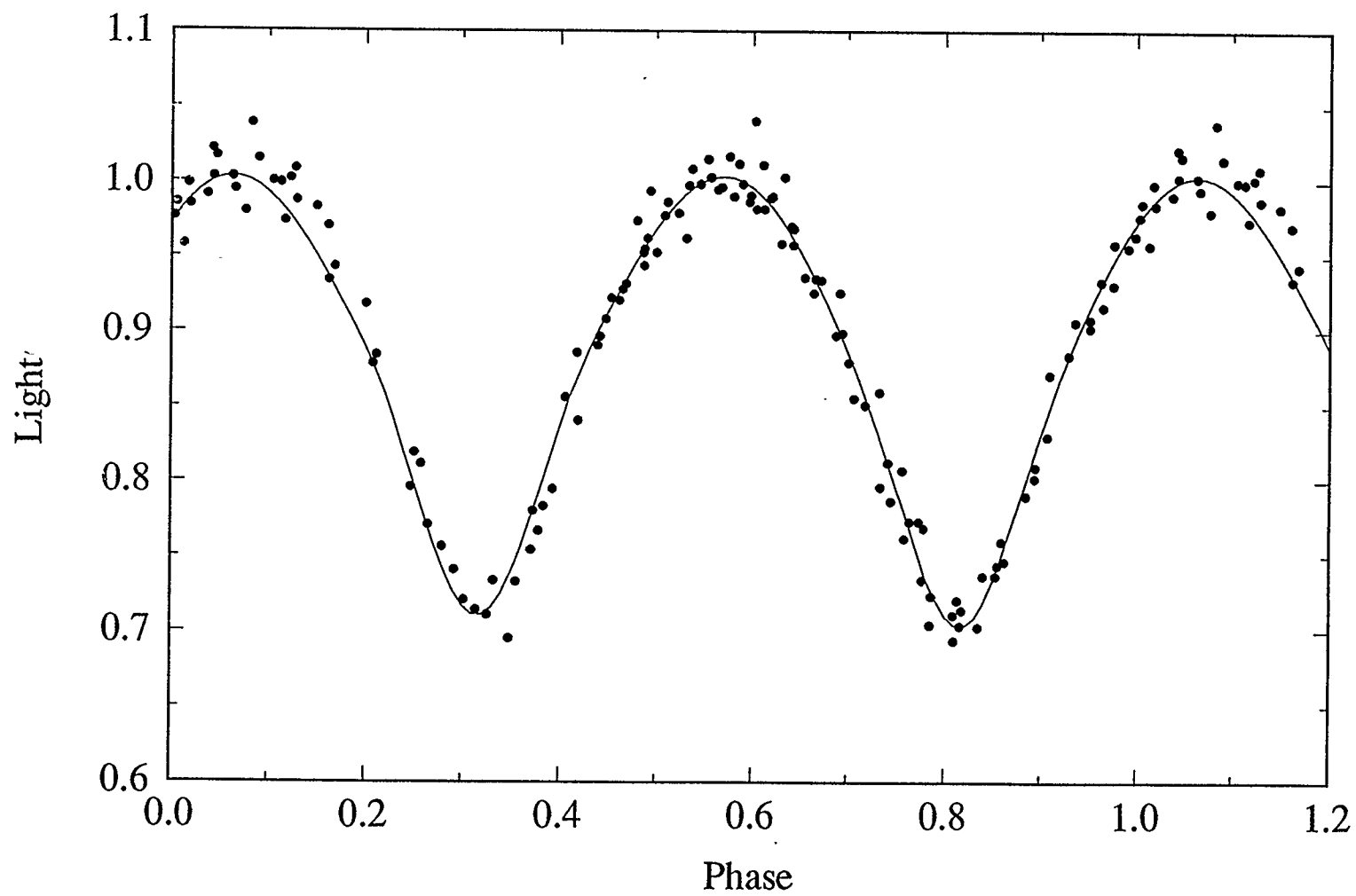
Figure 11j - The observed and model light curves for V5 in the Cousins I passband.
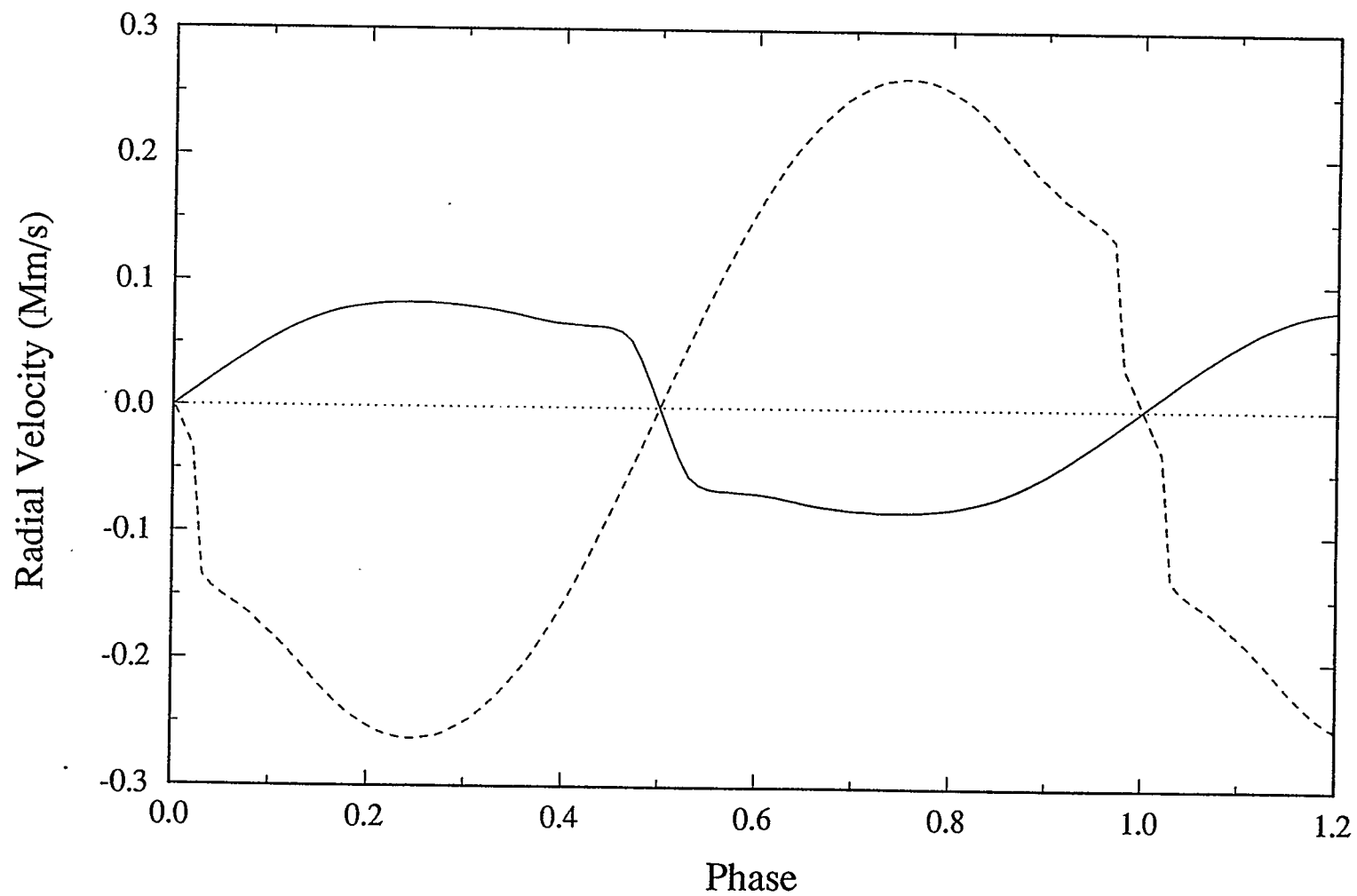
Figure 12a - The predicted radial velocity curves of V1 assuming a semi-major axis of 2.49 solar radii. The solid line represents the primary star; the dashed line represents the secondary.
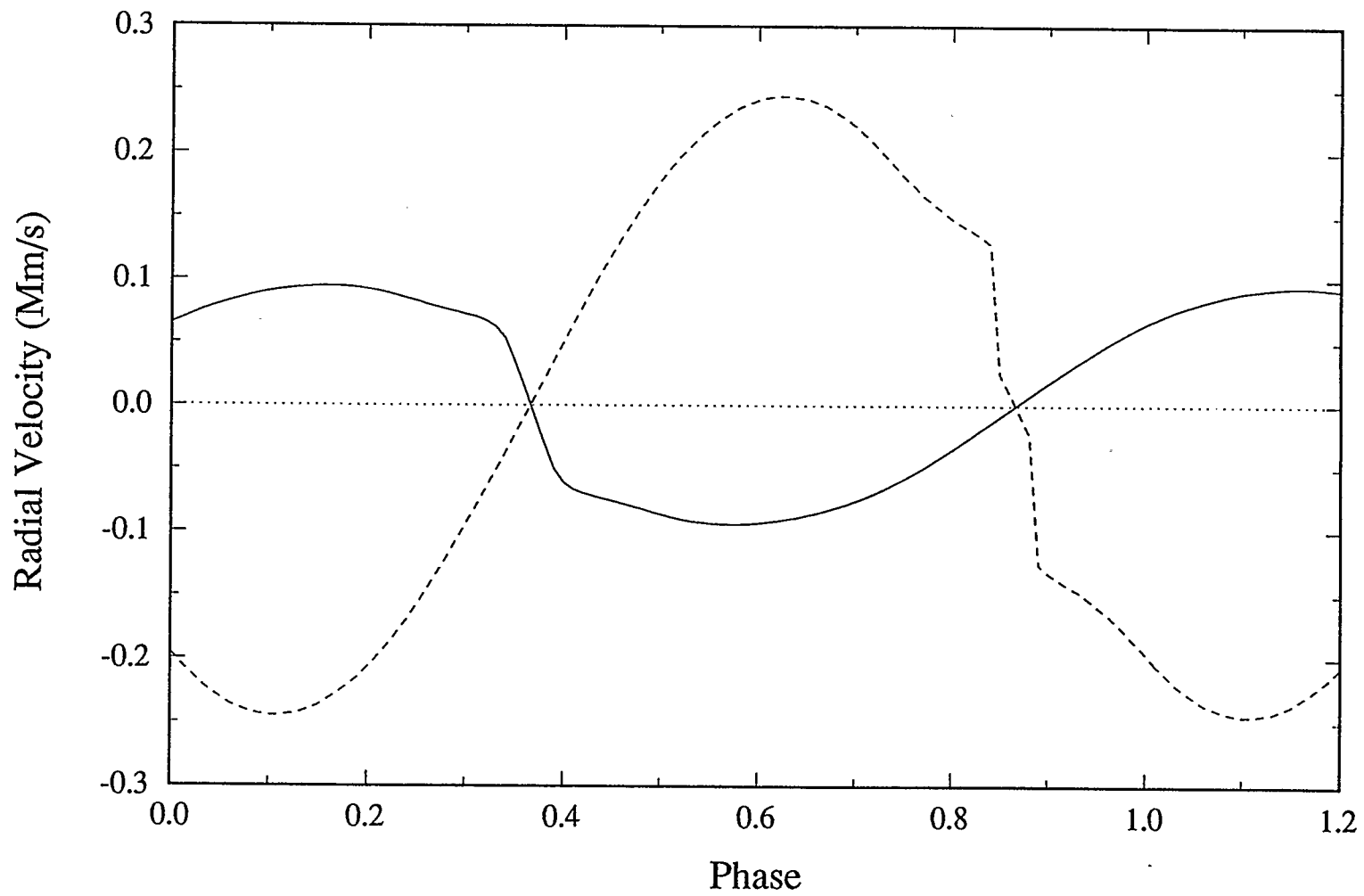
Figure 12b - The predicted radial velocity curves of V2 assuming a semi-major axis of 2.57 solar radii. The solid line represents the primary star; the dashed line represents the secondary.
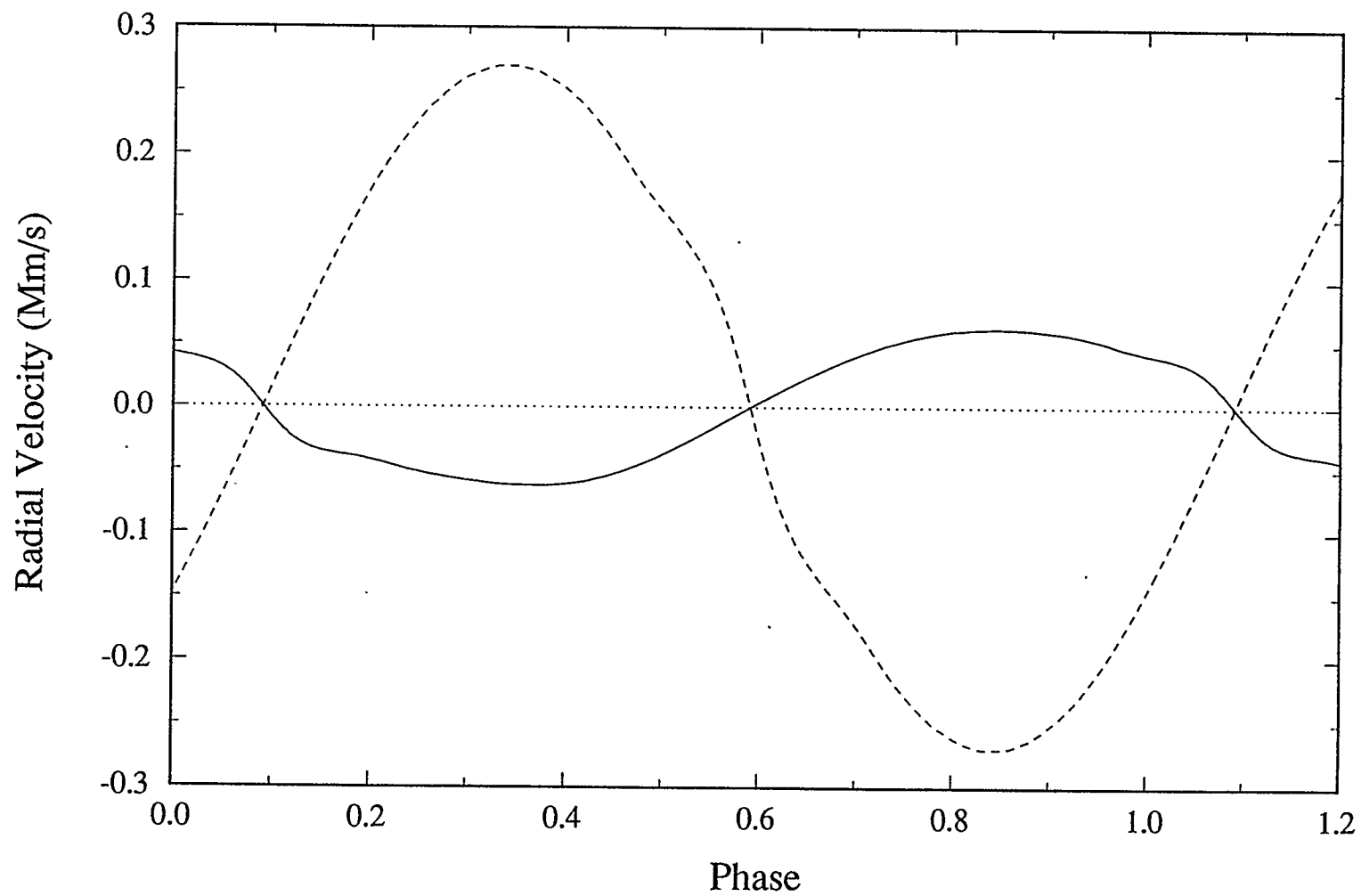
Figure 12c - The predicted radial velocity curves of V3 assuming a semi-major axis of 2.61 solar radii. The solid line represents the primary star; the dashed line represents the secondary.
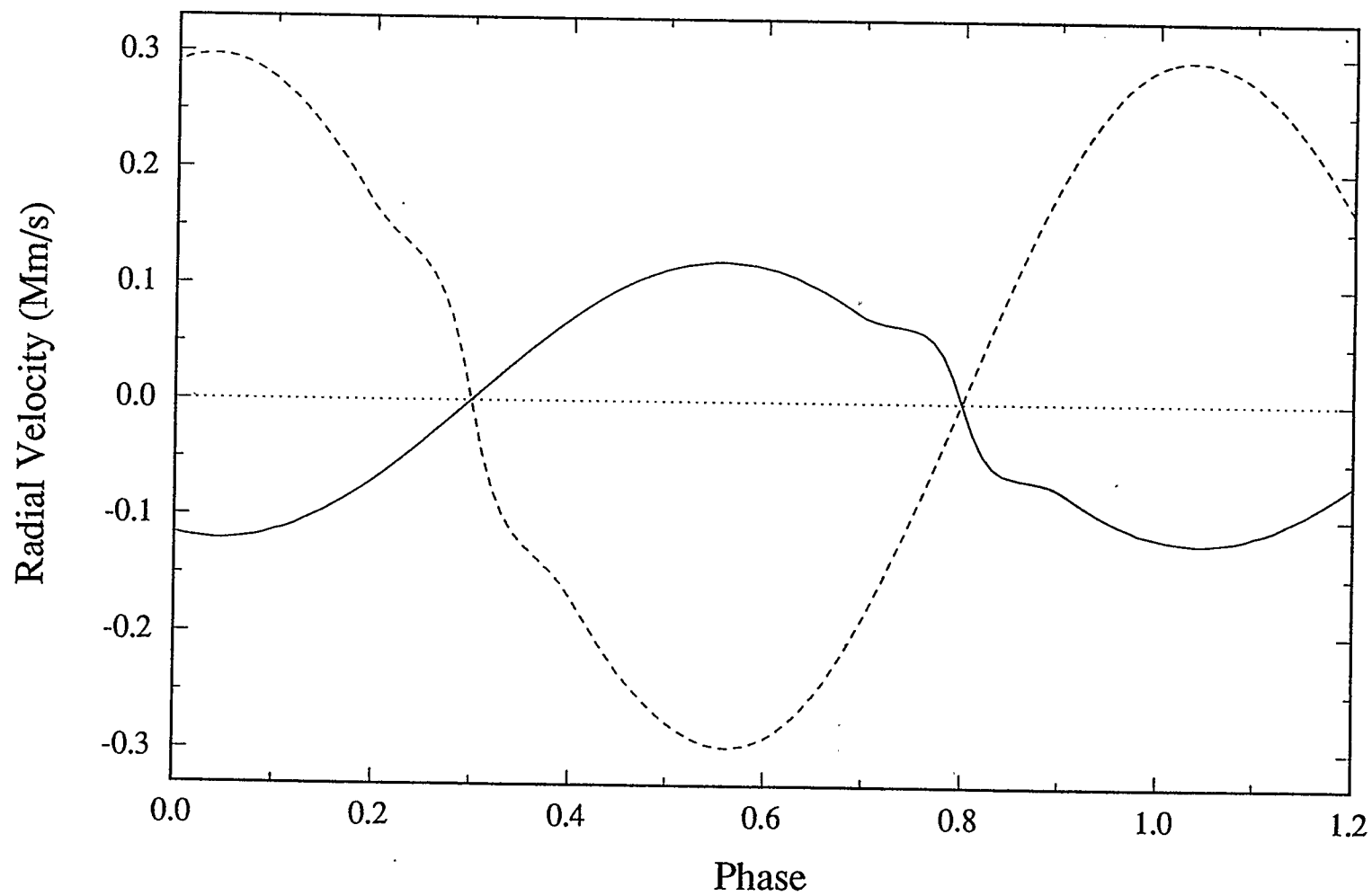
Figure 12d - The predicted radial velocity curves of V4 assuming a semi-major axis of 4.97 solar radii. The solid line represents the primary star; the dashed line represents the secondary.
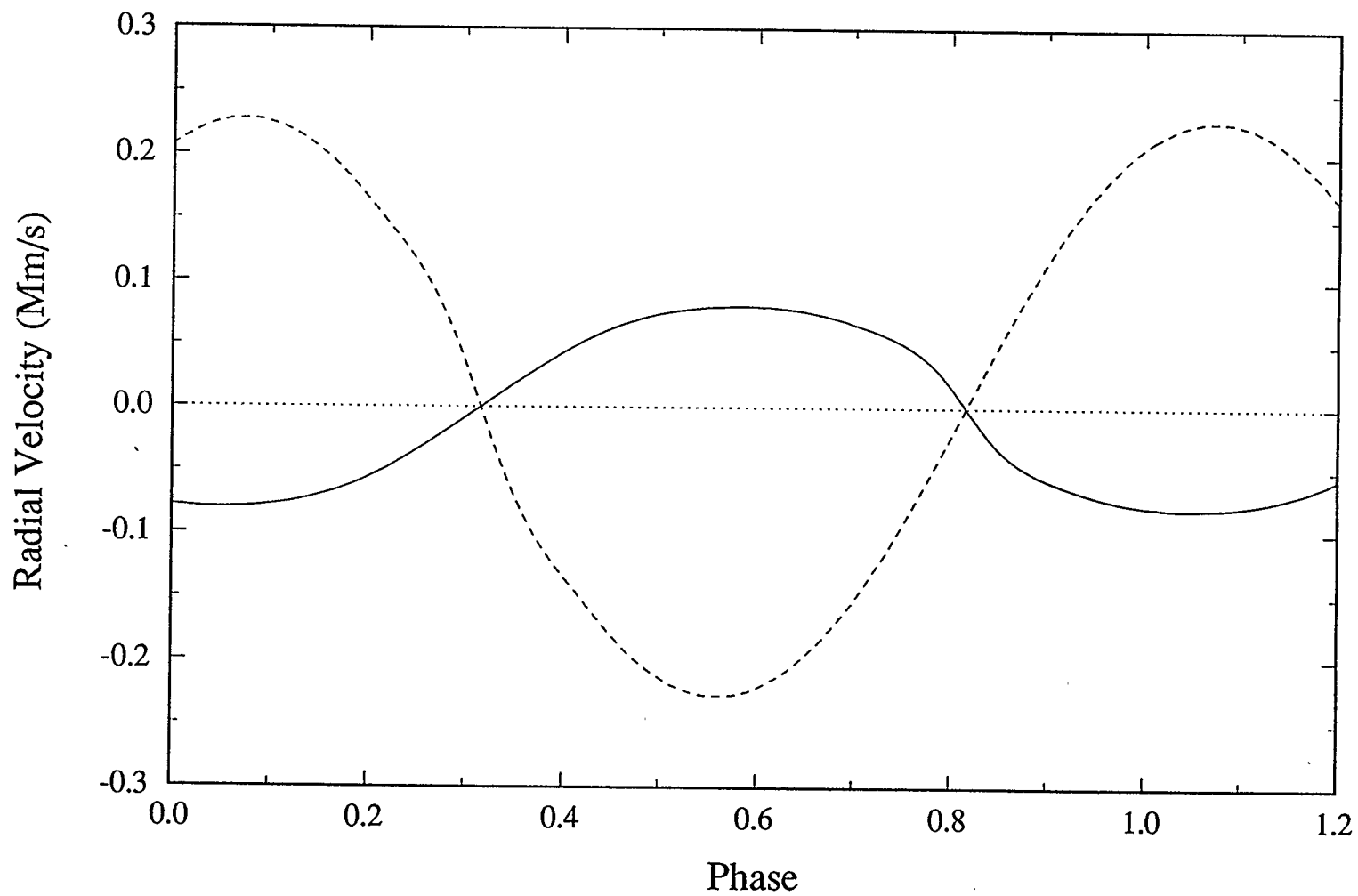
Figure 12e - The predicted radial velocity curves of V5 assuming a semi-major axis of 2.75 solar radii. The solid line represents the primary star; the dashed line represents the secondary.

therefore justifiable to adjust the semi-major axes to allow for more appropriate masses and not expect significantly different light curve solutions. As described, the values of the semi-major axis used in the models were calculated on the assumption that the total mass was equal to 1.7 solar masses. Better information did not become available until after the modelling was nearly complete. Based on the positions of the binary systems on the M71 colour magnitude diagram, Yan & Mateo (1994) gave approximations for the total masses. They assumed the total mass of each system, M_{tot}, to fall between M_{MS} and M_{max}, where M_{MS} is the mass of a single star in M71 that has the same luminosity as the binary, and

$$M_{max} = M_{MS}(1+q).$$

(53)

In this equation, the mass ratio, q, is assumed to be less than one. Their estimates of q, based on the Fourier analysis described by Rucinski (1993), have now been improved through modelling and the total mass estimates were changed accordingly.

While the semi-major axis is not required for light curve modelling, it is crucial to the calculation of absolute parameters. Using the new mass estimates (M was taken to be the mid-point between M_{MS} and M_{max} and ΔM was taken to be half the difference between the extremes), a was calculated for each of the systems using equation (4). These values of a were then used to find the effective radii, R_{eff}, of each binary component:

$$R_{eff} = \left(\frac{S}{4\pi}\right)^{1/2},$$

(54)

where S is the surface area calculated and printed out by WD in units of a^2. The bolometric luminosity, L_{bol}, of each component was then calculated from

$$L_{bol} = 4\pi R_{eff}^2 \sigma T^4.$$

(55)

The absolute bolometric magnitude of each component was then calculated by means of the expression

$$M_{bol} = M_{\odot}^{bol} - 2.5 \cdot \log\left(L_{bol}\Big/L_{\odot}\right),$$ (56)

where $M_{\odot}^{bol}$ was taken to be 4.76 (Mihalas & Binney 1981). Using bolometric corrections based on the models of VandenBerg & Bell (1985), the absolute visual magnitudes were then found. An uncertainty in the bolometric corrections of 0.05 was assumed based on an uncertainty of 150 K for each effective temperature. The combined absolute visual magnitudes were then found from:

$$M_{both}^{V} = M_{1}^{V} - 2.5 \cdot \log\left(1 + 10^{\left(\frac{M_{2}^{V} - M_{1}^{V}}{-2.5}\right)}\right).$$ (57)

The distance moduli (DM) were then calculated. No uncertainty in the reddening-removed magnitudes were specified by Yan & Mateo (1994). Therefore, ΔV_O, the uncertainty in V_O, was calculated to be $0^m.165$ from the expression

$$\Delta V_O = \sqrt{\left(\Delta V\right)^2 + \left(R_V \cdot \Delta E_{(B-V)}\right)^2 + \left(E_{(B-V)} \cdot \Delta R_V\right)^2},$$ (58)

where it was assumed that $\Delta V = 0.05$, $E_{(B-V)} = 0.28 \pm 0.05$ and $R_V = 3.1 \pm 0.1$ (Cardelli *et al.* 1989). In all cases, the different metallicity models were not different enough to affect the calculations of absolute parameters, given the reported uncertainties.

The individual components of the binary systems were placed on the CMD of Hodder *et al.* (1992) (see Figure 13). The $(B-V)_o$ values were found using the effective temperatures of the components and the models of VandenBerg & Bell (1985). An uncertainty of 0.06 was assumed based on the 150 K uncertainty in the effective temperatures. Combined with an uncertainty of 0.05 in the colour excess (needed because the Hodder *et al.* CMD is not corrected for reddening), the total uncertainty in (B-V) is 0.08. Combining the uncertainties in M_V, DM, R_V, and $E_{(B-V)}$ gave a net uncertainty in V of roughly 0.29. These errors are clearly quite large, especially in the (B-V) direction.
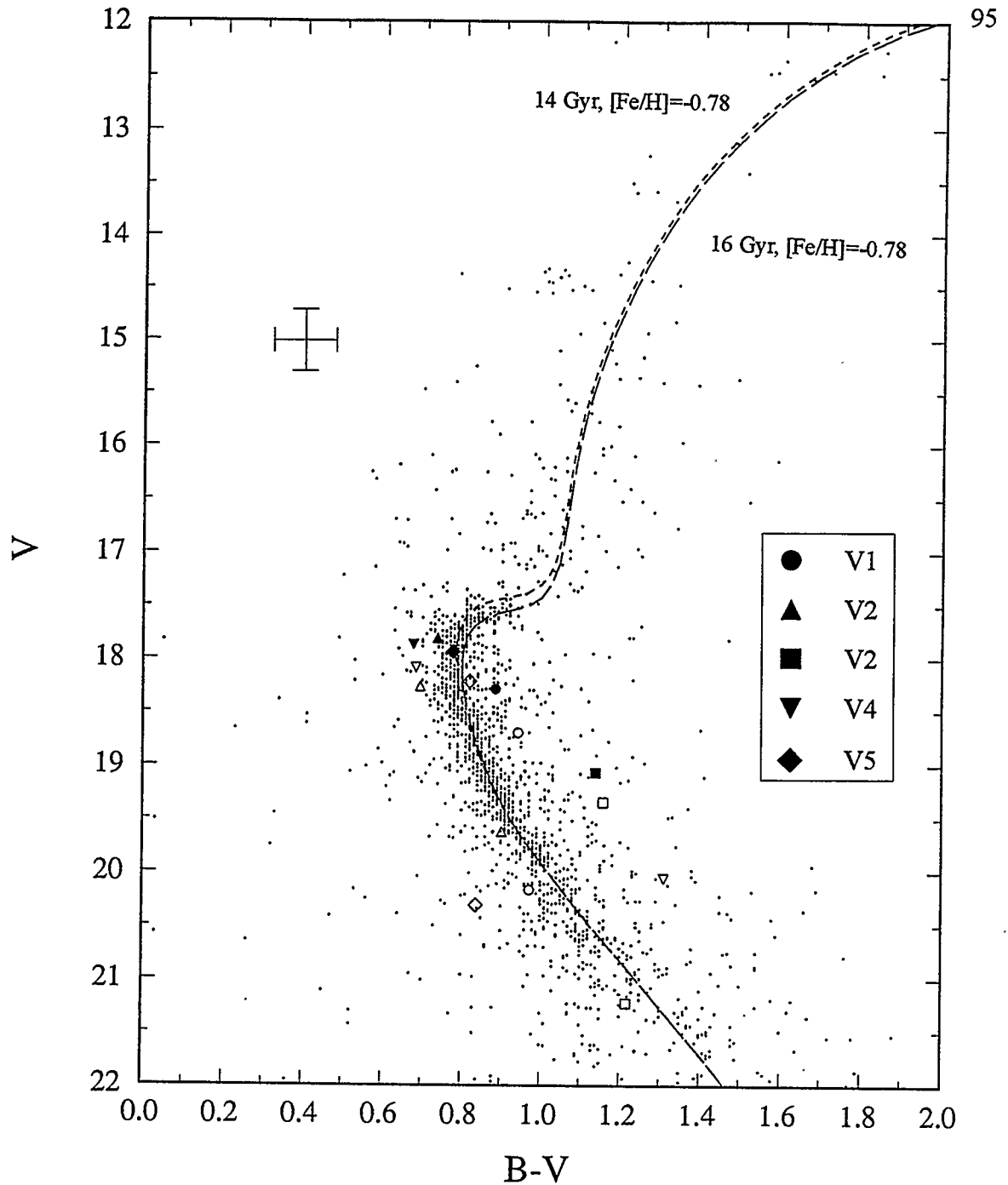
Figure 13 - The uncorrected colour magnitude diagram of M71 using data from Hodder *et al.* (1992). The isochrones are those of Bergbusch & VandenBerg (1992). The positions of the systems and the individual components of each of the systems are indicated. The filled symbols represent the unresolved binary systems. The empty symbols represent the primary and secondary components of the binary systems—the primary being the brighter of the two components. The cross represents the estimated error in the positions of the components. To place the isochrones on the diagram, an additional shift of 0.015 was added to B-V values, as suggested by Hodder *et al.* (1992)

Improvements to the precision of $E_{(B-V)}$ and the $(B-V)_o$ values would greatly reduce this error. The former may be difficult to improve but the latter would be helped significantly with the aid of spectral information.

5.1 V1, V2, and V5

Of the four binaries suspected of being contact systems, only three proved to be in contact. The parameter sets for the best fit solutions with stellar atmosphere flux ratios of [Fe/H]=-0.3, -0.5, and -1.0 for these three systems are given in Tables 4a through 4c. The other W UMa-type system, V3, is most likely a detached system. Of the three, V1 required the addition of a cool spot on the hotter component in order to obtain a satisfactory fit (see Table 5). The reason for this is the fairly obvious O'Connell effect exhibited in the light curves. Semi-detached models were also investigated with simplex but did not fit the observations as well as the contact models. The model radii and surface areas calculated by WD for the contact systems are given in Tables 6a through 6c. The absolute parameters and related quantities for these systems are given in Table 7. Three dimensional representations of the contact systems are shown in Figures 14a through 14c and their Roche lobe configurations are shown in Figure 15.

Using the mass ranges discussed above (see Table 7), the distances to the three systems were calculated. The results for V1, V2, and V5 are 3.99 ± 0.42 kpc, 3.68 ± 0.35 kpc, and 3.57 ± 0.38 kpc respectively. All are comparable with Richer & Fahlman's (1988) 3.6 ± 0.5 kpc.

The positions of the individual components of the contact systems on the M71 CMD can be seen in Figure 13. All of the components, with the exception of the

TABLE 4a
Final Parameter Sets for V1

Parameter	[Fe/H]=-0.3	[Fe/H]=-0.5	[Fe/H]=-1.0
$\log(g_1)$	4.351	4.351	4.351
$\log(g_2)$	4.300	4.300	4.300
a (R_{sun})	2.49	2.49	2.49
$\Delta\phi$	0.5003(4)	0.5003(4)	0.5003(4)
i	84°.51(81)	84°.51(81)	84°.55(78)
g_1	0.32	0.32	0.32
g_2	0.32	0.32	0.32
T_1 (K)	5460	5460	5460
T_2 (K)	5335(15)	5334(15)	5333(15)
A_1	0.50	0.50	0.50
A_2	0.50	0.50	0.50
Ω	2.5010(75)	2.5008(76)	2.5007(75)
q	0.3297(30)	0.3297(30)	0.3297(30)
L_1^V	9.091(36)	9.088(36)	9.085(36)
L_1^I	9.201(31)	9.197(31)	9.198(31)
X_1^{bol}	0.527	0.527	0.527
X_1^V	0.674	0.674	0.674
X_1^I	0.491	0.491	0.492
L_1^V	2.985	2.985	2.991
L_1^I	3.108	3.109	3.110
X_2^{bol}	0.527	0.527	0.527
X_2^V	0.677	0.677	0.677
X_2^I	0.492	0.492	0.492
Σwr^2	0.20002	0.20027	0.20136
σ	0.016498	0.016509	0.016554

Quantities in parentheses are the probable errors calculated by the WD program. They are applies to the least significant digits of the parameter value.

TABLE 4b
Final Parameter Sets for V2

Parameter	[Fe/H]=-0.3	[Fe/H]=-0.5	[Fe/H]=-1.0
$\log(g_1)$	4.331	4.331	4.331
$\log(g_2)$	4.291	4.291	4.291
a (R_{sun})	2.57	2.57	2.57
$\Delta\phi$	0.3663(6)	0.3663(6)	0.3663(6)
i	85°.4(14)	85°.3(15)	85°.6(14)
g_1	1.00	1.00	1.00
g_2	0.32	0.32	0.32
T_1 (K)	6050	6050	6050
T_2 (K)	5586(37)	5585(36)	5581(38)
A_1	1.00	1.00	1.00
A_2	0.50	0.50	0.50
Ω	2.632(16)	2.616(19)	2.615(19)
q	0.3844(80)	0.3800(80)	0.3795(86)
L_1^V	9.212(79)	9.235(81)	9.235(84)
L_1^I	9.131(73)	9.147(74)	9.149(77)
X_1^{bol}	0.495	0.495	0.495
X_1^V	0.572	0.572	0.572
X_1^I	0.411	0.411	0.411
L_1^V	2.693	2.687	2.694
L_1^I	2.915	2.912	2.915
X_2^{bol}	0.517	0.517	0.517
X_2^V	0.637	0.637	0.637
X_2^I	0.464	0.464	0.464
Σwr^2	0.35645	0.35712	0.36850
σ	0.026537	0.026562	0.026613

Quantities in parentheses are the probable errors calculated by the WD program. They are applies to the least significant digits of the parameter value.

<div align="center">

TABLE 4c
Final Parameter Sets for V5

</div>

Parameter	[Fe/H]=-0.3	[Fe/H]=-0.5	[Fe/H]=-1.0
$\log(g_1)$	4.260	4.260	4.260
$\log(g_2)$	4.208	4.208	4.208
a (R_{sun})	2.75	2.75	2.75
$\Delta\phi$	0.8168(6)	0.8168(6)	0.8168(6)
i	69°.22(34)	69°.22(34)	69°.23(34)
g_1	0.32	0.32	0.32
g_2	0.32	0.32	0.32
T_1 (K)	5900	5900	5900
T_2 (K)	5829(32)	5829(33)	5829(33)
A_1	0.50	0.50	0.50
A_2	0.50	0.50	0.50
Ω	2.556(14)	2.555(13)	2.556(13)
q	0.3705(71)	0.3705(72)	0.3705(69)
$L_1{}^V$	8.408(73)	8.407(74)	8.406(72)
$L_1{}^I$	8.489(65)	8.488(65)	8.487(64)
$X_1{}^{bol}$	0.505	0.505	0.505
$X_1{}^V$	0.597	0.597	0.597
$X_1{}^I$	0.433	0.433	0.433
$L_1{}^V$	3.306	3.307	3.310
$L_1{}^I$	3.382	3.384	3.386
$X_2{}^{bol}$	0.505	0.505	0.505
$X_2{}^V$	0.599	0.599	0.599
$X_2{}^I$	0.434	0.434	0.434
Σwr^2	0.25445	0.25435	0.25445
σ	0.018470	0.018467	0.018470

Quantities in parentheses are the probable errors calculated by the WD program. They are applies to the least significant digits of the parameter value.

TABLE 5
Spot Parameters for V1

Parameter	Value
latitude	91°(26)
longitude	81°(15)
size	11°(7)
temp. factor	0.91(23)

Quantities in parentheses are the probable errors calculated by WD.

TABLE 6a
V1 Model Radii and Surface Areas

Quantity	[Fe/H]=-0.3	[Fe/H]=-0.5	[Fe/H]=-1.0
R_1^{pole} (a)	0.4544(11)	0.4544(11)	0.4544(11)
R_1^{side} (a)	0.4888(15)	0.4888(15)	0.4889(15)
R_1^{back} (a)	0.5166(17)	0.5166(17)	0.5167(17)
R_2^{pole} (a)	0.2744(34)	0.2745(34)	0.2745(34)
R_2^{side} (a)	0.2867(41)	0.2868(41)	0.2868(41)
R_2^{back} (a)	0.3244(75)	0.3245(75)	0.3245(75)
S_1 (a^2)	2.996	2.997	2.997
S_2 (a^2)	1.103	1.103	1.103

Quantities in parentheses are the probable errors calculated by the WD program.

TABLE 6b
V2 Model Radii and Surface Areas

Quantity	[Fe/H]=-0.3	[Fe/H]=-0.5	[Fe/H]=-1.0
R_1^{pole} (a)	0.4386(20)	0.4409(24)	0.4411(23)
R_1^{side} (a)	0.4691(25)	0.4720(30)	0.4722(29)
R_1^{back} (a)	0.4966(28)	0.5000(34)	0.5002(33)
R_2^{pole} (a)	0.2823(69)	0.2828(75)	0.2828(79)
R_2^{side} (a)	0.2946(84)	0.2953(91)	0.2953(96)
R_2^{back} (a)	0.329(15)	0.331(16)	0.331(17)
S_1 (a^2)	2.782	2.813	2.816
S_2 (a^2)	1.163	1.168	1.168

Quantities in parentheses are the probable errors calculated by the WD program.

TABLE 6c
V5 Model Radii and Surface Areas

Quantity	[Fe/H]=-0.3	[Fe/H]=-0.5	[Fe/H]=-1.0
R_1^{pole} (a)	0.4509(17)	0.4509(17)	0.4509(16)
R_1^{side} (a)	0.4851(22)	0.4853(21)	0.4852(21)
R_1^{back} (a)	0.5161(24)	0.5162(24)	0.5162(24)
R_2^{pole} (a)	0.2894(66)	0.2895(67)	0.2894(64)
R_2^{side} (a)	0.3035(82)	0.3036(83)	0.3035(80)
R_2^{back} (a)	0.346(16)	0.347(16)	0.347(16)
S_1 (a^2)	2.955	2.956	2.956
S_2 (a^2)	1.226	1.226	1.226

Quantities in parentheses are the probable errors calculated by the WD program.

TABLE 7
Assumed and Calculated Quantities for Contact Systems

Quantity	V1	V2	V5
M_{tot} (M_{sun})	0.7-1.0	0.9-1.3	0.8-1.1
M_1 (M_{sun})	0.63(11)	0.79(14)	0.69(11)
M_2 (M_{sun})	0.21(4)	0.30(6)	0.25(4)
f_1	0.147	0.060	0.271
BC_1	-0.188(50)	-0.104(50)	-0.119(50)
BC_2	-0.222(50)	-0.165(50)	-0.130(50)
$(B-V)_{o,1}$	0.662(60)	0.415(60)	0.539(60)
$(B-V)_{o,2}$	0.692(60)	0.622(60)	0.557(60)
R_1^{eff} (R_{sun})	0.961(7)	1.044(14)	1.094(12)
R_2^{eff} (R_{sun})	0.583(27)	0.675(60)	0.704(85)
L_1^{bol} (L_{sun})	1.12(11)	1.31(14)	1.31(14)
L_2^{bol} (L_{sun})	0.30(4)	0.40(8)	0.19(5)
M_1^{bol}	$4^m.64(11)$	$4^m.46(11)$	$4^m.47(11)$
M_2^{bol}	$6^m.07(16)$	$5^m.76(23)$	$6^m.54(30)$
M_1^{V}	$4^m.83(12)$	$4^m.57(12)$	$4^m.59(12)$
M_2^{V}	$6^m.30(17)$	$5^m.92(23)$	$6^m.67(30)$
DM_O	13.00(18)	12.82(17)	12.76(18)
d (kpc)	3.99(42)	3.68(35)	3.57(38)

Quantities in parentheses are standard errors.

0.25

0.42

0.50

0.75

0.92

1.00
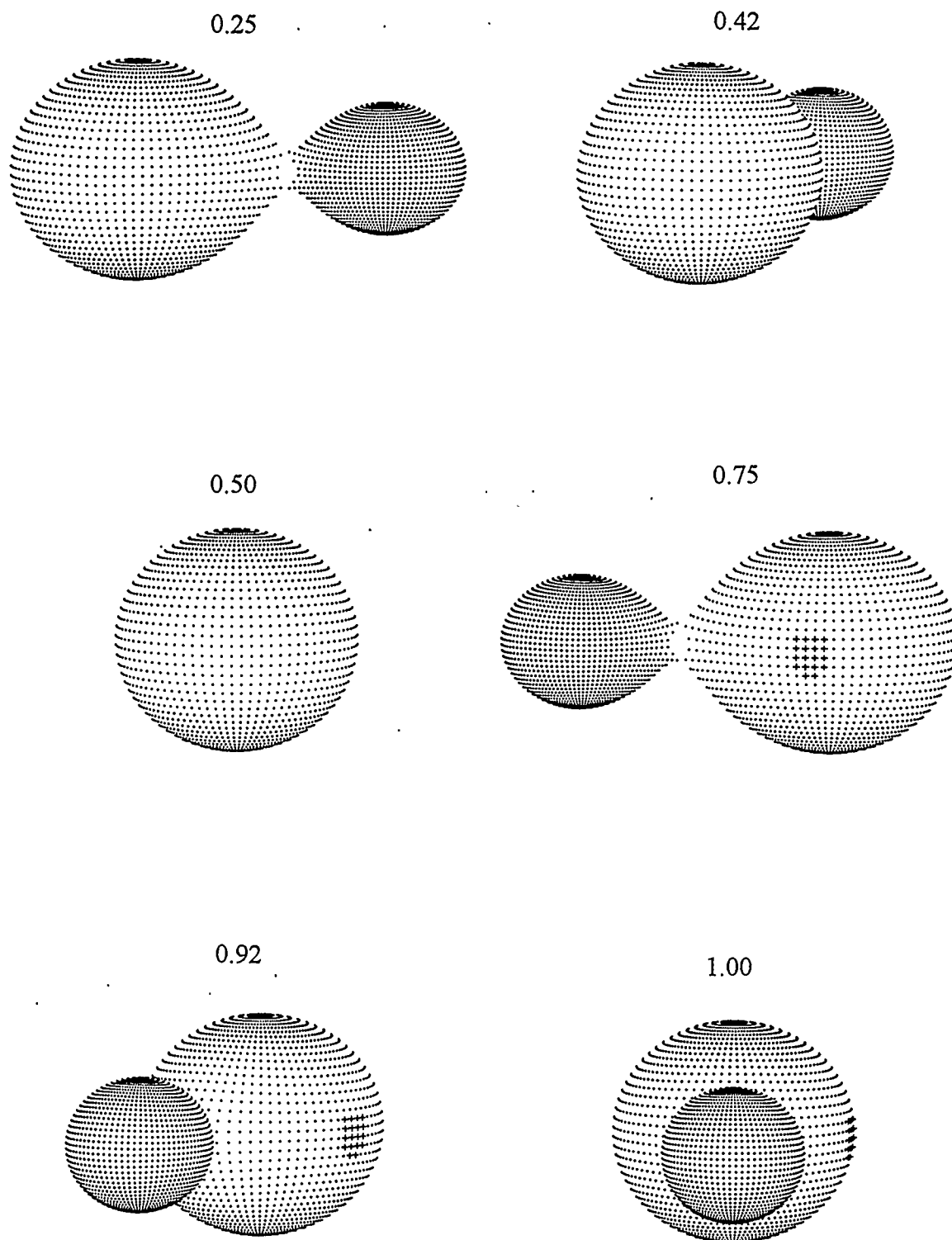
Figure 14a - Three-dimensional representation of the V1 system (see Table 4a for model parameters) produced with D. H. Bradstreet's *Binary Maker II*. The phases represented by each picture are indicated.

0.25　　　　　　　　　　　　　0.42

0.50　　　　　　　　　　　　　0.75

0.92　　　　　　　　　　　　　1.00
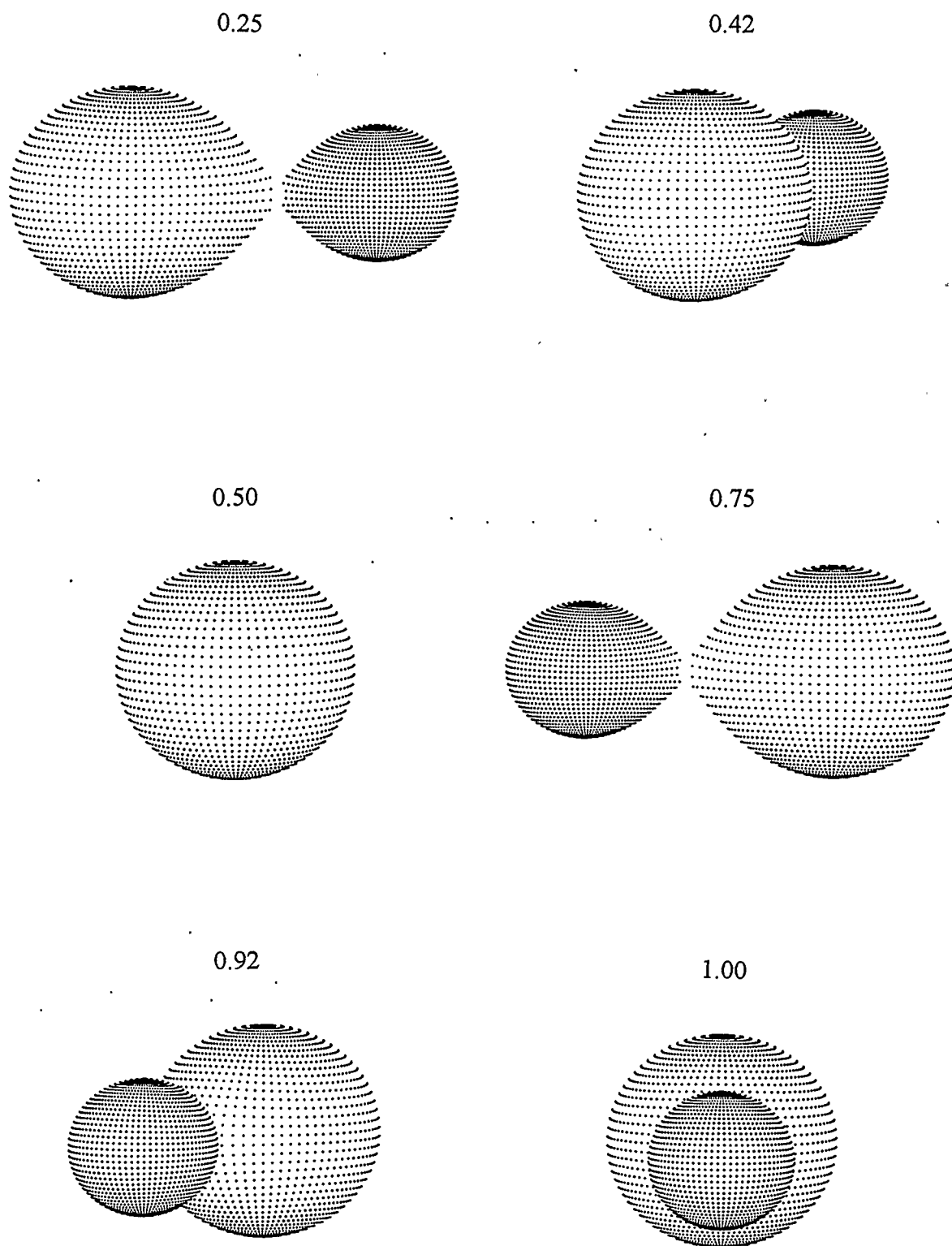
Figure 14b - Three-dimensional representation of the V2 system (see Table 4b for model parameters). The phases represented by each picture are indicated.

0.25

0.42

0.50

0.75

0.92

1.00
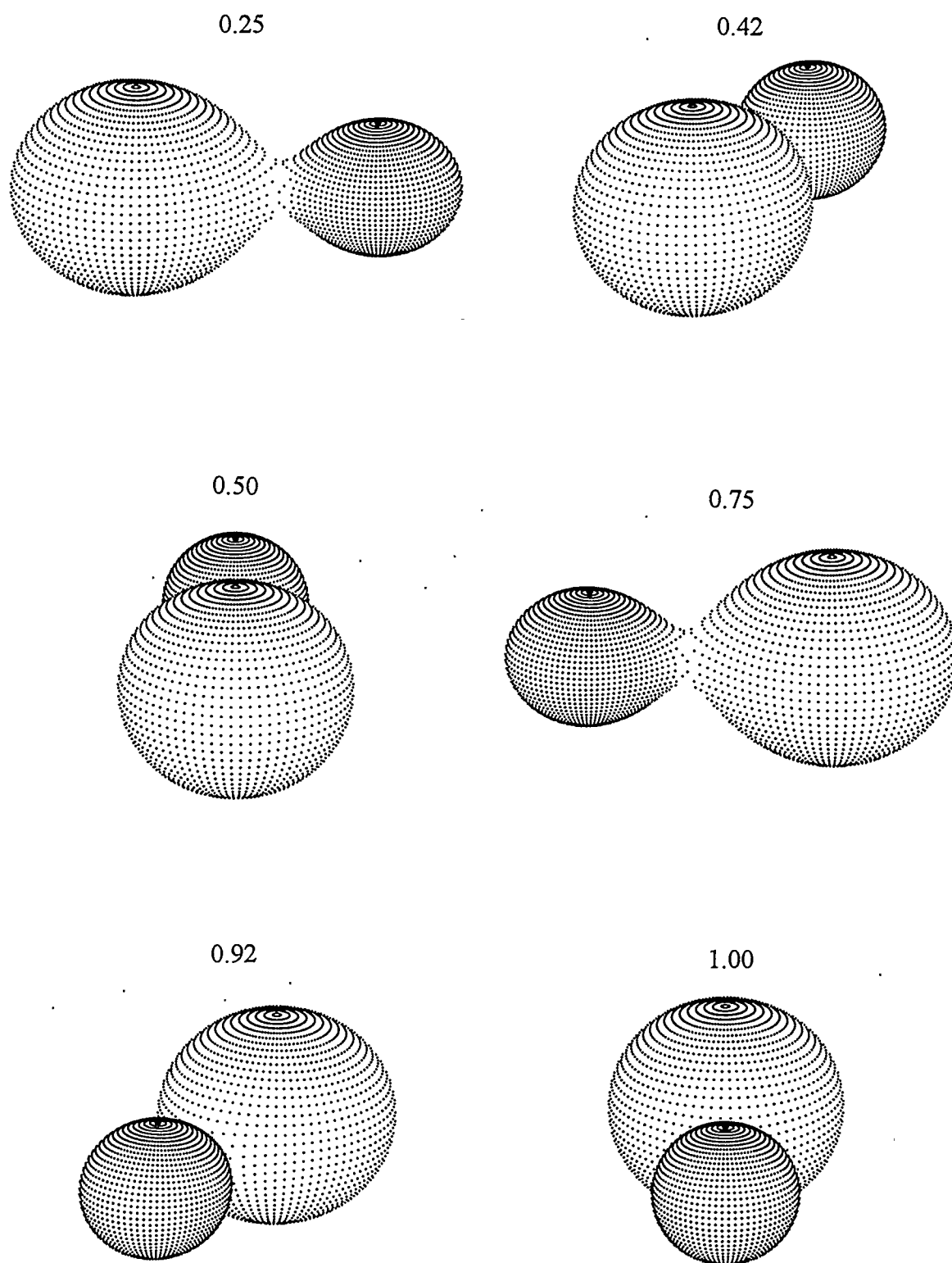
Figure 14c - Three-dimensional representation of the V5 system (see Table 4c for model parameters). The phases represented by each picture are indicated.
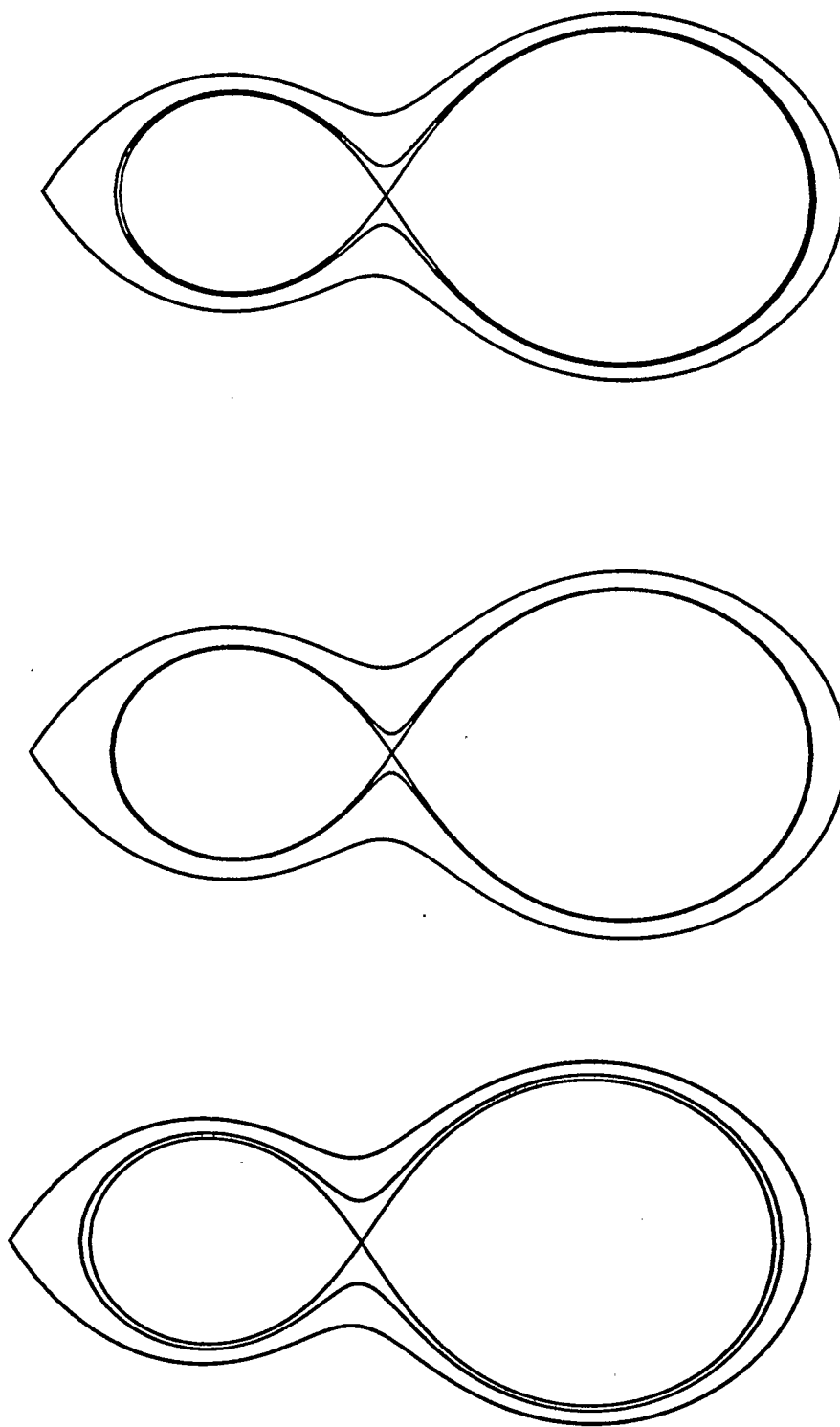
Figure 15 - The Roche lobe configurations of V1, V2, and V5, produced with D. H. Bradstreet's *Binary Maker II*. The less massive star is on the left.

secondary star of V5 are quite close to the main sequence. The primaries are roughly 1.5-2.0 magnitudes brighter than their lower mass companions. They are also consistently bluer than their companions, although none of them is sufficiently blue to be conclusively classified as a blue straggler given the uncertainty of these determinations. Two of the systems (V1 and V5) have their primary components located above the main sequence while their companions are both found below the main sequence. This fact suggests the possibility that the more massive stars acquired mass and luminosity from their companions.

It is interesting to compare these binaries with those found in NGC 5466 by Mateo *et al.* (1990) and modelled by Kallrath *et al.* (1992). In that case, the two contact systems were found to be blue stragglers. Of the M71 contact systems, before being resolved into individual stars, V2 and V5 are very near the main sequence, and V1 is *redward* of the main sequence. This is not surprising given the state of contact of the systems. Kallrath *et al.* found the outer critical surfaces to be nearly filled by the stars, their fill-out factors both being equal to ~0.95. The present work shows V1, V2, and V5 to have fill-out factors of 0.15, 0.06, and 0.27 respectively. The M71 systems are only slightly in contact so that their degree of mutual influence is not expected to be as high as in the case of the NGC 5466 contact binaries.

Rucinski (1994) has proposed that W UMa might be used as standard candles for distance determinations. He has found an empirical relationship between period, colour, and luminosity. Based on B-V colours he finds a linear relation of the form

$$a_{P(BV)} \log P + a_{BV}(B-V) + a_{0(BV)} = M_V$$
$$a_{P(BV)} = -2.44^{+0.70}_{-1.50}$$
$$a_{BV} = +4.20^{+0.29}_{-0.68}$$
$$a_{0(BV)} = +0.23^{+0.30}_{-0.28}$$

(59)

This relation can be tested for the M71 contact systems. The periods and V magnitudes from Table 2b were used, along with $(B-V)_o$ values found from the models of VandenBerg (1985), to find the distance moduli of the three binaries. In determining the uncertainty in DM, the values of the coefficients in equation (59) were chosen such that the maximum range was achieved. The values were found to be 13.69 (+1.01, -1.16), 13.91 (+0.89, -1.09), and 13.92 (+0.90, -1.03) for V1, V2, and V5 respectively. As can be seen from Table 9, the agreement between these values and those derived in the present work is quite poor. Only the two determinations for V1 fell within each other's uncertainty range. However, the fact that the Rucinski values are consistently higher than those listed in Table 9 implies a systematic error possibly due to the transformation between V-I and B-V. Rucinski also determines a relationship using V-I colours:

$$a_{P(VI)} \log P + a_{VI}(V - I_c) + a_{0(VI)} = M_V$$
$$a_{P(VI)} = -4.28^{+1.30}_{-2.84}$$
$$a_{VI} = +3.67^{+0.63}_{-1.27}$$
$$a_{0(VI)} = -0.37^{+0.38}_{-0.35}$$

(60)

If this relationship is used to avoid the colour transformation, the results are in better agreement with the DM determined through modelling: 13.23 (+4.62, -2.16), 13.41 (+4.28, -2.00), and 13.52 (+4.03, -1.90) for V1, V2, and V5 respectively. Obviously, this relationship suffers from an even greater lack of precision than the B-V relationship. This is due to the very small sample size used for its determination: only 3 binaries with V-I colours were available; the rest of the sample was composed of half-weighted systems with V-I colours transformed from B-V values. The three M71 contact systems studied here will, therefore, be a valuable addition to the V-I sample. When the reduction of the 5-colour Mt. Laguna CCD frames is completed, these stars will also supplement the relatively small (less than 20) B-V sample.

The origin of these stars is also of interest. Do the binaries represent the result of collisions? This possibility cannot be ruled out but M71's age is sufficient for merger hypotheses to be important competitors. The magnetic braking theory of contact system formation predicts that considerable time is required to bring initially detached components into contact. Vilhu (1982), for instance, estimates that two 1 solar mass stars with an initial period of 4 days will come into contact in $\sim 10^{10}$ years. In young clusters, therefore, it can be argued that contact systems must be caused by some other mechanism. This argument cannot be applied to M71 because of its large age. However, one might ask if binary systems could survive the effects of collisions over the time interval required for them to come into contact. This question is considered by Yan & Mateo (1994) who find the timescale required to destroy binaries with periods less that 2.5-5 days and component masses of 0.7 solar masses exceeds 10^{11} years. Binary-binary interactions are expected to be more common because the interaction cross-section increases as the semi-major axis, but interactions with large period, low orbital velocity binaries will tend to harden binaries rather than destroy them (Hills 1990).

It is also possible that the binary systems discussed here were produced through binary-binary interactions but Yan & Mateo (1994) argue against this scenario. Adapting the work of Leonard & Fahlman (1991), they conclude that only 3-4 short-period binaries are expected to be created during wide-binary interactions in M71, assuming that the maximum stable orbital period in M71 is ~ 800 years (Hills 1984). Contact binaries are expected to merge completely from the time of initial contact within $\sim 5 \times 10^8$ years (Stryker 1993). This would imply that all of the short-period binaries expected to be formed in this manner were formed within a small fraction of the M71's lifetime. While not impossible, assuming that the figures of Yan & Mateo are accurate, it seems unlikely that more than one, if any, of the contact binaries observed in M71 were formed in this fashion.

The origin of the M71 contact systems may be in question but their ultimate fate is fairly certain: within ~10^9 years, these stars will have merged. Whether they will become blue stragglers depends on the mass of the merged star. If it exceeds the turn-off mass of the cluster, the recently-formed 'high' mass star will appear above and blueward of the other cluster members on the main sequence. Merged stars of mass less than the turn-off mass will move up the main sequence but remain among other stars of comparable mass. These stars will form *latent blue stragglers*, being exposed after the stars near them on the CMD evolve off the main sequence. The precise fate of the M71 contact systems, therefore, obviously depends largely on their current mass. Also, their final, merged mass may be affected by mass loss during the merger process. As the stars of a binary system merge, the Roche lobes become increasingly small. If the outer critical surface of the system can no longer contain the stars, material will be lost from the system. The NGC 5466 contact systems, which are very close to filling their outer critical surfaces, may have already lost mass and could represent the fate of the M71 contact systems as they merge further. A quantitative investigation of how these systems fit into current binary star evolutionary models is beyond the scope of the present work but would be an interesting subject of future study.

5.2 V4

Three models of V4, the Algol-type system, were produced. The initial model, which has the lowest Σwr^2, is a detached system with the secondary star smaller than the primary star so that the primary eclipse is a transit eclipse. The secondary star in this model is close to filling its Roche lobe (f=-0.11). Because of this, the possibility of a semi-detached system in which the secondary star fills its Roche lobe was also investigated.

The Σwr^2 of this model was not as small as that of the detached system (0.262 as compared to 0.257). This result was expected as the potentials Ω_i of the two stars in the initial detached model were not constrained and the secondary potential would be expected to migrate to a smaller value, had the semi-detached system been more desirable. Careful spectroscopy or infrared photometry could reveal the existence of circumstellar matter, which would lend support to the semi-detached model in which the secondary star is slowly losing mass to form an accretion disk around its companion. However, in the absence of such evidence, the detached model is the more likely of the two. A third model investigated was for the case in which the primary star is the smaller of the two, meaning that the primary eclipse is an occultation eclipse. The fit of this model to the observed light curve was the worst of the three models (Σwr^2=0.264). The model parameters for each of these models are given in Tables 8 and 9. The radii and surface areas calculated by the WD program for the three models are given in Tables 10 and 11. The absolute parameters and related quantities for the models are given in Table 12. Three dimensional representations of the models are shown in Figures 16a through 16c and their Roche lobe configurations are shown in Figure 17.

The calculated distances (using the assumed mass ranges discussed earlier and given in Table 10) for the two transit case models were 3.33±0.39 kpc (detached) and 3.32±0.42 kpc (semi-detached), both in agreement with the Richer & Fahlman (1988) distance for M71 of 3.6±0.5 kpc. The occultation model implies a distance 3.03±0.36 kpc and so V4 would be less likely to be a cluster member if it were accurately represented by this model. The fact that the better models (smaller Σwr^2 and σ) indicate cluster membership lends weight to V4 being a cluster member.

The positions of the detached model components on the M71 CMD of Hodder *et al.* (1992) are shown in Figure 13. The primary is slightly blueward of the main sequence near the turn-off but there is considerable uncertainty in V and B-V. The secondary component is redward of the main sequence and just fainter than 20th magnitude. The fact

TABLE 8
Final Parameter Sets for Adopted V4 Model

Parameter	[Fe/H]=-0.3	[Fe/H]=-0.5	[Fe/H]=-1.0
$\log(g_1)$	4.599	4.594	4.599
$\log(g_2)$	4.263	4.264	4.263
a (R_{sun})	4.97	4.97	4.97
$\Delta\phi$	0.7998(3)	0.7998(3)	0.7998(3)
i	79°.40(49)	79°.46(50)	79°.42(50)
g_1	1.00	1.00	1.00
g_2	0.32	0.32	0.32
T_1 (K)	6500	6500	6500
T_2 (K)	4286(28)	4285(28)	4244(30)
A_1	1.00	1.00	1.00
A_2	0.50	0.50	0.50
Ω_1	3.469(43)	3.456(42)	3.469(49)
Ω_2	2.653(24)	2.654(26)	2.652(25)
q	0.3755(67)	0.3752(74)	0.3754(86)
L_1^V	11.495(88)	11.498(88)	11.495(93)
L_1^I	10.67(12)	10.67(11)	10.67(12)
X_1^{bol}	0.482	0.482	0.482
X_1^V	0.526	0.526	0.526
X_1^I	0.374	0.374	0.374
L_1^V	1.021	1.027	1.028
L_1^I	1.723	1.738	1.736
X_2^{bol}	0.526	0.526	0.466
X_2^V	0.826	0.826	0.749
X_2^I	0.595	0.596	0.553
Σwr^2	0.25681	0.25815	0.26040
σ	0.018307	0.018355	0.018435

Quantities in parentheses are the probable errors calculated by the WD program.

TABLE 9
Alternative V4 Model Parameter Sets ([Fe/H]=-0.3)

Parameter	Semi-detached	Occultation
$\log(g_1)$	4.608	4.610
$\log(g_2)$	4.224	4.389
a (R_{sun})	4.97	4.97
$\Delta\phi$	0.7998(3)	0.7998(3)
i	$79°.19(38)$	$75°.50(31)$
g_1	1.00	1.00
g_2	0.32	0.32
T_1 (K)	6500	6500
T_2 (K)	4285(27)	4326(31)
A_1	1.00	1.00
A_2	0.50	0.50
Ω_1	3.468(44)	4.610(65)
Ω_2	2.597	3.847(42)
q	0.361(16)	0.918(14)
L_1^V	11.454(64)	10.50(17)
L_1^I	10.615(82)	9.27(20)
X_1^{bol}	0.482	0.482
X_1^V	0.526	0.526
X_1^I	0.374	0.374
L_1^V	1.056	1.900
L_1^I	1.776	3.008
X_2^{bol}	0.522	0.526
X_2^V	0.820	0.826
X_2^I	0.592	0.596
Σwr^2	0.26157	0.26428
σ	0.018476	0.018572

Quantities in parentheses are the probable errors calculated by the WD program.

TABLE 10
V4 Adopted Model Radii and Surface Areas

Quantity	[Fe/H]=-0.3	[Fe/H]=-0.5	[Fe/H]=-1.0
R_1^{pole} (a)	0.3214(41)	0.3227(41)	0.3214(45)
R_1^{side} (a)	0.3292(46)	0.3307(45)	0.3292(50)
R_1^{back} (a)	0.3350(48)	0.3366(48)	0.3350(52)
R_1^{point} (a)	0.3391(52)	0.3408(51)	0.3391(56)
R_2^{pole} (a)	0.2729(69)	0.2726(77)	0.2730(81)
R_2^{side} (a)	0.2837(82)	0.2834(92)	0.2838(96)
R_2^{back} (a)	0.313(13)	0.313(15)	0.313(16)
R_2^{point} (a)	0.354(37)	0.353(41)	0.355(45)
S_1 (a^2)	1.358	1.370	1.358
S_2 (a^2)	1.069	1.066	1.070

Quantities in parentheses are the probable errors calculated by the WD program.

TABLE 11
Alternative V4 Model Radii and Surface Areas

Quantity	Semi-detached	Occultation
R_1^{pole} (a)	0.3201(34)	0.2686(41)
R_1^{side} (a)	0.3276(37)	0.2738(44)
R_1^{back} (a)	0.3332(38)	0.2810(48)
R_1^{point} (a)	0.3369(40)	0.2849(52)
R_2^{pole} (a)	0.2747(32)	0.3216(55)
R_2^{side} (a)	0.2862(34)	0.3337(65)
R_2^{back} (a)	0.3190(34)	0.3540(85)
R_2^{point} (a)	0.3968(42)	0.375(13)
S_1 (a^2)	1.345	0.948
S_2 (a^2)	1.100	1.431

Quantities in parentheses are the probable errors calculated by the WD program.

TABLE 12
Assumed and Calculated Quantities for V4 Models

Quantity	Adopted	Semi-detached	Occultation
M_{tot} (M_{sun})	0.7-1.0	0.7-1.0	0.7-1.3
M_1 (M_{sun})	0.61(11)	0.62(11)	0.51(16)
M_2 (M_{sun})	0.23(4)	0.22(4)	0.46(14)
f_1	-3.654	-3.920	-1.966
f_2	-0.110	0	-0.458
BC_1	-0.093(50)	-0.093(50)	-0.093(50)
BC_2	-0.606(50)	-0.606(50)	-0.606(50)
$(B-V)_{0,1}$	0.404(60)	—	—
$(B-V)_{0,2}$	1.029(60)	—	—
R_1^{eff} (R_{sun})	0.883(38)	0.878(30)	0.773(39)
R_2^{eff} (R_{sun})	0.78(16)	0.794(29)	0.950(74)
L_1^{bol} (L_{sun})	1.25(16)	1.24(14)	0.96(13)
L_2^{bol} (L_{sun})	0.19(8)	0.19(3)	0.28(6)
M_1^{bol}	$4^m.51(14)$	$4^m.52(12)$	$4^m.80(15)$
M_2^{bol}	$6^m.58(48)$	$6^m.55(17)$	$6^m.12(23)$
M_1^{V}	$4^m.61(15)$	$4^m.62(13)$	$4^m.89(16)$
M_2^{V}	$7^m.19(49)$	$7^m.16(18)$	$6^m.73(24)$
DM_O	12.61(19)	12.60(20)	12.41(19)
d (kpc)	3.33(39)	3.32(42)	3.03(36)

Quantities in parentheses are standard errors.

that the primary component is near the main sequence and slightly fainter than the turn off magnitude is interesting because it may provide an observationally determined limit to the turn-off mass of M71. However, the displacement of the stars from the main sequence may imply that the evolution of the two components was influenced by mass exchange. Considering how close the secondary component is to filling its Roche lobe, this is not an unreasonable concern. To test this hypothesis, evolutionary models must be consulted.

0.25　　　　　　　　　　　　　0.42

0.50　　　　　　　　　　　　　0.75

0.92　　　　　　　　　　　　　1.00
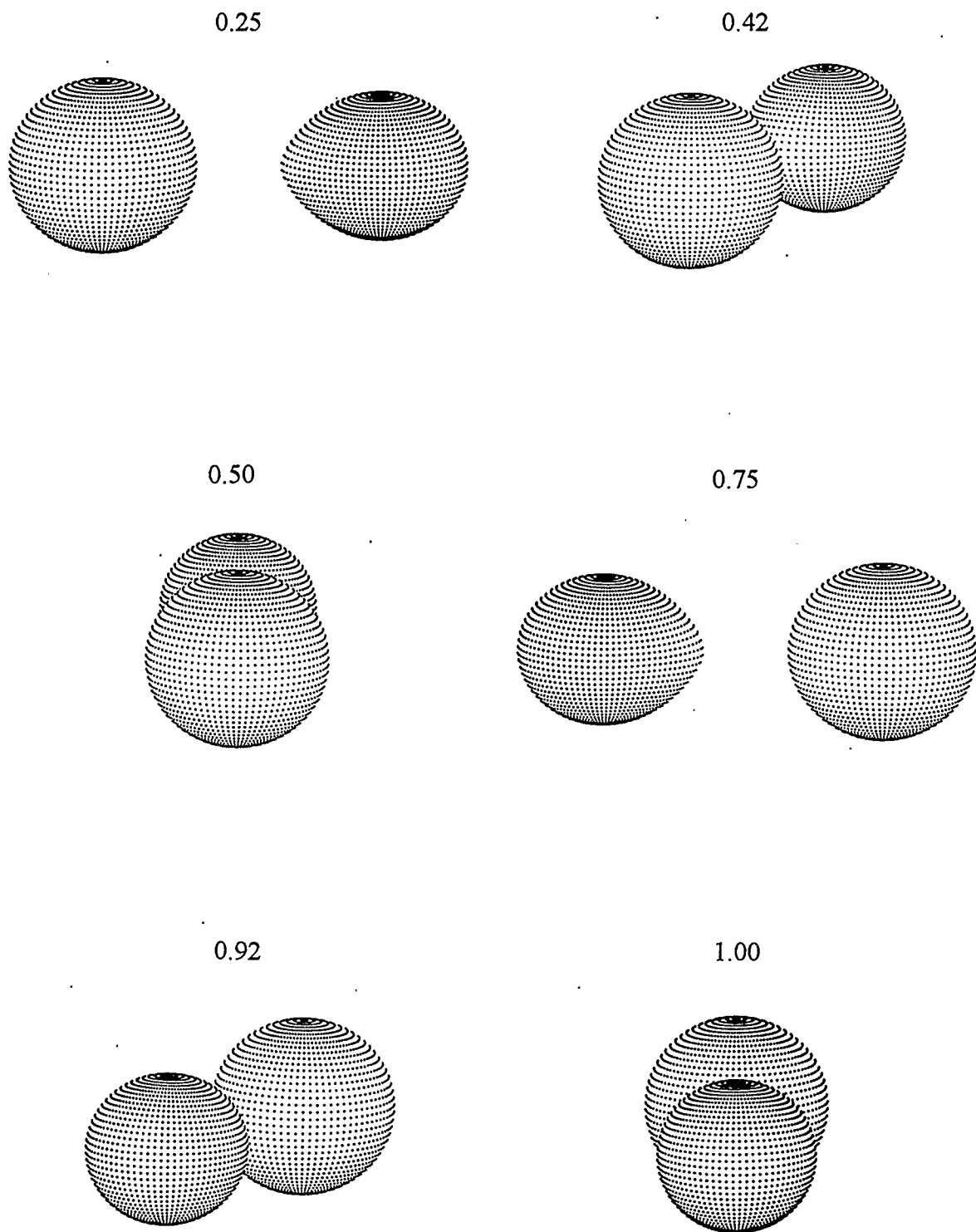
Figure 16a - Three-dimensional representation of the V4 system (see Table 8 for model parameters). The phases represented by each picture are indicated.

0.25

0.42

0.50

0.75

0.92

1.00
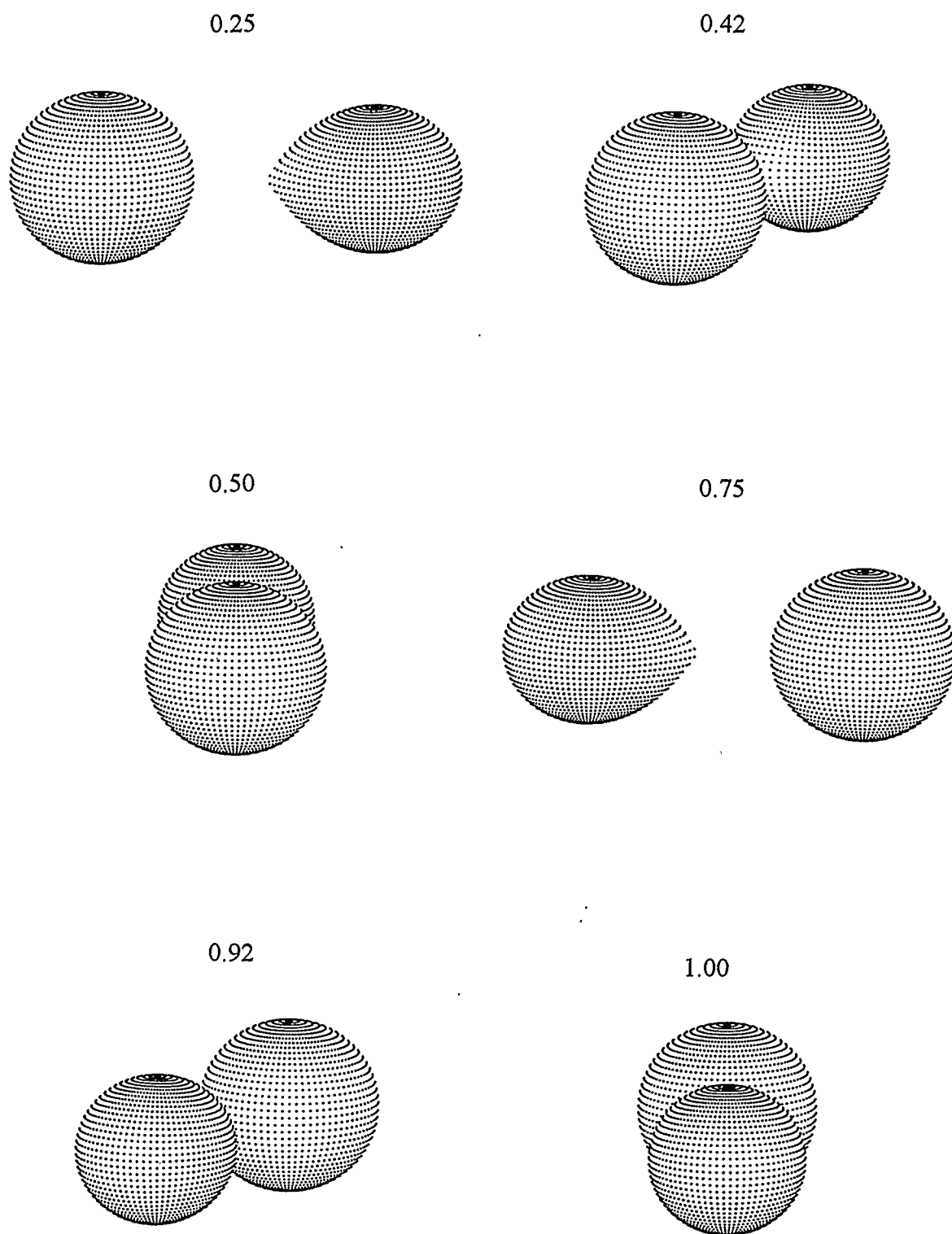
Figure 16b - Three dimensional representation of the semi-detached model of V4 (see Table 9 for model parameters). The phases represented by each picture are indicated.

0.25

0.42

0.50

0.75

0.92

1.00
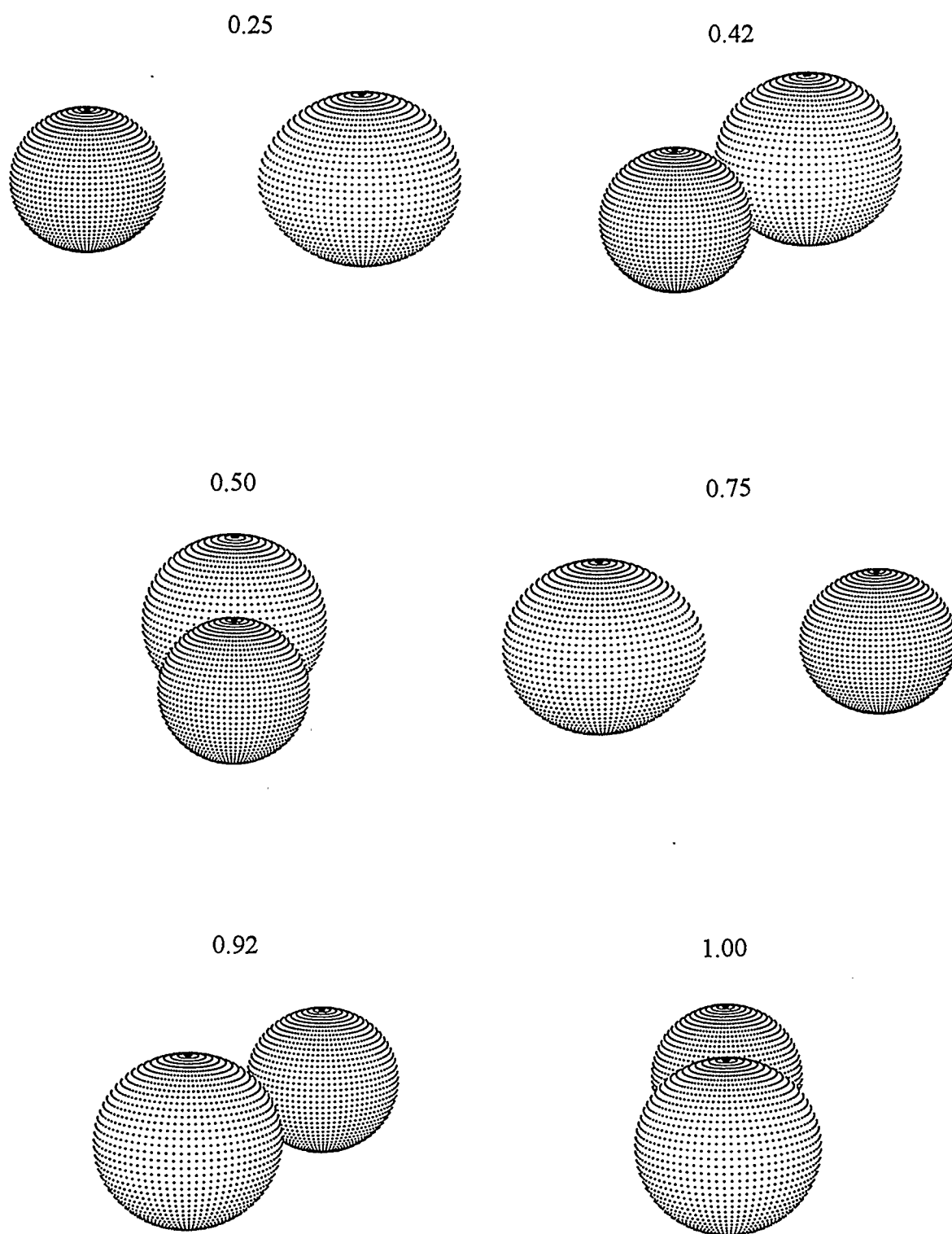
Figure 16c - Three dimensional representation of the occultation model of V4 (see Table 9 for model parameters). The phases represented by each picture are indicated.
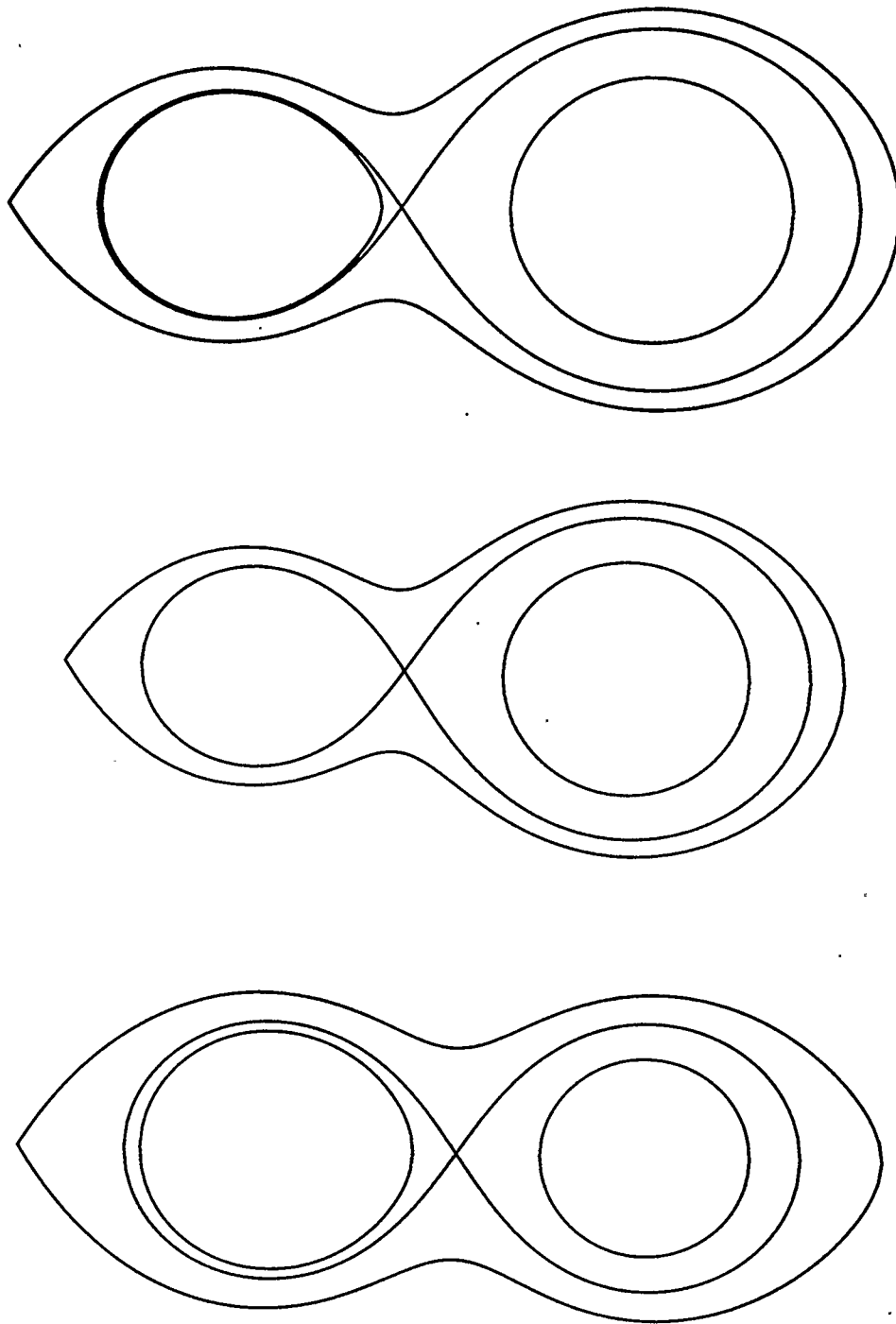
Figure 17 - The Roche lobe configurations of the V4 models (adopted, semi-detached, and occultation from top to bottom). The less massive star is on the left.

The evolutionary tracks of VandenBerg & Bell[7] indicate that a 0.6 solar mass star (the detached model predicts a primary mass of 0.61±0.11 solar masses) would not have exceeded its current size since it moved on to the main sequence within the lifetime of M71. Therefore, it is not expected to have filled its Roche lobe in the past since it does not currently. This assumes Y=0.2 and Z=0.006. Even under the more unfavorable circumstances of a 0.7 solar mass star with Z=0.003 (since lower metallicity stars evolve at a greater rate), the star is not expected to have exceeded its current size in the past. The same argument can be made for the less massive star (0.23±0.04 solar masses) since its main sequence lifetime is expected to be much longer.

This represents the most obvious scenario and makes V4 very similar to DS And (Schiller & Milone 1988), which also has its primary component near the cluster turn-off and its secondary component, which nearly fills its Roche lobe, somewhat redward of the main sequence.

It is, however, possible to argue that if the stars have exchanged mass in the past, the masses of the components could have been significantly different than they currently are, meaning that the above argument is not valid. Suppose the system had a fairly extreme initial mass ratio of 0.15. This mass ratio would imply a primary component of mass 0.87 solar masses, assuming that the upper end of V4's assumed total mass range is adopted, *i.e.*, 1.0 solar mass. Such a star will evolve faster than the 0.61 solar mass star considered above. In order to determine how long it would take for this hypothetical star to start transferring mass to its companion, the size of the corresponding hypothetical

---

[7] Single star evolutionary tracks are consulted because, up until the time that binaries exchange mass, the components are assumed to evolve in the same manner as single stars, although it is likely that the proximity of the stars actually affects their evolution to an extent that has not yet been clearly established.

Roche lobe must be calculated. Using equation (46), the effective radius of the Roche lobe of the primary component of a binary system with q=0.15 was found to be 0.5451· a. The semi-major axis is affected by mass transfer and must be calculated for this 'primordial' mass ratio.

The total angular momentum of a binary system, J, can be expressed as

$$J = M_1 a_1^2 \omega + M_2 a_2^2 \omega + I_1 \omega_1 + I_2 \omega_2 , \qquad (61)$$

where a_1 and a_2 are the same as in equation (4), I_1 and I_2 are the moments of inertia of the two stars, ω_1 and ω_2 are the angular rotation rates of the stars, and ω is the angular orbital revolution rate. Assuming that the stars are centrally condensed, and hence that the stellar moments of inertia are negligible, the equation can be simplified:

$$J_{orb} = \frac{M_1 M_2}{M_1 + M_2} a^2 \frac{2\pi}{P} . \qquad (62)$$

Combining this with equation (4) gives:

$$J_{orb} = G^{1/2} \frac{M_1 M_2}{\left(M_1 + M_2\right)^{1/2}} a^{1/2} \qquad (63)$$

If mass exchange conserves angular momentum and total mass, then the current angular momentum should be equal to the primordial angular momentum. Equating the two and simplifying gives:

$$a'\left(M_1' M_2'\right)^2 = a\left(M_1 M_2\right)^2 , \qquad (64)$$

where the primed quantities refer to the primordial system. So if the primordial mass ratio q' was 0.15, then a'=3.06 · a. Using a value of a appropriate for a 1.0 solar mass system yields a'=8.71 solar radii. Therefore, the Roche lobe of this hypothetical primordial system would have had an effective radius of 4.75 solar radii. The isochrones of Bergbusch and VandenBerg (1992) indicate that a 0.87 solar mass star with a metallicity

in the range of [Fe/H]=-0.47 to -0.78 will not exceed this size in 14 Gyr. However, in 16 Gyr, 0.87 solar mass stars with [Fe/H]=-0.65 and -0.78 will exceed this size, while a [Fe/H]=-0.47 star will not. It should be noted that the assumption that angular momentum is conserved represents a worst-case scenario for the argument that mass has not been exchanged. If the mass exchange does not conserve angular momentum, the primordial semimajor axis would be even larger, strengthening the case for there having been no past mass exchange. In conclusion, the precise values for M71's age and metallicity are crucial in determining if mass transfer could have taken place in the V4 system. Considering the uncertainties in the age[8] and metallicity of M71, and the mass of the V4 system, mass transfer in V4's past cannot be ruled out by this argument.

Is it likely that the mass ratio could have changed from 0.15 to its current 0.376? This question would be logically addressed by consulting binary star evolutionary models (reviews of this topic can be found in Paczynski 1971, Thomas 1979, and Iben, 1991 for example). As was noted above, the evolutionary status of V4 is very sensitive to mass, mass ratio, metallicity, and separation—small changes in any of these quantities are enough to significantly affect conclusions concerning V4's status. Unfortunately, the author was unable to locate binary star evolutionary models that are suited to the

---

[8] Demarque *et al.* (1992) argue that most isochrones calibrated with the same observational data will give approximately the same ages. In particular, mixing lengths for isochrones of near solar metallicities must be chosen to reproduce the radius of the Sun. Ages derived from inappropriately calibrated isochrones will not be accurate. For instance, estimates of the age of NGC 6791 based on VandenBerg's (1985) isochrones are too old by ~4 Gyr. Based on these isochrone, the Sun would have an age of greater than ~8-10 Gyr. VandenBerg (1992) claims that until globular cluster distance estimates are refined, age uncertainties of ~3Gyr will persist.

hypothetical primordial V4 system. When suitable binary star evolutionary models become available, the question of the likelyhood of a change in V4's mass ratio from 0.15 to 0.376 can be investigated by this means. Until then, the question must be addressed less directly.

If the more massive component of a binary system loses mass to its companion, its Roche lobe will contract. This can lead to runaway mass transfer if the rate of contraction for the star due to mass loss is not as great as the Roche lobe contraction rate. Under these circumstances, mass loss will occur on a dynamical timescale, τ_d. Such a timescale is a measure of the time required for the system's motions representing its response to an arbitrary disturbance (Kopal, 1978) and is given by

$$\tau_d \approx \left(\frac{R^3}{GM}\right)^{1/2}. \tag{65}$$

A second possibility is that as the star loses mass, it cannot remain in thermal equilibrium and contracts to just within its Roche lobe. In this case mass loss will proceed on a thermal timescale, τ_{th}, the time needed for the system to contract from infinity to the current form, which is given by

$$\tau_{th} \approx \frac{GM^2}{RL}, \tag{66}$$

where L is the luminosity of the system (Kopal, 1978). The ability of a star to contract rapidly enough to avoid an exponential increase in mass loss rate as its Roche lobe contracts depends on its thermal structure. Specifically, stars with radiative envelopes will respond to initial mass loss by rapidly contracting. Conversely, stars with convective envelopes may expand as a result of mass loss and tend to be unstable to dynamical timescale mass loss (Webbink 1985).

The proposed hypothetical star of mass 0.87 solar masses will have a convective envelope when it reaches a size large enough to fill its Roche lobe (Webbink 1985) and so dynamical mass loss would be expected to occur. Mass would be lost by the primary component very quickly, possibly faster than its accreting companion could accommodate, thereby causing mass to be lost from the system if the mass loss rate was sufficiently large. The mass loss would halt only after the primary star's Roche lobe stopped its rapid contraction or when the star became capable of remaining within its Roche lobe. The former circumstance would only occur after the system's mass ratio slightly exceeded unity. The latter circumstance would most likely result in mass exchange proceeding on a slower thermal timescale. In either of these cases, mass exchange would be expected to proceed past mass equalization before halting. Since the current mass ratio of V4 is only 0.376, it seems reasonable to conclude that mass exchange probably did not occur in the past.

A caveat is necessary, however, since binary star evolution is still not well understood. All of the uncertainties that limit single star evolution studies apply to binary stars, and additional problems make matters much more complicated: tidal distortion for close binaries means models must be three-dimensional rather than one-dimensional; tidal effects may cause currents that cannot be dealt with in normal evolutionary models; tidal heating may be significant; mass transfer and/or loss, which is very sensitive to the structure of the stars; non-conservation of angular momentum; physical processes such as turbulent viscosity and meteorological phenomena such as electrodynamical storms that may result from mass transfer but for which we do not yet have quantitative descriptions; and potentially many other complications that are not normally considered for single star evolution (Iben 1991). Given these complications and the fact that even models that do not consider many of these complications predict very complicated evolutionary paths for

binary systems (see Iben & Tutukov (1985) for some well-annotated examples of binary evolutionary tracks), caution is required before making firm conclusions about the V4 system.

The displacement of the V4 secondary component from the CMD main sequence is problematic for the hypothesis that mass exchange has not occurred, although the width of the main sequence and the uncertainty in the secondary's position determination still allow that the secondary could be a normal main sequence object. The model radii of the V4 components are also problematic. The ratio of the radii of the V4 components is expected to be ~2.5 (Milhalas & Binney 1981) if the stars were main sequence objects while the adopted model indicates as ratio of ~1. How can this observation be consistent with the argument that mass exchange has not taken place because the current mass ratio of V4 is unlikely if mass exchange had occurred? Lucy (1976) has proposed that contact binaries go through short-lived intervals during which the contact between the stars is broken. During these intervals, the system assumes a semi-detached configuration. XZ Canis Minoris is possibly an example of such a system (Terrell *et al.* 1994) and is very similar to V4 in many respects, including mass ratio. However, given that such broken-contact systems are expected to be difficult to observe due to the fact that the duration of the broken-contact interval is only of the order of 10^6 years, and that the preferred model for V4 is not semi-detached, there are some problems with this evolutionary interpretation of V4.

In conclusion, the evolutionary status of V4 is unsettled. If mass exchange has occurred, then, as was the case for the contact systems, it will be interesting to see how V4 fits into current binary star evolutionary models. On the other hand, if mass exchange has not occurred, V4 could provide important checks for single star evolutionary models.

The resolution of this question will certainly be accelerated by the acquisition of spectral information.

5.3 V3

The best-fit model of V3 indicates that it is a detached system. The parameters for this model are given in Table 13. Because the light curves exhibit a strong O'Connell effect, they were modelled with a single cool spot in the primary component (see Table 14). The radii and surface areas of the V3 stars are given in Table 15. The absolute parameters and related quantities for this system are given in Table 16. A three dimensional representation and the Roche lobe configuration for the system are given in Figures 18 and 19.

If V3 is a member of M71, it is potentially of interest for the same reasons as V4. In this case though, the small mass ratio of V3 implies that it is less likely that the primary star is unevolved. With a calculated mass of 0.80 ± 0.08 solar masses, arguments concerning changes in mass ratio are not required for the primary component to exceed the current turn-off mass of M71 (based on Bergbusch and VandenBerg (1992) models).

The location of the individual components of V3 on the CMD is suggestive of mass and luminosity being gained by the more massive component at the expense of its companion, as was the case for V1 and V5. Again, this is only true if V3 is a member of M71.

Unfortunately, the calculated absolute parameters for this system suggest that it is not a member of M71. The derived distance of V3 (3.17 ± 0.35 kpc) make the membership of this system the least likely of the five binaries. Yan and Mateo (1994) also found this star to be the most likely non-member, because of its position on the CMD. The

individual components of V3 have been placed on M71's CMD (see Figure 13) assuming a reddening value appropriate for cluster membership. Of all of the binaries, V3 is the only system to have its primary located significantly off the main sequence. While not precluded by these observations, the cluster membership of V3 seems unlikely.

TABLE 13
Final Parameter Sets for V3

Parameter	[Fe/H]=-0.3	[Fe/H]=-0.5	[Fe/H]=-1.0
$\log(g_1)$	4.383	4.383	4.383
$\log(g_2)$	4.419	4.419	4.419
a (R_{sun})	2.61	2.61	2.61
$\Delta\phi$	0.0917(6)	0.0917(6)	0.0917(6)
i	73°.94(73)	73°.89(73)	73°.94(73)
g_1	0.32	0.32	0.32
g_2	0.32	0.32	0.32
T_1 (K)	4740	4740	4740
T_2 (K)	4562(19)	4562(19)	4560(20)
A_1	0.50	0.50	0.50
A_2	0.50	0.50	0.50
Ω_1	2.448(20)	2.445(21)	2.447(20)
Ω_2	2.473(34)	2.474(34)	2.473(34)
q	0.2387(55)	0.2387(59)	0.2387(55)
L_1^V	10.53(13)	10.54(13)	10.52(13)
L_1^I	10.49(14)	10.49(14)	10.48(13)
X_1^{bol}	0.534	0.534	0.534
X_1^V	0.788	0.788	0.788
X_1^I	0.567	0.567	0.567
L_1^V	1.840	1.833	1.844
L_1^I	1.970	1.960	1.968
X_2^{bol}	0.535	0.535	0.535
X_2^V	0.798	0.798	0.798
X_2^I	0.572	0.572	0.572
Σwr^2	0.27633	0.27642	0.27638
σ	0.017637	0.017640	0.017639

Quantities in parentheses are the probable errors calculated by the WD program.

TABLE 14
Spot Parameters for V3

Parameter	Value
latitude	96°(19)
longitude	267°(5)
size	13°(4)
temp. factor	0.65(11)

Quantities in parentheses are the probable errors calculated by WD.

TABLE 15
V3 Model Radii and Surface Areas

Quantity	[Fe/H]=-0.3	[Fe/H]=-0.5	[Fe/H]=-1.0
R_1^{pole} (a)	0.4485(34)	0.4490(35)	0.4486(34)
R_1^{side} (a)	0.4783(44)	0.4790(45)	0.4785(43)
R_1^{back} (a)	0.4956(49)	0.4965(50)	0.4958(49)
R_1^{point} (a)	0.5273(74)	0.5287(74)	0.5277(73)
R_2^{pole} (a)	0.2143(88)	0.2140(92)	0.2141(87)
R_2^{side} (a)	0.2199(99)	0.220(10)	0.2198(98)
R_2^{back} (a)	0.236(14)	0.235(14)	0.236(13)
R_2^{point} (a)	0.245(17)	0.244(18)	0.244(17)
S_1 (a^2)	2.834	2.833	2.836
S_2 (a^2)	0.629	0.627	0.628

Quantities in parentheses are the probable errors calculated by the WD program.

TABLE 16

Assumed and Calculated Quantities for V3

Quantity	Value
M_{tot} (M_{sun})	0.9-1.1
M_1 (M_{sun})	0.80(8)
M_2 (M_{sun})	0.19(2)
f_1	-0.803
f_2	-0.968
BC_1	-0.437(50)
BC_2	-0.523(50)
$(B-V)_{0,1}$	0.876(60)
$(B-V)_{0,2}$	0.936(60)
R_1^{eff} (R_{sun})	1.036(20)
R_2^{eff} (R_{sun})	0.488(87)
L_1^{bol} (L_{sun})	0.49(7)
L_2^{bol} (L_{sun})	0.09(4)
M_1^{bol}	$5^m.54(15)$
M_2^{bol}	$7^m.34(41)$
M_1^V	$5^m.98(16)$
M_2^V	$7^m.86(41)$
DM_0	12.50(18)
d (kpc)	3.17(35)

Quantities in parentheses are standard errors.
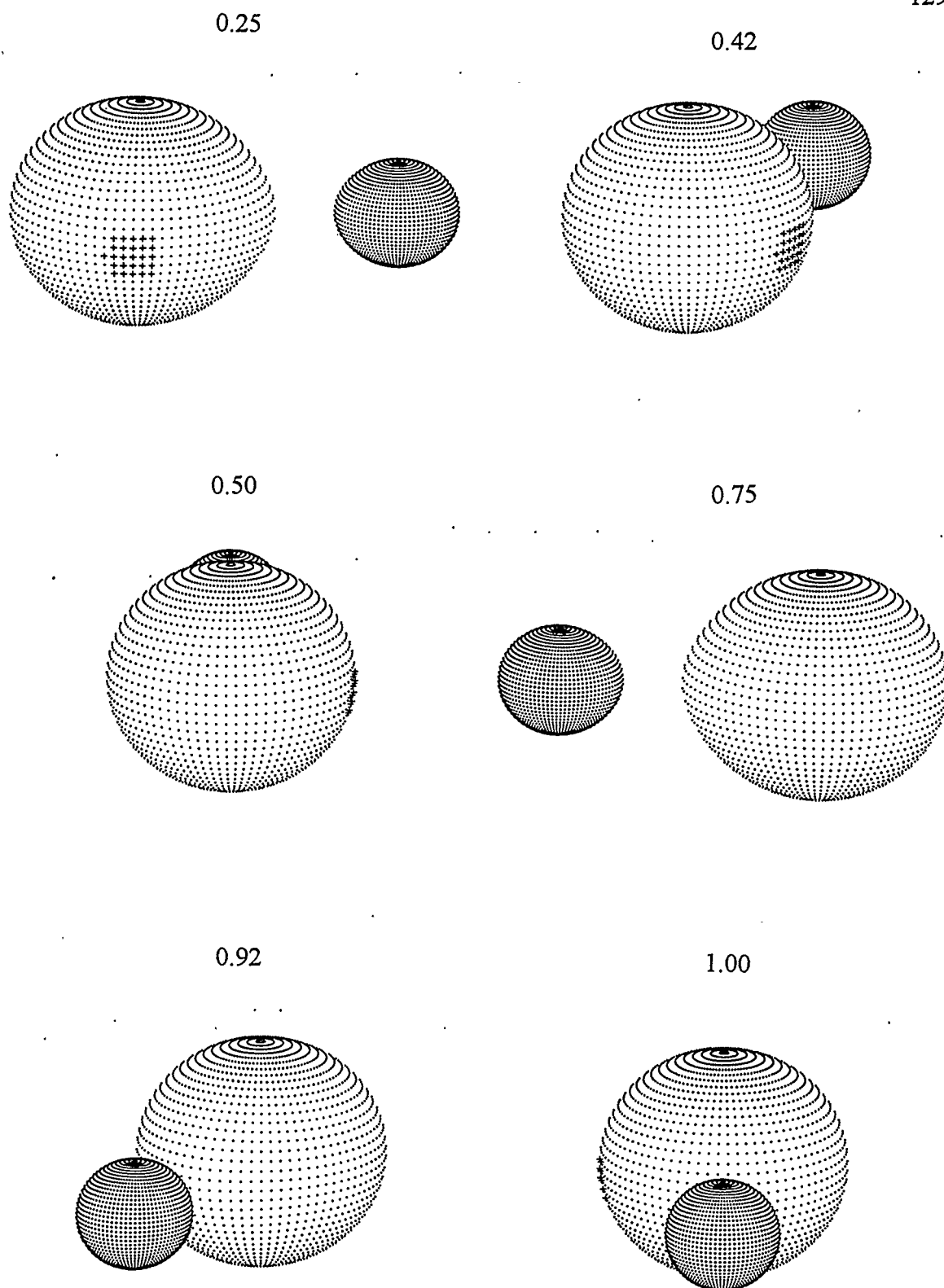
Figure 18 - Three-dimensional representation of the V3 system (see Table 13 for model parameters. The phases represented by each picture are indicated.
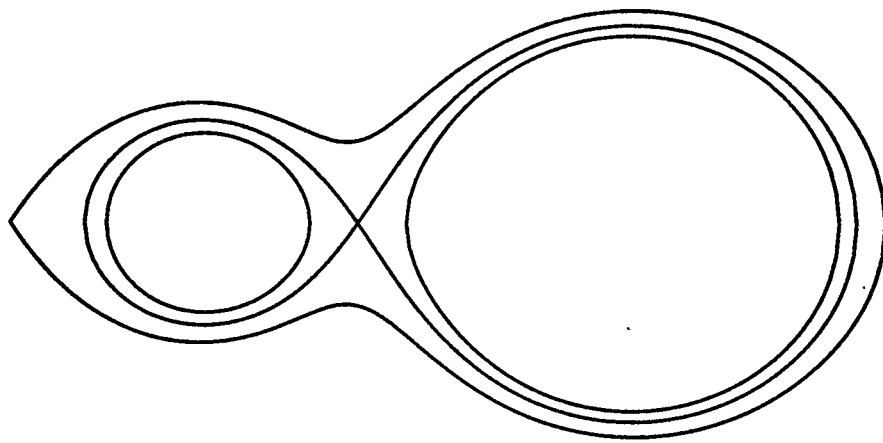
Figure 19 - The Roche lobe configurations of the V3 system. The less massive star is on the left.

6.0 SUMMARY

The Johnson V and Cousins I eclipsing light curves of Yan & Mateo (1994) have been analyzed using the University of Calgary improved Wilson-Devinney light curve modelling program and a simplex enhanced version of the same. Using the results, absolute parameters for the binaries have been calculated and the individual components have been placed on the colour magnitude diagram of Hodder *et al.* (1992). Of the five binaries, four are probable M71 cluster members based on distance determinations.

Three binaries are contact systems, but the degree of contact is not nearly so great as that demonstrated by the W UMa stars in NGC 5466 (Kallrath *et al.* 1992). This is consistent with the fact that the M71 contact systems are on or near the main sequence while the NGC 5466 systems were blue stragglers. The individual components of two of the contact systems (V1 and V5) demonstrate the common trait of having their primary components above the main sequence while their secondary components are to be found below the main sequence. This is suggestive of the more massive star having gained mass and luminosity at the expense of its companion, a result common with other W UMa systems. The contact systems have been used to test Rucinski's (1994) period-colour-luminosity relationship for W UMa stars. The results were not impressive, and imprecise colour transformations and small sample sizes are the probable cause. These systems are an important addition to the available sample of W UMa systems with derived distances and will help to refine the P-C-L relationship.

The fourth probable member, V4, is most likely a detached system although the semi-detached model was also considered since the less massive star nearly fills its Roche lobe in the detached model. A third model, the least likely based on goodness-of-fit measurements, has the hotter star more massive but smaller in size (mass ratio ~0.9) and

represents the occultation eclipse possibility. If the system is detached, the location of the primary component near the main sequence turn-off is potentially important for evolutionary model calibrations. The primary is notably blueward of the main sequence but the large error in (B-V) encompasses the main sequence. The theoretical evolutionary tracks of VandenBerg & Bell (1985) and the isochrones of Bergbusch & VandenBerg (1992) have been used to check for the possibility of mass exchange. Stars of masses equal to the current component masses would not have expanded past their current size and, hence, would not have exchanged mass. This fact makes V4 very similar to DS And, the components of which have similar positions on the CMD of NGC 752, and whose less massive star nearly fills its Roche lobe. The possibility of past mass exchange has also been investigated. A primordial mass ratio smaller that its current value would imply a correspondingly more massive primary star, which would be expected to have evolved faster than of the current primary star. Evolutionary tracks have been consulted and it has been concluded that past mass exchange cannot be ruled out on this basis, despite the larger size of the primordial Roche lobe required by the smaller primordial mass ratio, because of uncertainties in the cluster age and metallicity. The likelihood of mass exchange leading to a change in mass ratio to its current value of 0.38 from a smaller value has been considered. It has been argued that such a change was unlikely to occur because, once begun, mass exchange will proceed until component mass equalization was achieved. However, given the complicated nature of binary star evolution, past mass exchange cannot be definitively ruled out. The final resolution of the question V4's evolutionary status will require further information, particularly spectral information.

The fifth binary, V3, is the least likely to be a M71 member, based on its calculated distance. The resolved and combined positions of V3 on the CMD also argue against membership.

The continuing work on the Mt. Laguna 5-colour CCD images is expected to provide valuable additional information, and may help to confirm the conclusions discussed here. In particular, precise colour excess determinations will greatly reduce the uncertainty in the component positions on the CMD. B-V colour information will allow the M71 contact systems to be added to the Rucinski (1994) B-V sample and hence aid in the determination of a period-colour-luminosity relationship for W UMa stars, as can already be done for the V-I sample. The pursuit of spectroscopic information is an extremely important task to be included in future work. Radial velocity information will help in the confirmation of the membership of the M71 binaries. The large uncertainty in the total mass of the binary systems will also be addressed by the addition of radial velocity curves to the light curves analyzed here. Spectroscopic analysis will also provide better estimates for the temperatures of the stars. It may also, along with infrared observation, provide evidence for mass loss in the binary systems. This would be useful in establishing the status of the V4 binary because mass loss is an expected symptom of dynamical timescale mass transfer. Finally, spectroscopic information may provide clues concerning the composition and evolutionary state of the V4 components, which would be helpful in determining if large scale mass transfer has occurred.

References

Abt, H. A. & Levy, S. G. 1969, AJ, 74, 908

Allen, C. & Martos, M. A. 1988, Rev Mexicana Astron Astrof, 16, 25

Arp, H. C. & Hartwick, F. D. A. 1971, ApJ, 167, 499

Bergbusch, P.A. & VandenBerg, D.A. 1992, ApJS, 81, 163

Burstein, D., Faber, S. M., & Gonzalez, J. J. 1986, AJ, 91, 1130

Buser, R. & Kurucz, R.L. 1992, A&A, 264, 557

Cannon, R.D. 1968, Observatory, 88, 206

Chernoff, D.F. & Djorgovski, S. 1989, ApJ, 339, 904

Chiosi, C. & Maeder, A. 1986, Ann Rev Astron Astrophys, 24, 329

Cudworth, K.M. 1985, AJ, 90, 65

Davidge, T.J. & Milone, E.F. 1984, ApJS, 55, 571

Davidge, T.J. & Simons, D.A. 1994, AJ preprint.

Demarque, P., Green, E.M., & Guenther, D.B. 1992, AJ, 103, 151

Djorgovski, S.G. 1993, in *Structure and Dynamics of Globular Clusters*, eds. S.G. Djorgovski & G Meylan, (San Francisco, A.S.P.), p. 373

Drukier, G.A., Fahlman, G.G., & Richer, H.B. 1989, ApJ, 342, L27

Drukier, G.A., Fahlman, G.G., & Richer, H.B. 1992, ApJ, 386, 106

Eggleton, P.P. 1983, ApJ, 268, 368

Frogel, J.A., Persson, S.E., & Cohen, J.G. 1979, ApJ, 227, 499

Gilliland, R.L. 1992, *Astronomical CCD Observing and Reduction Techniques*, ed. S.B. Howell, (San Francisco, A.S.P.), p. 68

Groisman, G. 1989, Master of Science thesis, University of Calgary.

Hardie, R.H. 1962, in *Astronomical Techniques*, ed. W.A. Hiltner, (Chicago, University of Chicago Press), p. 178

Harris, W.E. & Racine, R. 1979, Ann Rev Astron Astrophys, 17, 241

Hesser, J.E., Harris, W.E., VandenBerg, D.A., Allwright, J.W.B., Shott, P., & Stetson,

P.B. 1987, PASP, 99, 739

Heasley, J.N. & Christian, C.A. 1991, in *Formation and Evolution of Star Clusters*, ed. K. Janes (San Francisco, A.S.P.), p. 266

Heggie, D.C. & Aarseth. S.J. 1992, MNRAS, 257, 513

Hills, J.G. 1984, AJ, 89, 1811

Hills, J.G. 1990, AJ, 99, 979

Hodder, P.J.C., Nemec, J.M., Richer, H.B., & Fahlman, G.G. 1992, AJ, 103, 460

Hoyle, F. 1964, R.O.B., No. 82, p. 91

Iben, I., Jr. 1991, ApJS, 76, 55

Iben, I., Jr. & Tutukov, A.V. 1985, ApJS, 58, 661

Janes, K.A. & Heasley, J.N. 1993, PASP, 105, 527

Kallrath, J. & Linnell, A.P. 1987, ApJ, 313, 346

Kallrath, J., Milone, E.F., & Stagg, C.R. 1992, ApJ, 389, 590

Kopal, Z. 1978, *Dynamics of Close Binary Systems*, (Dordrecht, Reidel Publishing)

Landolt, A.U. 1983, AJ, 88, 439

Leonard, P.J.T. & Fahlman, G.G. 1991, AJ, 102, 994

Liller, M.H. & Tokarz, S.P. 1981, AJ, 86, 669

Livio, M, 1993, in *Blue Stragglers*, ed. R. Saffer, (San Francisco, A.S.P.), p. 3

Lucy, L.B. 1967, Zs. Ap., 65, 89

Lucy, L.B. 1976, ApJ, 205, 208

Lucy, L.B. 1979, ApJ, 231, 502

Mateo, M. & Schecter, P.L. 1989, in ESO Conference and Workshop Proceedings 31, 1st ESO/ST-ECF Data Analysis Workshop, eds. P.J. Grosbol, F. Murtagh, & R.H. Harris, (Garching, ESO), p. 69

Mateo, M., Harris, H.C., Nemec, J., & Olszewski, E.W. 1990, AJ, 100, 469

McCrea, W.H. 1964, MNRAS, 128, 147

McMillan, S.L.W. 1991, in *Formation and Evolution of Star Clusters*, ed. K. Janes (San Francisco, A.S.P.), p. 324

Mihalas, D. & Binney, J. 1981, *Galactic Astronomy*, (New York, Freeman & Company)

Milone, E.F. 1993, in *Light Curve Modelling of Eclipsing Binary Stars*, ed. E.F. Milone (New York, Springer-Verlag), p. 1, 195.

Milone, E.F., Groisman, G., Fry, D.J.I., & Bradstreet, D.H. 1991, ApJ, 370, 677

Milone, E.F., Stagg, C.R., & Kurucz, R.L. 1992, ApJS, 79, 123

Milone, E.F., Stagg, C.R., Sugars, B.A., McVean, J.R., Schiller, S.J., & Kallrath, J. 1994, AJ, in press

Murray, W. 1972, *Numerical Methods for Unconstrained Optimization*, (London and New York, Academic)

Nelder, J.A. & Mead, R. 1965, Comput J, 7, 308

Paczynski, B. 1971, Ann Rev Astron Astrophys, 9, 183

Peterson, R.C. & Latham, D.W. 1986, ApJ, 305, 645

Popper, D.M. 1980, Ann Rev Astron Astrophys, 18, 115

Popper, D.M. 1984, AJ, 89, 132

Richer, H.B. & Fahlman, G.G. 1988, ApJ, 325, 218

Richer, H.B. & Fahlman, G.G. 1989, ApJ, 339, 178

Rucinski, S.M. 1973, Acta Astron, 23, 79

Rucinski, S.M. 1974, Acta Astron, 24, 119

Rucinski, S.M. 1993, PASP, 105, 1433

Rucinski, S.M. 1994, AJ, 107, 738

Rucinski, S.M. 1994, PASP, 106, 462

Sawyer Hogg, H. 1973, Pub DDO, 3, No. 6

Schiller, S.J. & Milone, E.F. 1988, AJ, 95, 1466

Sneden, C., Kraft, R.P., Langer, G.E., Prosser, C.F., & Shetrone, M.D. 1994, AJ, 107, 1773

Stagg, C.R. & Milone, E.F. 1993, in *Light Curve Modelling of Eclipsing Binary Stars*, ed. E.F. Milone (New York, Springer-Verlag), p. 75

Stagg, C.R. et al. 1994, in preparation

Strom, S.E. & Strom, K.M. 1970, ApJ, 162, 523

Stryker, L.L. 1993, PASP, 105, 1081

Terrell, D., Gunn, J.B., & Kaiser, D.H. 1994, PASP, 106, 149

Thomas, H.C. 1977, Ann Rev Astron Astrophys, 15, 127

VandenBerg, D.A. & Bell, R.A. 1985, ApJS, 58, 561

VandenBerg, D.A. 1992, ApJ, 391, 685

Van Hamme, W. 1993, AJ, 106, 2096

Vihlu, O. 1982, A&A, 109, 17

Webbink, R.F. 1981, ApJS, 45, 259

Webbink, R.F. 1985, in *Interacting Binary Stars*, ed. J.E. Pringle & R.A. Wade,
    (Cambridge, Cambridge University Press), p 39

Wilson, R.E. 1979, ApJ, 234, 1054

Wilson, R.E. 1990, in *Report of IAU Commision 42*, ed. R.H. Koch, to appear in
    Reports on Astronomy, XXIA (Dordrecht, Kluwer)

Wilson, R.E. 1992, *Documentation of Eclipsing Binary Computer Model*, (Gainesville,
    University of Florida Astronomy Department).

Wilson, R.E. & Devinney, E.J. 1971, ApJ, 166, 605

Yan, L., & Mateo, M. 1994, AJ, in press

Zinn, R, & West, M.J. 1984, ApJS, 55, 45

Zinn, R. 1985, ApJ, 293, 424

Appendix A: Light Curve Data

The following tables contain Yan & Mateo (1994) the I_C and V_J light curves.

TABLE 17a
M71-V1 Light Curves

Phase	V_J	Error	Phase	I_C	Error
0.009493	18.761	0.026	0.000997	17.658	0.025
0.029040	18.761	0.032	0.015041	17.681	0.030
0.068142	18.575	0.029	0.042009	17.594	0.015
0.081221	18.517	0.023	0.043528	17.560	0.023
0.107299	18.402	0.026	0.068119	17.503	0.032
0.115382	18.413	0.028	0.091797	17.393	0.023
0.163034	18.328	0.024	0.094227	17.379	0.027
0.167864	18.308	0.022	0.097363	17.341	0.013
0.174814	18.321	0.023	0.136428	17.272	0.014
0.180959	18.296	0.022	0.138572	17.296	0.016
0.188910	18.276	0.023	0.157076	17.224	0.021
0.191584	18.311	0.023	0.191317	17.191	0.021
0.197878	18.246	0.026	0.198070	17.235	0.024
0.215998	18.278	0.018	0.213478	17.207	0.026
0.220893	18.292	0.027	0.216786	17.207	0.026
0.237362	18.275	0.031	0.237545	17.197	0.025
0.260569	18.275	0.028	0.243584	17.213	0.024
0.274842	18.296	0.027	0.248866	17.207	0.018
0.284997	18.264	0.021	0.261245	17.191	0.029
0.289709	18.292	0.021	0.266321	17.207	0.017
0.296330	18.269	0.018	0.276499	17.202	0.025
0.298390	18.260	0.022	0.296330	17.230	0.027
0.306330	18.310	0.024	0.306092	17.259	0.038
0.316049	18.297	0.023	0.308250	17.191	0.025
0.319350	18.314	0.024	0.313825	17.210	0.028
0.332271	18.337	0.024	0.319333	17.237	0.028
0.337708	18.373	0.025	0.332357	17.220	0.025
0.356111	18.366	0.030	0.336209	17.243	0.017
0.358103	18.366	0.023	0.342308	17.274	0.028
0.358278	18.360	0.026	0.345341	17.281	0.027
0.364933	18.388	0.024	0.350184	17.269	0.017
0.375022	18.413	0.014	0.359602	17.261	0.027
0.376521	18.388	0.021	0.369127	17.310	0.020

TABLE 17a - *Continued*

Phase	V$_J$	Error	Phase	I$_C$	Error
0.378966	18.404	0.019	0.376060	17.306	0.020
0.391729	18.461	0.026	0.379665	17.314	0.026
0.395429	18.455	0.017	0.389413	17.356	0.025
0.401892	18.484	0.026	0.393930	17.366	0.011
0.411522	18.518	0.021	0.398484	17.372	0.028
0.412038	18.527	0.023	0.401657	17.376	0.022
0.412348	18.534	0.019	0.401935	17.368	0.020
0.415825	18.565	0.019	0.414552	17.443	0.029
0.422139	18.686	0.034	0.418289	17.425	0.023
0.424414	18.592	0.021	0.426375	17.463	0.025
0.434732	18.653	0.030	0.427811	17.503	0.021
0.437808	18.663	0.016	0.429636	17.510	0.021
0.442276	18.684	0.020	0.431256	17.496	0.031
0.449665	18.693	0.020	0.447105	17.594	0.029
0.455142	18.766	0.026	0.451651	17.618	0.022
0.467521	18.820	0.023	0.453686	17.619	0.022
0.469929	18.828	0.024	0.454715	17.623	0.015
0.471900	18.844	0.019	0.460333	17.665	0.014
0.472058	18.839	0.020	0.466360	17.639	0.021
0.475535	18.846	0.017	0.475506	17.664	0.033
0.483322	18.844	0.020	0.479562	17.710	0.027
0.494445	18.838	0.022	0.490969	17.685	0.020
0.499427	18.795	0.021	0.492886	17.695	0.021
0.506432	18.829	0.020	0.493594	17.692	0.028
0.514852	18.838	0.017	0.505440	17.711	0.017
0.516073	18.436	0.017	0.506045	17.694	0.026
0.529432	18.830	0.023	0.511364	17.690	0.017
0.531771	18.794	0.025	0.519338	17.718	0.015
0.535248	18.803	0.013	0.524273	17.682	0.030
0.541568	18.750	0.022	0.533304	17.658	0.025
0.542823	18.734	0.028	0.538699	17.632	0.011
0.546557	18.716	0.024	0.548690	17.618	0.016
0.547197	18.717	0.028	0.552754	17.568	0.018
0.552167	18.685	0.017	0.555594	17.556	0.028
0.561954	18.660	0.024	0.559180	17.561	0.022
0.568300	18.593	0.017	0.559395	17.530	0.024
0.572467	18.565	0.032	0.566016	17.515	0.025
0.572573	18.612	0.023	0.571074	17.480	0.025
0.575445	18.578	0.013	0.571516	17.478	0.023

TABLE 17a - *Continued*

Phase	V$_J$	Error	Phase	I$_C$	Error
0.589337	18.501	0.013	0.581106	17.444	0.018
0.589492	18.521	0.030	0.585703	17.415	0.030
0.592969	18.480	0.024	0.598733	17.346	0.017
0.593777	18.487	0.023	0.606411	17.379	0.022
0.594969	18.474	0.021	0.610934	17.355	0.018
0.597549	18.782	0.026	0.611645	17.337	0.022
0.598707	18.497	0.024	0.614519	17.340	0.031
0.609888	18.425	0.028	0.620504	17.320	0.022
0.621091	18.404	0.026	0.628795	17.286	0.023
0.624516	18.405	0.016	0.636809	17.285	0.019
0.630294	18.392	0.021	0.637388	17.288	0.028
0.637110	18.383	0.015	0.644146	17.266	0.017
0.643295	18.382	0.017	0.661724	17.262	0.021
0.647213	18.360	0.021	0.662963	17.273	0.022
0.650257	18.344	0.026	0.666121	17.250	0.020
0.652679	18.326	0.023	0.666250	17.250	0.025
0.666938	18.313	0.024	0.682590	17.206	0.022
0.669598	18.316	0.021	0.686517	17.208	0.030
0.676531	18.299	0.025	0.688907	17.237	0.030
0.684883	18.321	0.017	0.689861	17.223	0.023
0.688016	18.340	0.030	0.691730	17.216	0.031
0.689242	18.290	0.030	0.708465	17.214	0.025
0.706923	18.261	0.021	0.709497	17.198	0.030
0.710400	18.261	0.029	0.713822	17.189	0.021
0.711231	18.273	0.020	0.717671	17.217	0.022
0.712982	18.266	0.027	0.724602	17.195	0.021
0.727319	18.211	0.029	0.725834	17.221	0.020
0.732653	18.263	0.026	0.744238	17.185	0.023
0.741091	18.628	0.023	0.746763	17.187	0.023
0.749718	18.318	0.018	0.750245	17.201	0.017
0.763280	18.271	0.017	0.763914	17.171	0.018
0.766636	18.251	0.039	0.772440	17.185	0.028
0.768124	18.229	0.024	0.792308	17.218	0.030
0.785040	18.248	0.024	0.805940	17.200	0.025
0.785344	18.254	0.026	0.809826	17.193	0.030
0.786805	18.253	0.023	0.824091	17.232	0.018
0.810890	18.276	0.017	0.842334	17.246	0.029
0.824358	18.273	0.027	0.843265	17.264	0.028
0.827834	18.287	0.028	0.849901	17.257	0.026

Table 17a - *Continued*

Phase	V$_J$	Error	Phase	I$_C$	Error
0.832386	18.285	0.013	0.855375	17.251	0.028
0.836865	18.347	0.023	0.863661	17.252	0.021
0.844753	18.308	0.022	0.874417	17.282	0.021
0.863105	18.338	0.028	0.901319	17.356	0.009
0.865160	18.368	0.026	0.902282	17.370	0.019
0.878166	18.336	0.030	0.921382	17.413	0.025
0.884068	18.365	0.025	0.928656	17.449	0.028
0.885555	18.379	0.019	0.947266	17.536	0.013
0.889112	18.445	0.033	0.955492	17.553	0.024
0.902474	18.404	0.022	0.980639	17.663	0.019
0.915386	18.522	0.033	0.985142	17.641	0.031
0.923778	18.502	0.026			
0.942588	18.631	0.034			
0.943276	18.611	0.023			
0.965171	18.695	0.026			
0.968232	18.762	0.028			
0.969957	18.774	0.017			
0.984079	18.754	0.025			

TABLE 17b
M71-V2 Light Curves

Phase	V$_J$	Error	Phase	I$_C$	Error
0.020382	17.873	0.024	0.011651	16.907	0.030
0.038348	17.839	0.019	0.023211	16.959	0.020
0.038762	17.814	0.020	0.069550	16.868	0.015
0.045941	17.860	0.024	0.103894	16.865	0.015
0.079338	17.761	0.026	0.114439	16.869	0.019
0.087734	17.777	0.025	0.118260	16.867	0.020
0.091331	17.825	0.014	0.128293	16.900	0.026
0.094768	17.836	0.026	0.163937	16.879	0.022
0.112383	17.759	0.026	0.177371	16.912	0.026
0.116033	17.766	0.020	0.225191	16.995	0.017
0.121245	17.799	0.030	0.251668	17.068	0.021
0.121918	17.801	0.033	0.257423	17.095	0.016
0.122678	17.836	0.030	0.258629	17.053	0.020
0.136725	17.813	0.028	0.265672	17.078	0.030
0.137095	17.816	0.020	0.276729	17.145	0.023
0.140554	17.761	0.031	0.290133	17.190	0.026

TABLE 17b - *Contintued*

Phase	V_J	Error	Phase	I_C	Error
0.145835	17.832	0.018	0.302228	17.268	0.024
0.164827	17.782	0.023	0.304717	17.236	0.023
0.166557	17.848	0.018	0.310379	17.349	0.017
0.169201	17.853	0.027	0.324584	17.396	0.027
0.170421	17.839	0.019	0.326123	17.404	0.019
0.187688	17.863	0.017	0.348825	17.457	0.025
0.189510	17.853	0.024	0.349571	17.485	0.030
0.195008	17.884	0.023	0.352360	17.456	0.028
0.214442	17.909	0.024	0.376947	17.465	0.013
0.216910	17.907	0.026	0.384436	17.431	0.028
0.219595	17.921	0.015	0.394964	17.477	0.015
0.235399	17.893	0.023	0.409246	17.310	0.029
0.239154	17.975	0.027	0.412509	17.368	0.021
0.240897	17.971	0.017	0.420447	17.308	0.020
0.244181	17.944	0.020	0.434053	17.287	0.020
0.264119	18.039	0.027	0.437095	17.192	0.024
0.270661	18.020	0.022	0.445034	17.192	0.028
0.275228	18.059	0.026	0.458861	17.081	0.032
0.277870	18.086	0.020	0.470849	17.013	0.031
0.280789	18.084	0.031	0.488161	16.996	0.028
0.289967	18.168	0.020	0.514347	16.927	0.025
0.291304	18.143	0.017	0.518794	16.946	0.021
0.299030	18.191	0.017	0.543381	16.936	0.019
0.311634	18.343	0.025	0.559735	16.842	0.027
0.312449	18.285	0.021	0.594447	16.873	0.017
0.314333	18.279	0.022	0.604398	16.862	0.009
0.318296	18.318	0.030	0.627027	16.874	0.014
0.323617	18.323	0.021	0.652025	16.865	0.026
0.326183	18.357	0.021	0.676674	16.903	0.024
0.329600	18.409	0.027	0.701021	16.869	0.021
0.336657	18.389	0.019	0.701136	16.909	0.013
0.339486	18.343	0.031	0.725436	16.893	0.021
0.345677	18.422	0.023	0.737506	16.952	0.019
0.348204	18.409	0.024	0.750089	16.984	0.018
0.360865	18.399	0.031	0.760884	17.035	0.014
0.362080	18.422	0.017	0.781696	17.057	0.027
0.371576	18.461	0.015	0.797102	17.069	0.023
0.372113	18.336	0.026	0.808372	17.213	0.014
0.372791	18.381	0.031	0.848340	17.374	0.022

TABLE 17b - *Continued*

Phase	V_J	Error	Phase	I_C	Error
0.386339	18.454	0.019	0.873368	17.538	0.028
0.386811	18.389	0.017	0.887192	17.430	0.029
0.396699	18.330	0.022	0.932144	17.247	0.018
0.399270	18.308	0.025	0.957276	17.093	0.025
0.402413	18.385	0.019	0.976527	17.041	0.024
0.402887	18.277	0.032			
0.405327	18.326	0.029			
0.416967	18.353	0.022			
0.421694	18.233	0.020			
0.423857	18.247	0.024			
0.443076	18.093	0.025			
0.443550	18.110	0.022			
0.446850	18.072	0.020			
0.449141	18.103	0.021			
0.450336	18.060	0.017			
0.459152	18.076	0.020			
0.459626	18.041	0.011			
0.476813	18.005	0.023			
0.492862	17.936	0.017			
0.497922	17.958	0.022			
0.501400	17.941	0.024			
0.506849	17.902	0.025			
0.513998	17.936	0.020			
0.516362	17.894	0.024			
0.536235	17.880	0.025			
0.537041	17.826	0.017			
0.562578	17.784	0.029			
0.568844	17.867	0.022			
0.573101	17.876	0.022			
0.579798	17.794	0.021			
0.582303	17.783	0.016			
0.605000	17.795	0.025			
0.607465	17.769	0.027			
0.607615	17.761	0.026			
0.614829	17.778	0.019			
0.623549	17.785	0.023			
0.625581	17.824	0.019			
0.626651	17.776	0.028			
0.627947	17.828	0.023			

TABLE 17b - *Continued*

Phase	V_J	Error
0.639448	17.739	0.023
0.648185	17.783	0.026
0.657333	17.758	0.028
0.664381	17.787	0.022
0.666244	17.779	0.022
0.670906	17.779	0.016
0.673344	17.843	0.032
0.682320	17.856	0.023
0.682794	17.846	0.028
0.688905	17.812	0.027
0.691432	17.801	0.016
0.703069	17.817	0.021
0.713364	17.853	0.014
0.715412	17.819	0.021
0.721090	17.855	0.032
0.726302	17.863	0.028
0.737166	17.951	0.029
0.738329	17.887	0.026
0.739530	17.944	0.021
0.759634	17.905	0.020
0.762575	17.930	0.023
0.771301	17.994	0.027
0.771696	17.934	0.028
0.773109	18.043	0.021
0.775936	18.028	0.023
0.778875	18.016	0.016
0.793902	18.104	0.023
0.794376	18.157	0.026
0.796266	18.096	0.023
0.798137	18.163	0.025
0.813353	18.178	0.020
0.818979	18.137	0.020
0.820758	18.202	0.029
0.849222	18.384	0.023
0.857137	18.347	0.018
0.883927	18.329	0.031
0.899823	18.294	0.028
0.905961	18.277	0.028
0.909763	18.248	0.023

TABLE 17b - *Continued*

Phase	V$_J$	Error
0.928816	18.263	0.019
0.928999	18.170	0.023
0.944732	18.068	0.028
0.949089	17.958	0.022
0.950690	18.022	0.018
0.953264	18.046	0.025
0.960808	18.007	0.028
0.981958	17.920	0.020
0.992527	17.941	0.013
0.994003	17.882	0.030
0.998657	17.939	0.021
0.999578	17.909	0.015

TABLE 17c
M71-V3 Light Curves

Phase	V$_J$	Error	Phase	I$_C$	Error
0.004431	19.148	0.018	0.006019	17.772	0.027
0.004607	19.143	0.028	0.023348	17.832	0.021
0.010346	19.188	0.019	0.026944	17.862	0.018
0.012297	19.211	0.032	0.033293	17.822	0.025
0.020220	19.191	0.022	0.037865	17.863	0.022
0.022252	19.193	0.024	0.038041	17.857	0.011
0.027134	19.226	0.021	0.047496	17.911	0.017
0.034494	19.301	0.030	0.049979	17.906	0.031
0.055462	19.296	0.025	0.066936	17.943	0.017
0.058298	19.309	0.017	0.071646	17.978	0.016
0.058641	19.367	0.028	0.073629	17.971	0.022
0.060330	19.332	0.026	0.077443	17.920	0.020
0.061895	19.320	0.034	0.093591	17.964	0.024
0.071093	19.383	0.023	0.093767	17.975	0.015
0.075943	19.350	0.024	0.099509	18.007	0.017
0.077978	19.394	0.023	0.109628	17.962	0.016
0.084648	19.428	0.026	0.121033	17.968	0.028
0.088206	19.418	0.024	0.123657	17.935	0.017
0.098185	19.374	0.032	0.124016	17.928	0.020
0.112511	19.370	0.022	0.149314	17.856	0.018
0.115880	19.361	0.021	0.149490	17.851	0.016
0.116055	19.374	0.021	0.149660	17.855	0.013

TABLE 17c - *Continued*

Phase	V_J	Error	Phase	I_C	Error
0.127931	19.361	0.034	0.154024	17.844	0.025
0.131085	19.309	0.022	0.155702	17.866	0.019
0.131669	19.350	0.031	0.166737	17.817	0.023
0.131845	19.324	0.031	0.166884	17.799	0.030
0.136659	19.338	0.025	0.173808	17.795	0.016
0.142768	19.304	0.024	0.184903	17.774	0.015
0.146305	19.278	0.028	0.197958	17.776	0.021
0.160806	19.231	0.023	0.200770	17.755	0.014
0.169747	19.184	0.024	0.203181	17.752	0.023
0.169922	19.186	0.014	0.203357	17.772	0.018
0.172768·	19.198	0.027	0.209107	17.753	0.035
0.179944	19.179	0.032	0.209174	17.761	0.021
0.184954	19.208	0.021	0.211315	17.744	0.016
0.185536	19.141	0.026	0.212395	17.733	0.026
0.185711	19.177	0.021	0.218465	17.758	0.027
0.189026	19.137	0.023	0.223962	17.779	0.025
0.189207	19.157	0.021	0.231371	17.772	0.024
0.196977	19.161	0.033	0.242613	17.746	0.022
0.210960	19.190	0.033	0.243617	17.736	0.021
0.221247	19.137	0.023	0.248110	17.733	0.019
0.222133	19.160	0.029 ·	0.255180	17.712	0.027
0.223613	19.152	0.032	0.256482	17.709	0.028
0.225645	19.148	0.015	0.257223	17.727	0.020
0.233480	19.124	0.018	0.258769	17.759	0.021
0.233787	19.129	0.029	0.274117	17.720	0.020
0.235108	19.169	0.020	0.285336	17.729	0.019
0.241259	19.143	0.034	0.286124	17.735	0.022
0.241434	19.142	0.022	0.287841	17.750	0.023
0.261115	19.152	0.029	0.298264	17.720	0.022
0.264670	19.137	0.021	0.298830	17.717	0.019
0.270936	19.130	0.022	0.309484	17.723	0.017
0.277036	19.105	0.023	0.310469	17.712	0.021
0.278370	19.137	0.028	0.311090	17.734	0.023
0.279512	19.123	0.014	0.311245	17.727	0.020
0.287118	19.128	0.031	0.313812	17.684	0.022
0.287747	19.116	0.029	0.329000	17.718	0.014
0.295301	19.126	0.031	0.333632	17.713	0.013
0.299636	19.155	0.029	0.333731	17.755	0.031
0.311266	19.128	0.029	0.347528	17.716	0.016

TABLE 17c - *Continued*

Phase	V_J	Error	Phase	I_C	Error
0.317404	19.075	0.028	0.357779	17.713	0.014
0.320500	19.117	0.029	0.357940	17.766	0.028
0.323196	19.093	0.025	0.358673	17.685	0.030
0.333381	19.125	0.019	0.368672	17.714	0.018
0.349168	19.137	0.031	0.371552	17.722	0.028
0.349960	19.114	0.021	0.371879	17.719	0.016
0.359508	19.159	0.032	0.381927	17.716	0.016
0.363843	19.111	0.029	0.385089	17.719	0.025
0.364211	19.110	0.024	0.385911	17.714	0.020
0.389105	19.123	0.025	0.398356	17.748	0.019
0.393055	19.161	0.021	0.405388	17.709	0.027
0.393469	19.136	0.023	0.406074	17.736	0.020
0.397010	19.123	0.035	0.409052	17.725	0.027
0.404894	19.107	0.020	0.422539	17.712	0.028
0.407644	19.138	0.021	0.429196	17.746	0.029
0.417245	19.131	0.026	0.429312	17.737	0.018
0.421094	19.174	0.036	0.430225	17.735	0.020
0.428859	19.117	0.034	0.442316	17.732	0.021
0.441021	19.182	0.035	0.451674	17.736	0.034
0.442316	19.149	0.025	0.456229	17.782	0.027
0.442971	19.126	0.019	0.457254	17.759	0.021
0.444934	19.173	0.027	0.472378	17.751	0.013
0.452789	19.162	0.021	0.474088	17.758	0.025
0.458760	19.149	0.025	0.476406	17.752	0.018
0.464110	19.132	0.031	0.480376	17.797	0.019
0.469175	19.179	0.027	0.481340	17.763	0.020
0.473439	19.168	0.023	0.486026	17.780	0.021
0.486026	19.224	0.019	0.496939	17.785	0.026
0.493662	19.226	0.033	0.502668	17.786	0.019
0.495103	19.159	0.019	0.504220	17.804	0.022
0.495791	19.144	0.022	0.516812	17.819	0.023
0.496838	19.152	0.023	0.526866	17.832	0.025
0.517270	19.179	0.030	0.528674	17.875	0.017
0.517933	19.277	0.035	0.529553	17.853	0.014
0.518021	19.215	0.019	0.530223	17.853	0.028
0.534916	19.210	0.031	0.540992	17.856	0.024
0.538266	19.270	0.018	0.550705	17.871	0.017
0.542452	19.276	0.037	0.552822	17.896	0.019
0.549836	19.306	0.024	0.554836	17.907	0.017

TABLE 17c - *Continued*

Phase	V_J	Error	Phase	I_C	Error
0.551253	19.288	0.024	0.559471	17.897	0.016
0.562604	19.316	0.025	0.571911	17.930	0.024
0.567838	19.306	0.031	0.572924	17.946	0.018
0.581297	19.345	0.021	0.579880	17.950	0.021
0.591769	19.304	0.036	0.585575	17.952	0.023
0.593922	19.343	0.022	0.595546	17.940	0.021
0.594996	19.374	0.026	0.603062	17.906	0.019
0.607184	19.375	0.030	0.603348	17.938	0.019
0.616473	19.373	0.038	0.615563	17.905	0.022
0.624238	19.290	0.026	0.616728	17.959	0.031
0.638645	19.362	0.027	0.619693	17.898	0.028
0.642899	19.268	0.023	0.635453	17.874	0.018
0.648517	19.266	0.040	0.643841	17.855	0.036
0.666836	19.169	0.026	0.645970	17.837	0.014
0.672665	19.228	0.041	0.660620	17.785	0.025
0.687819	19.153	0.026	0.662450	17.853	0.030
0.697213	19.113	0.036	0.664786	17.752	0.021
0.709621	19.094	0.032	0.684987	17.754	0.027
0.721920	19.125	0.031	0.688351	17.739	0.014
0.727770	19.161	0.022	0.706038	17.808	0.019
0.731382	19.091	0.022	0.707410	17.715	0.014
0.752591	19.087	0.032	0.709093	17.730	0.017
0.756608	19.074	0.021	0.709351	17.694	0.031
0.767603	19.059	0.021	0.731014	17.714	0.022
0.781189	19.079	0.019	0.733716	17.693	0.018
0.785424	19.071	0.022	0.734782	17.712	0.024
0.797603	19.089	0.029	0.749532	17.730	0.025
0.801038	19.040	0.022	0.751814	17.691	0.021
0.801213	19.074	0.030	0.763136	17.692	0.015
0.821783	19.067	0.025	0.809584	17.680	0.026
0.840974	19.041	0.018	0.818683	17.673	0.017
0.841527	19.034	0.019	0.818859	17.641	0.037
0.846270	19.096	0.031	0.834135	17.672	0.029
0.849710	19.063	0.026	0.858344	17.693	0.019
0.856761	19.034	0.026	0.862703	17.692	0.021
0.870357	19.084	0.032	0.871413	17.681	0.024
0.875277	19.112	0.024	0.874409	17.651	0.022
0.883941	19.053	0.023	0.874585	17.667	0.022
0.892712	19.074	0.027	0.882369	17.676	0.024

TABLE 17c - *Continued*

Phase	V$_J$	Error	Phase	I$_C$	Error
0.894378	19.044	0.030	0.905117	17.693	0.017
0.895014	19.079	0.018	0.906236	17.683	0.021
0.896697	19.041	0.021	0.913888	17.673	0.029
0.910803	19.092	0.024	0.924899	17.690	0.023
0.911897	19.069	0.024	0.928276	17.682	0.015
0.912487	19.074	0.024	0.930308	17.690	0.011
0.918898	19.064	0.032	0.930447	17.681	0.019
0.919860	19.134	0.022	0.944813	17.743	0.025
0.926416	19.118	0.025	0.947841	17.725	0.019
0.937901	19.097	0.025	0.949046	17.718	0.019
0.950564	19.071	0.026	0.963111	17.725	0.019
0.950740	19.106	0.023	0.963759	17.713	0.021
0.951281	19.149	0.028	0.973197	17.739	0.016
0.962051	19.087	0.022	0.982142	17.733	0.018
0.963111	19.099	0.023	0.984174	17.720	0.010
0.966299	19.125	0.031	0.987690	17.756	0.015
0.966353	19.088	0.022	0.988868	17.765	0.031
0.966529	19.088	0.014	0.990594	17.791	0.022
0.975800	19.078	0.032	0.999201	17.759	0.018
0.984595	19.122	0.028			
0.986199	19.130	0.019			
0.999854	19.152	0.035			

TABLE 17d
M71-V4 Light Curves

Phase	V$_J$	Error	Phase	I$_C$	Error
0.008237	17.881	0.021	0.004091	17.026	0.021
0.018700	17.871	0.026	0.023678	17.035	0.027
0.024619	17.892	0.019	0.025320	17.023	0.025
0.025320	17.873	0.026	0.030362	17.045	0.027
0.026911	17.872	0.020	0.031570	17.064	0.031
0.038207	17.868	0.018	0.033266	17.035	0.017
0.039971	17.903	0.031	0.046595	17.034	0.021
0.046553	17.874	0.032	0.053648	17.024	0.027
0.051260	17.873	0.021	0.054704	17.031	0.027
0.054704	17.882	0.019	0.062829	17.033	0.021
0.057167	17.855	0.022	0.080310	17.030	0.025
0.063122	17.872	0.020	0.083963	17.026	0.016

TABLE 17d - *Continued*

Phase	V_J	Error	Phase	I_C	Error
0.068175	17.862	0.022	0.096542	17.011	0.021
0.073736	17.876	0.020	0.097021	17.036	0.018
0.082412	17.874	0.017	0.106489	17.046	0.032
0.098551	17.867	0.017	0.111527	17.018	0.014
0.111047	17.882	0.027	0.113119	17.003	0.018
0.111195	17.871	0.022	0.123058	17.006	0.026
0.120223	17.873	0.027	0.129010	17.038	0.028
0.127956	17.868	0.015	0.142565	17.027	0.032
0.130836	17.879	0.026	0.143948	17.035	0.017
0.138041	17.915	0.023	0.145242	17.029	0.021
0.139809	17.876	0.016	0.154189	17.011	0.026
0.148655	17.879	0.016	0.159269	17.045	0.018
0.157298	17.872	0.021	0.173301	17.020	0.021
0.157683	17.880	0.019	0.173963	17.033	0.024
0.168297	17.882	0.012	0.190195	17.033	0.016
0.168694	17.896	0.018	0.190319	17.055	0.021
0.174252	17.873	0.026	0.202602	17.038	0.024
0.182266	17.895	0.021	0.206428	17.049	0.026
0.184866	17.890	0.022	0.206824	17.071	0.020
0.193894	17.905	0.021	0.223098	17.082	0.017
0.195106	17.878	0.014	0.231840	17.070	0.018
0.198520	17.890	0.022	0.237852	17.142	0.014
0.205756	17.877	0.025	0.239248	17.125	0.013
0.214981	17.929	0.031	0.253830	17.201	0.023
0.217211	17.894	0.015	0.255292	17.157	0.029
0.221077	17.911	0.021	0.266573	17.220	0.024
0.223617	17.918	0.022	0.271568	17.185	0.013
0.231173	17.937	0.030	0.291288	17.190	0.023
0.243216	17.936	0.023	0.293960	17.219	0.016
0.246674	17.957	0.023	0.310047	17.202	0.020
0.247321	17.940	0.017	0.327499	17.152	0.020
0.252170	17.960	0.021	0.336436	17.154	0.024
0.258535	17.978	0.024	0.346632	17.135	0.023
0.263804	17.965	0.024	0.367819	17.073	0.029
0.268813	18.020	0.017	0.375331	17.106	0.020
0.279427	17.992	0.019	0.394787	17.026	0.024
0.285382	18.015	0.023	0.474840	17.015	0.034
0.285572	17.989	0.024	0.487502	17.033	0.032
0.295996	18.001	0.026	0.493977	16.964	0.025

TABLE 17d - *Continued*

Phase	V_J	Error	Phase	I_C	Error
0.302055	17.997	0.017	0.509292	17.001	0.029
0.305024	17.996	0.016	0.522799	16.954	0.018
0.309902	17.985	0.028	0.525566	17.024	0.019
0.315638	17.992	0.019	0.534555	17.009	0.025
0.318225	17.991	0.025	0.543817	17.024	0.028
0.321593	18.005	0.021	0.559925	17.022	0.015
0.332207	17.985	0.024	0.560997	17.032	0.018
0.342482	17.962	0.016	0.576162	17.022	0.028
0.353096	17.934	0.018	0.592328	17.034	0.025
0.357804	17.934	0.024	0.608519	17.031	0.025
0.359931	17.925	0.021	0.639597	17.028	0.032
0.360930	17.920	0.024	0.650912	17.022	0.028
0.369665	17.921	0.031	0.657926	17.057	0.024
0.373436	17.897	0.024	0.669212	17.045	0.030
0.389307	17.886	0.020	0.674761	17.067	0.022
0.389755	17.878	0.020	0.690537	17.081	0.020
0.410229	17.887	0.025	0.699076	17.096	0.026
0.414906	17.852	0.021	0.700201	17.139	0.020
0.422281	17.873	0.026	0.712119	17.136	0.024
0.425518	17.879	0.022	0.728754	17.141	0.019
0.439864	17.914	0.021	0.729037	17.228	0.029
0.450960	17.882	0.020	0.739821	17.299	0.016
0.452364	17.894	0.025	0.745417	17.351	0.030
0.462978	17.868	0.022	0.756054	17.481	0.023
0.472788	17.868	0.025	0.758057	17.374	0.025
0.479554	17.887	0.025	0.764676	17.427	0.027
0.488575	17.853	0.021	0.772289	17.659	0.020
0.499189	17.878	0.019	0.778174	17.683	0.033
0.524786	17.879	0.015	0.788879	17.696	0.027
0.536889	17.878	0.026	0.789769	17.731	0.019
0.538521	17.869	0.016	0.800575	17.718	0.025
0.550383	17.884	0.021	0.803765	17.720	0.020
0.551830	17.874	0.028	0.806002	17.739	0.024
0.557888	17.857	0.019	0.819473	17.716	0.024
0.565859	17.880	0.023	0.820081	17.652	0.028
0.568020	17.873	0.021	0.828037	17.662	0.031
0.584046	17.881	0.024	0.835003	17.478	0.024
0.592853	17.874	0.021	0.838469	17.461	0.024
0.595126	17.880	0.021	0.849110	17.434	0.029

TABLE 17d - *Continued*

Phase	V$_J$	Error	Phase	I$_C$	Error
0.600342	17.868	0.028	0.853420	17.317	0.017
0.609086	17.896	0.024	0.856755	17.345	0.031
0.616803	17.875	0.023	0.857199	17.270	0.017
0.622823	17.859	0.019	0.870962	17.241	0.029
0.624033	17.895	0.026	0.873432	17.154	0.023
0.633118	17.880	0.030	0.886721	17.140	0.030
0.649601	17.878	0.030	0.888696	17.114	0.025
0.654040	17.878	0.019	0.890913	17.100	0.016
0.666666	17.938	0.027	0.901118	17.120	0.026
0.671357	17.889	0.027	0.907145	17.103	0.020
0.682753	17.900	0.028	0.913086	17.075	0.021
0.685799	17.911	0.024	0.916209	17.081	0.021
0.699360	17.923	0.019	0.923380	17.068	0.021
0.713978	17.923	0.031	0.929236	17.062	0.022
0.720900	18.013	0.020	0.936689	17.061	0.021
0.731081	18.080	0.018	0.936711	17.035	0.026
0.737133	18.168	0.033	0.940861	17.060	0.028
0.742698	18.087	0.021	0.945552	17.052	0.021
0.743946	18.194	0.021	0.951981	17.059	0.017
0.746007	18.092	0.018	0.957093	17.046	0.020
0.748562	18.236	0.017	0.963636	17.052	0.025
0.753636	18.300	0.031	0.965431	17.047	0.021
0.764796	18.435	0.025	0.967986	17.064	0.023
0.770244	18.527	0.035	0.974576	17.039	0.019
0.772668	18.411	0.024	0.981664	17.045	0.016
0.780971	18.476	0.022	0.990808	17.046	0.025
0.781029	18.611	0.022	0.994065	17.035	0.016
0.795607	18.657	0.030	0.994110	17.057	0.021
0.797262	18.648	0.021	0.995769	17.039	0.029
0.803886	18.647	0.023			
0.811881	18.611	0.022			
0.813494	18.617	0.021			
0.828197	18.432	0.029			
0.829727	18.397	0.024			
0.833854	18.498	0.019			
0.843020	18.345	0.021			
0.847209	18.214	0.028			
0.861599	18.077	0.017			
0.863823	18.157	0.027			

TABLE 17d - *Continued*

Phase	V_J	Error
0.865940	18.058	0.029
0.871738	18.074	0.022
0.873376	17.981	0.033
0.880892	17.966	0.023
0.882172	17.952	0.017
0.896729	17.919	0.024
0.898405	17.921	0.023
0.901622	17.933	0.025
0.904594	17.900	0.033
0.914638	17.929	0.030
0.921140	17.896	0.011
0.921415	17.923	0.030
0.930901	17.906	0.025
0.932120	17.907	0.029
0.943969	17.905	0.027
0.948299	17.896	0.023
0.948353	17.904	0.028
0.959952	17.900	0.027
0.960119	17.898	0.020
0.965835	17.909	0.023
0.967159	17.903	0.021
0.975935	17.907	0.027
0.978267	17.890	0.022
0.983316	17.909	0.025
0.989503	17.871	0.025
0.996066	17.885	0.017
0.999549	17.905	0.021

TABLE 17e
M71-V5 Light Curves

Phase	V_J	Error	Phase	I_C	Error
0.022329	17.926	0.021	0.002499	16.981	0.022
0.024638	17.926	0.027	0.004806	16.971	0.018
0.031303	17.924	0.026	0.012418	17.002	0.019
0.036346	17.934	0.022	0.016613	16.957	0.022
0.045896	18.017	0.032	0.018658	16.972	0.013
0.056203	17.910	0.024	0.036346	16.965	0.020
0.062101	17.903	0.024	0.041928	16.932	0.031
0.069360	17.910	0.017	0.042695	16.952	0.028
0.082806	18.102	0.024	0.045839	16.937	0.028
0.095520	17.938	0.029	0.062205	16.952	0.023
0.101790	17.900	0.029	0.065014	16.961	0.019
0.108791	18.015	0.026	0.076005	16.977	0.026
0.132593	17.956	0.032	0.082218	16.914	0.029
0.136151	17.980	0.026	0.089046	16.939	0.023
0.141162	18.027	0.027	0.104502	16.955	0.026
0.147187	17.897	0.019	0.111993	16.956	0.027
0.148106	18.005	0.020	0.116635	16.984	0.025
0.180707	18.166	0.015	0.121876	16.953	0.027
0.182383	18.014	0.032	0.126821	16.946	0.030
0.187595	18.075	0.024	0.128648	16.969	0.023
0.196974	18.038	0.026	0.149140	16.974	0.026
0.220423	18.132	0.017	0.161048	16.988	0.016
0.226937	18.103	0.030	0.161780	17.029	0.027
0.231876	18.094	0.025	0.167936	17.019	0.014
0.245434	18.127	0.024	0.200480	17.048	0.025
0.248480	18.175	0.035	0.207565	17.096	0.021
0.266769	18.235	0.022	0.211276	17.089	0.028
0.269468	18.186	0.021	0.247197	17.203	0.030
0.271362	18.208	0.026	0.250761	17.172	0.031
0.283674	18.249	0.023	0.257451	17.182	0.025
0.291790	18.261	0.022	0.264789	17.238	0.028
0.298267	18.302	0.018	0.279770	17.259	0.023
0.312450	18.289	0.025	0.291963	17.281	0.025
0.314109	18.314	0.022	0.302091	17.311	0.026
0.333461	18.262	0.030	0.314576	17.321	0.019
0.336428	18.301	0.022	0.326126	17.326	0.019
0.352346	18.237	0.031	0.332507	17.292	0.023
0.352707	18.265	0.026	0.348445	17.350	0.031

TABLE 17e - *Continued*

Phase	V_J	Error	Phase	I_C	Error
0.358747	18.270	0.025	0.355585	17.293	0.017
0.368655	18.195	0.026	0.370764	17.262	0.021
0.376588	18.178	0.024	0.372850	17.225	0.009
0.381066	18.213	0.014	0.378180	17.244	0.030
0.392880	18.139	0.029	0.383248	17.221	0.026
0.398781	18.171	0.028	0.393085	17.205	0.026
0.405103	18.148	0.029	0.405946	17.124	0.016
0.427177	18.062	0.026	0.417666	17.087	0.029
0.430855	18.080	0.031	0.418838	17.144	0.023
0.432260	18.035	0.021	0.439130	17.081	0.029
0.433281	18.033	0.019	0.441157	17.074	0.028
0.448569	18.006	0.025	0.447580	17.060	0.017
0.453174	18.042	0.020	0.453337	17.043	0.021
0.457318	18.009	0.030	0.461506	17.045	0.030
0.463162	17.987	0.023	0.465192	17.036	0.024
0.467923	17.988	0.025	0.468534	17.032	0.026
0.473424	17.974	0.023	0.479471	16.984	0.033
0.475493	17.998	0.015	0.486598	17.008	0.019
0.479693	17.976	0.031	0.487511	17.018	0.025
0.489219	18.016	0.026	0.487926	17.005	0.018
0.497617	17.946	0.027	0.490967	16.997	0.026
0.497812	17.969	0.016	0.493451	16.962	0.030
0.500074	17.966	0.019	0.500292	17.008	0.025
0.502126	17.946	0.027	0.508747	16.980	0.026
0.511567	17.964	0.029	0.511483	16.970	0.021
0.513192	17.939	0.026	0.522984	16.978	0.019
0.514665	17.936	0.032	0.530977	16.997	0.031
0.519876	17.955	0.029	0.533867	16.958	0.031
0.521849	17.943	0.026	0.536806	16.946	0.022
0.534200	17.928	0.024	0.545360	16.957	0.021
0.541911	17.931	0.019	0.553298	16.939	0.024
0.544168	17.924	0.023	0.556185	16.952	0.023
0.548052	17.939	0.027	0.563676	16.961	0.030
0.551577	17.908	0.022	0.567565	16.959	0.029
0.554710	17.909	0.024	0.575560	16.937	0.017
0.556462	17.942	0.024	0.580222	16.966	0.020
0.564316	17.936	0.029	0.585308	16.942	0.032
0.566171	17.889	0.018	0.589624	16.957	0.015
0.568205	17.920	0.028	0.596707	16.970	0.025

TABLE 17e - *Continued*

Phase	V$_J$	Error	Phase	I$_C$	Error
0.574578	17.908	0.019	0.598116	16.965	0.020
0.578665	17.931	0.030	0.602541	16.912	0.031
0.586949	17.936	0.030	0.603817	16.975	0.021
0.589800	17.890	0.024	0.610801	16.943	0.022
0.592240	17.913	0.015	0.612002	16.975	0.026
0.596354	17.871	0.031	0.618843	16.967	0.018
0.601328	17.938	0.027	0.620742	16.966	0.019
0.601365	17.905	0.017	0.630551	17.001	0.029
0.609382	17.993	0.020	0.633847	16.952	0.020
0.614559	17.919	0.024	0.641048	16.988	0.027
0.615958	17.953	0.025	0.642791	17.002	0.017
0.618289	17.938	0.029	0.643491	16.990	0.019
0.629916	17.983	0.023	0.655323	17.027	0.018
0.631258	17.962	0.022	0.664910	17.039	0.029
0.632044	17.976	0.022	0.666638	17.028	0.016
0.641009	17.965	0.028	0.672321	17.029	0.027
0.651152	17.965	0.021	0.688329	17.073	0.012
0.653921	17.992	0.019	0.692032	17.039	0.023
0.655508	18.005	0.021	0.694326	17.071	0.025
0.661305	18.057	0.022	0.701192	17.095	0.026
0.665745	17.954	0.031	0.706826	17.125	0.026
0.675923	18.036	0.016	0.718002	17.131	0.017
0.676153	18.020	0.030	0.732663	17.120	0.022
0.677627	18.006	0.020	0.733560	17.203	0.034
0.683281	18.044	0.014	0.741263	17.181	0.022
0.690517	18.073	0.021	0.744341	17.216	0.027
0.700460	18.069	0.023	0.755978	17.188	0.024
0.700939	18.068	0.024	0.758331	17.251	0.018
0.705256	18.062	0.025	0.763785	17.235	0.026
0.717248	18.095	0.029	0.773063	17.235	0.020
0.730077	18.129	0.029	0.776581	17.291	0.026
0.732663	18.047	0.031	0.778297	17.241	0.032
0.733496	18.147	0.024	0.785063	17.336	0.025
0.752396	18.242	0.022	0.786304	17.307	0.029
0.752806	18.152	0.027	0.808823	17.326	0.025
0.754161	18.191	0.019	0.809834	17.352	0.022
0.757009	18.207	0.021	0.813293	17.311	0.016
0.768754	18.209	0.024	0.815782	17.337	0.020
0.773063	18.281	0.029	0.817785	17.321	0.028

TABLE 17e - *Continued*

Phase	V_J	Error	Phase	I_C	Error
0.775085	18.270	0.023	0.834850	17.338	0.035
0.777214	18.298	0.027	0.840104	17.287	0.033
0.791807	18.310	0.031	0.853379	17.287	0.025
0.796210	18.300	0.022	0.855271	17.277	0.024
0.797921	18.355	0.023	0.859622	17.254	0.010
0.818541	18.339	0.026	0.862423	17.273	0.026
0.828719	18.302	0.024	0.884742	17.211	0.022
0.833350	18.316	0.022	0.893867	17.195	0.026
0.835468	18.312	0.027	0.894786	17.185	0.027
0.843313	18.249	0.014	0.907061	17.158	0.020
0.853735	18.241	0.019	0.909409	17.105	0.022
0.870044	18.257	0.032	0.929379	17.089	0.025
0.873780	18.202	0.031	0.936126	17.062	0.025
0.878507	18.158	0.024	0.951592	17.060	0.019
0.894816	18.126	0.022	0.951701	17.067	0.022
0.914124	18.142	0.028	0.963011	17.030	0.020
0.914845	18.113	0.024	0.965347	17.050	0.030
0.930010	18.069	0.028	0.975735	17.033	0.025
0.931533	18.051	0.020	0.976413	17.001	0.026
0.943325	18.044	0.023	0.990850	17.004	0.015
0.945548	17.960	0.019	0.998054	16.995	0.028
0.946321	17.982	0.028			
0.971278	17.984	0.018			
0.981515	17.936	0.017			
0.983070	17.974	0.027			
0.985006	17.952	0.025			
0.996109	17.945	0.017			
0.996499	17.942	0.021			

Appendix B: Sample LC Input File

The following is and example of an LC input file for the University of Calgary enhanced

Wilson-Devinney light curve analysis program.

```
1
 4.351  4.300
Vfm10
Ifm10
END
0 1 1 1 1 1 1 2
03 0 1 1 30 30 .34890E00 .0000 1000.000 .250 +000.0000 +001.2000 000.01
.0000  90.00 002.490 +1.000 +1.000  0.0000 0.5003 +84.545 00.320 00.320
0.5460 0.5333 +0.500 +0.500 02.5007 02.5495 00.32970 0.527 0.527 0.000 0.000
 0.5500 09.0847 03.5317 0.674 0.677 0.000 0.000 0.0000 +0.000 1.0000
 90.80 081.10 011.15 000.913
300.
300.
0 1 1 1 1 1 1 2
03 0 1 1 30 30 .34890E00 .0000 1000.000 .250 +000.0000 +001.2000 000.01
.0000  90.00 002.490 +1.000 +1.000  0.0000 0.5003 +84.545 00.320 00.320
0.5460 0.5333 +0.500 +0.500 02.5007 02.5495 00.32970 0.527 0.527 0.000 0.000
 0.7900 09.1980 03.5017 0.492 0.492 0.000 0.000 0.0000 +0.000 1.0000
 90.80 081.10 011.15 000.913
300.
300.
9
```

Appendix C: Sample Flux File

The following is an example of a flux file, which required for the University of Calgary

enhanced version of the Wilson-Devinney light curve analysis program.

```
FILTER: Vfm03  WAVELENGTH: .5500
model   ratio of PHOTON flux: star/BB
  0 .61276 .60646 .59230 .58286 .56291 .55037 .60535 .71653
  8 .77958 .80226 .80677 .78303 .79312 .79479 .79931 .79076
 16 .77875 .76910 .78911 .84582 .88258 .89510 .88348 .89480
 24 .89926 .89898 .90286 .89748 .88901 .87975 .88235 .90736
 32 .93150 .95352 .96407 .96792 .97333 .97036 .96597 .95956
 40 .95179 .94300 .93969 .94903 1.00308 1.01093 1.01853 1.01901
 48 1.01478 1.01110 1.00541 .99919 .99228 .98478 .98030 1.03977
 56 1.04744 1.04871 1.04588 1.04273 1.03872 1.03429 1.02964 1.02478
 64 1.01926 1.01382 1.06962 1.06835 1.06642 1.06268 1.05846 1.05411
 72 1.05041 1.04692 1.04379 1.04045 1.03707 1.09101 1.08492 1.07931
 80 1.07319 1.06743 1.06229 1.05788 1.05445 1.05232 1.05091 1.04990
 88 1.11352 1.09738 1.08904 1.08042 1.07375 1.06602 1.06050 1.05623
 96 1.05392 1.05295 1.05335 1.12763 1.11519 1.09655 1.08676 1.07752
104 1.06838 1.06144 1.05578 1.05214 1.05042 1.05096 1.13680 1.12597
112 1.11317 1.09354 1.08246 1.07198 1.06246 1.05488 1.04934 1.04604
120 1.04526 1.13328 1.12389 1.11094 1.08967 1.07759 1.06605 1.05571
128 1.04734 1.04164 1.03879 1.13702 1.13147 1.12239 1.10870 1.08582
136 1.07260 1.05970 1.04813 1.03919 1.03321 1.14290 1.13614 1.13128
144 1.12138 1.10588 1.08133 1.06634 1.05204 1.03957 1.02980 1.14861
152 1.14306 1.13815 1.13107 1.11927 1.10162 1.07649 1.05973 1.04396
160 1.03045 1.15381 1.14859 1.14437 1.13760 1.12990 1.11529 1.09544
168 1.06989 1.05164 1.03496 1.15731 1.15052 1.14857 1.14401 1.13606
176 1.12645 1.10907 1.08213 1.06184 1.04211 1.14803 1.14817 1.14683
184 1.14127 1.13168 1.11981 1.09969 1.07344 1.05142 1.13640 1.14163
192 1.14337 1.14138 1.13445 1.12379 1.10974 1.08746 1.06152 1.10942
200 1.12839 1.13339 1.13489 1.13209 1.12384 1.11243 1.09668 1.07252
208 1.06775 1.10950 1.11823 1.12206 1.12243 1.11844 1.10906 1.09820
216 1.08059 1.08637 1.09956 1.10506 1.10764 1.10698 1.10173 1.09188
224 1.08216 1.06168 1.07965 1.08635 1.08995 1.09128 1.08923 1.08244
232 1.06981 1.05942 1.06707 1.07100 1.07316 1.07309 1.06956 1.06125
240 1.03952 1.04795 1.05183 1.05414 1.05523 1.05388 1.04887 1.02067
248 1.02938 1.03310 1.03540 1.03680 1.03687 1.03411 1.00291 1.01185
```

256	1.01518	1.01706	1.01866	1.01942	1.01800	.96994	.97946	.98206
264	.98275	.98341	.98444	.98503	.95012	.95242	.95224	.95176
272	.95200	.95279	.92314	.92547	.92488	.92361	.92287	.92305
280	.89837	.90080	.90013	.89848	.89702	.89641	.87589	.87821
288	.87753	.87583	.87402	.87280	.85581	.85770	.85690	.85527
296	.85342	.85189	.81361	.82266	.82274	.82116	.81944	.81785
304	.81638	.79843	.79561	.79241	.79004	.78844	.78728	.78144
312	.77544	.77001	.76639	.76429	.76321	.77080	.76141	.75330
320	.74796	.74495	.74354	.76580	.75266	.74160	.73423	.72997
328	.72786	.76538	.74855	.73417	.72450	.71876	.71575	.74858
336	.73058	.71843	.71099	.70687	.75165	.73033	.71552	.70623
344	.70091	.75694	.73284	.71539	.70412	.69745	.76346	.73746
352	.71776	.70447	.69640	.77179	.74338	.72200	.70701	.69749
360	.78429	.75046	.72768	.71143	.70061	.80150	.75952	.73451
368	.71734	.70556	.77187	.74284	.72445	.71202	.78806	.75347
376	.73300	.71996	.80613	.76702	.74362	.72938	.82280	.78307
384	.75655	.74057	.83523	.79971	.77136	.75361	.81577	.78686
392	.76781	.82817	.80249	.78242	.83675	.81556	.79703	.84127
400	.82579	.80923	.83656	.82907	.82893	.82997	.81897	.80579
408	.79399	.78376	.00000	.00000	.00000	.00000	.00000	.00000

Appendix D: Sample DC Input file

The following is and example of an DC input file for the University of Calgary enhanced

Wilson-Devinney light curve analysis program.

```
2
 4.400  4.360
Vfm03
Ifm03
END
 .5E+01 .5E+01 .3E+01 .3E-01 .5E+01 .5E+01 .3E+01 .3E-01
 .1E-01 .1E+00 .1E+00 .1E+00 .2E-02 -.1E+01 .1E-01 .1E-01 .1E-01 .1E-01 .
 .1E-01 .1E-01 .1E-01 .1E-01 .1E-01 .1E-01 .1E-01 .1E-01 .1E-01
 1111 1111 1111101 01110 11010 01111 0 1 1
   1 1 2 1
0 0 02 2 0 0 1 1 1 1 1 1 1
03 0 1 1 30 30 15 15 .34890E00 .0000 1000.000
 .0000  90.00 002.490 +1.000 +1.000  0.0000 0.4995 +84.848 01.000 01.000
0.5460 0.5152 +1.000 +1.000 02.5455 02.3790 00.32814 0.520 0.534 0.000 0.000
 0.5500 09.6036 03.5317 0.647 0.711 0.000 0.000 0.0000 0 0.0090
 0.7900 09.5741 03.5017 0.471 0.516 0.000 0.000 0.0000 0 0.0090
 300.
 300.
.0095 0.6304 57 .3377 0.9012 20 .4755 0.5829 29 .5987 0.8039 21 .7681 1.0290 21
.0290 0.6304 48 .3561 0.9070 17 .4833 0.5840 25 .6099 0.8590 18 .7850 1.0111 21
.0681 0.7482 17 .3581 0.9070 22 .4944 0.5872 23 .6211 0.8758 19 .7853 1.0055 19
.0812 0.7892 22 .3583 0.9120 19 .4994 0.6109 24 .6245 0.8750 31 .7868 1.0065 22
.1073 0.8774 19 .3649 0.8888 21 .5064 0.5921 25 .6303 0.8855 24 .8109 0.9854 29
.1154 0.8686 18 .3750 0.8686 36 .5149 0.5872 29 .6371 0.8929 33 .8244 0.9881 19
.1630 0.9393 21 .3765 0.8888 24 .5161 0.8504 00 .6433 0.8937 29 .8278 0.9754 18
.1679 0.9568 23 .3790 0.8758 26 .5294 0.5916 22 .6472 0.9120 24 .8324 0.9772 38
.1748 0.9454 22 .3917 0.8310 19 .5318 0.6115 20 .6503 0.9256 19 .8369 0.9230 22
.1810 0.9674 23 .3954 0.8356 29 .5352 0.6065 38 .6527 0.9410 22 .8448 0.9568 23
.1889 0.9854 22 .4019 0.8136 19 .5416 0.6368 23 .6669 0.9524 21 .8631 0.9307 18
.1916 0.9541 22 .4115 0.7885 24 .5428 0.6462 18 .6696 0.9497 24 .8652 0.9053 19
.1979 1.0130 19 .4120 0.7820 22 .5466 0.6571 21 .6765 0.9647 20 .8782 0.9324 17
.2160 0.9836 28 .4123 0.7770 26 .5472 0.6564 18 .6849 0.9454 29 .8841 0.9078 20
.2209 0.9710 19 .4158 0.7551 26 .5522 0.6761 29 .6880 0.9290 17 .8856 0.8962 26
.2374 0.9863 16 .4221 0.6755 15 .5620 0.6918 21 .6892 0.9727 17 .8891 0.8433 15
.2606 0.9863 18 .4244 0.7365 24 .5683 0.7359 29 .7069 0.9991 24 .9025 0.8758 23
```

.2748 0.9674 19 .4347 0.6963 17 .5725 0.7551 16 .7104 0.9991 17 .9154 0.7856 15
.2850 0.9963 24 .4378 0.6899 31 .5726 0.7231 22 .7112 0.9881 25 .9238 0.8002 19
.2897 0.9710 24 .4423 0.6767 25 .5754 0.7461 38 .7130 0.9945 19 .9426 0.7106 15
.2963 0.9917 28 .4497 0.6711 25 .5893 0.8009 38 .7273 1.0462 17 .9433 0.7238 22
.2984 1.0000 23 .4551 0.6275 19 .5895 0.7863 17 .7327 0.9972 19 .9652 0.6699 19
.3063 0.9550 21 .4675 0.5970 22 .5930 0.8166 21 .7411 0.7125 00 .9682 0.6298 54
.3160 0.9665 22 .4699 0.5927 21 .5938 0.8113 22 .7497 0.9480 00 .9700 0.6229 87
.3194 0.9515 21 .4719 0.5840 26 .5950 0.8211 24 .7633 0.9899 29 .9841 0.6345 60
.3323 0.9315 21 .4721 0.5867 25 .5975 0.6183 00 .7666 1.0083 13
14.
.0010 0.6558 60 .3193 0.9665 18 .4603 0.6516 36 .5987 0.8742 29 .7258 0.9808 25
.0150 0.6421 51 .3324 0.9817 20 .4664 0.6674 24 .6064 0.8480 23 .7442 1.0139 22
.0420 0.6957 33 .3362 0.9612 29 .4755 0.6522 15 .6109 0.8670 28 .7468 1.0120 22
.0435 0.7178 22 .3423 0.9341 18 .4796 0.6252 19 .6116 0.8815 23 .7502 0.9991 29
.0681 0.7565 16 .3453 0.9281 19 .4910 0.6397 25 .6145 0.8790 16 .7639 1.0271 28
.0918 0.8371 22 .3502 0.9384 29 .4929 0.6339 24 .6205 0.8954 23 .7724 1.0139 18
.0942 0.8480 19 .3596 0.9454 19 .4936 0.6356 18 .6288 0.9238 22 .7923 0.9836 17
.0974 0.8782 38 .3691 0.9036 25 .5054 0.6246 29 .6368 0.9247 26 .8059 1.0000 20
.1364 0.9358 36 .3761 0.9070 25 .5060 0.6345 19 .6374 0.9221 18 .8098 1.0065 17
.1386 0.9154 31 .3797 0.9003 19 .5114 0.6368 29 .6441 0.9410 29 .8241 0.9710 28
.1571 0.9781 24 .3894 0.8662 20 .5193 0.6206 33 .6617 0.9445 24 .8423 0.9585 17
.1913 1.0083 24 .3939 0.8582 45 .5243 0.6415 17 .6630 0.9350 23 .8433 0.9428 18
.1981 0.9683 21 .3985 0.8535 18 .5333 0.6558 20 .6661 0.9550 25 .8499 0.9489 19
.2135 0.9936 19 .4017 0.8504 23 .5387 0.6717 45 .6663 0.9550 20 .8554 0.9541 18
.2168 0.9936 19 .4019 0.8566 25 .5487 0.6805 31 .6826 0.9945 23 .8637 0.9532 24
.2375 1.0028 20 .4146 0.7995 17 .5528 0.7125 28 .6865 0.9927 17 .8744 0.9273 24
.2436 0.9881 21 .4183 0.8128 22 .5556 0.7204 18 .6889 0.9665 17 .9013 0.8662 56
.2489 0.9936 28 .4264 0.7849 20 .5592 0.7171 23 .6899 0.9790 22 .9023 0.8551 26
.2612 1.0083 17 .4278 0.7565 24 .5594 0.7379 21 .6917 0.9854 16 .9214 0.8219 20
.2663 0.9936 29 .4296 0.7516 24 .5660 0.7482 20 .7085 0.9872 20 .9287 0.7951 18
.2765 0.9982 20 .4313 0.7614 16 .5711 0.7727 20 .7095 1.0018 17 .9473 0.7338 38
.2963 0.9727 19 .4471 0.6957 17 .5715 0.7741 22 .7138 1.0102 24 .9555 0.7224 21
.3061 0.9471 13 .4517 0.6805 23 .5811 0.7987 28 .7177 0.9845 23 .9806 0.6528 78
.3083 1.0083 20 .4537 0.6798 23 .5857 0.8204 17 .7246 1.0046 24 .9851 0.6662 48
.3138 0.9908 18 .4547 0.6773 33
12.
1111 1111 1111101 11110 11011 11111 0 1 1
1111 1111 1111101 11111 11011 01111 0 1 1
1111 1111 1111101 01111 11111 11111 0 1 1
1111 1111 1111101 11111 11110 11111 0 1 1
2

Appendix E: Sample Simplex Files

The following are examples of the files required for the simplex enhanced version of the Wilson-Devinney light curve analysis program.

Constraint file:

This file contains constraints for SIMPLEX

0.10	100.00	a
0.00	0.90	e
0.00	360.00	PER
0.10	2.00	F1
0.10	2.00	F2
0.00	360.00	PSHIFT
-50.00	100.00	VGA
30.00	90.00	i
0.05	1.00	GR1
0.05	1.00	GR2
0.50	7.00	T1
0.50	6.00	T2
0.40	1.00	A1
0.40	1.00	A2
1.00	36.00	OMEGA1
1.00	36.00	OMEGA2
0.05	9.00	q
1.00	12.56	L1
1.00	12.56	L2
0.10	1.00	x1
0.10	1.00	x2
0.00	0.10	L3

Information file:

```
****************************************************************************


              I n p u t - file  for  L C 9 3 K S . E X E
-----------------------------------------------------------------------------


             UNIX name of this file :  lc93ks.inf


             ***************************************************
             *  Version 1.0 - Sep 20, 1993  by  Josef Kallrath  *
             *  Last Revise : Oct 29, 1993  by  Josef Kallrath  *
             *                                *
             *   Astronomische Institute der Universitat Bonn   *
             *             Auf dem Hugel 71             *
             *             D-53121  B o n n  1          *
             *        Federal Republic of Germany          *
             ***************************************************
```

This file contains parameters which define how LCDC will work !

                    Explanations to the parameters

TASK : 1 = invokes computation of simple light curves
        2 = invokes differential corrections
        3 = invokes the simplex algorithm
        4 = starts a test run - one light curve only

IWRITE 0 = no , 1 = yes ; produces lc93ks.spt

RESTRT 0 = no , 1 = yes ; requires lc93ks.spt to exists

IFSPOT 0 = use spot data from Wilson-Devinney input file
        1 = use spot data from 'spot.dat'

IGRAPH 0 = no
        1 = produces TopDRAWER compatible graphics after TASK=3 or TASK=4
        2 = produces gnuPLOT   compatible graphics after TASK=3 or TASK=4

MAXIT -1 = Shows initial simplex without evaluated vertices
     0 = Shows initial simplex with   evaluated vertices
     >0 = Number of iteration to be performed

ENTRY
     Never do change these four lines, because they tell the program 1
     where to find the beginning of data.   2
--- 3 ---
                               4
Specify the task (TASK = 1,2, 3 or 4)   TASK   : 3

Would you like to write Simplex tableau to lcj.spt ? IWRITE : 1

Specify RESTART-options for simplex-algorithm [0 or 1] RESTRT : 0

Specify if you would like to produce some graphics   IGRAPH : 0

Specify the source of spot data parameters   IFSPOT : 1

Specify G1   G1   : 4.353
Specify G2   G2   : 4.304

******************** TASK 3 **

Maximal number of iterations   MAXIT :300

Output of Simplex Tableau (YES=1,NO=0) ?   IOSTYN : 1
Reflection Coefficient, >0   ALPHA : 1.00
Contraction Coefficient, 0 < beta < 1   BETA   : 0.50
Expansion   Coefficient, 1 < gamma   GAMMA : 2.00

Format of size parameters of initial simplex   IFORM : F5.2
Format of minimal size of simplex   IFORM : E6.1

Format of parameter's and SSR Output-Vector   FORM1 : F9.5
Format of parameter's and SSR errors   FORM2 : F9.5
Format of Data-Points   FORM3 : F10.5

Divide all increments by ...   INITD : 1
Specify the mode for construction of init simplex   MINIT : 1

Specify stopping criteria for simplex   SGMINT : 0.004

Define the size of the simplex

```
0.1   AS1          is to be adjusted  1
0.1   AS1
0.1   AS1
0.1   AS1
0.1   AS1
0.1   AS1
0.1   AS1
0.1   AS1
2.0   a
0.1   e
2.0   omega
0.2   F1
0.2   F2
0.2   phi          is to be adjusted  2
0.1   Vgamma
2.0   XINCL         is to be adjusted  3
0.5   GR1
0.5   GR2
0.2   TP1
0.14  TP2           is to be adjusted  4
0.5   ALB1
0.05  ALB2
0.4   POTT1
0.3   POTT2         is to be adjusted  5
0.1   RM           is to be adjusted  6
0.2   HLA          is to be adjusted  7
0.2   CLA
0.1   X1A
0.1   X2A
0.2   L3
```

List of the parameters' errors

```
0.1E-2  AS1
0.1E-2  AS1
0.1E-2  AS1
0.1E-2  AS1
0.1E-2  AS1
0.1E-2  AS1
```

```
0.1E-2  AS1
0.1E-2  AS1
0.1E-2  a
0.1E-2  e
0.1E-2  omega
0.1E-2  F1
0.1E-2  F2
0.1E-2  phi
0.1E-2  Vgamma
0.1E-2  XINCL
0.1E-2  GR1
0.1E-2  GR2
0.1E-2  TP1
0.1E-2  TP2
0.1E-2  ALB1
0.1E-2  ALB2
0.1E-2  POTT1
0.1E-2  POTT2
0.1E-2  RM
0.1E-2  HLA
0.1E-2  CLA
0.1E-2  X1A
0.1E-2  X2A
0.1E-2  L3A
0.1E-2  Residuals
```

****************** End of h235.inf file   *******************************

Run file:

```
#!/bin/csh
#   run
#   This batch file copies 107.dci and 107.inf into lc93ks.dci and lc93ks.inf    :  run

    if ( $1 == 'clean' ) goto CLEAN

#   and then starts 'lc93ks' for simplex or differential corrections
    if ( -f 107.log ) rm 107.log
    if ( -f lc93ks.spo ) rm lc93ks.spo
    if ( -f lc93ks.out ) rm lc93ks.out
    if ( -f lc93ks.spt ) rm lc93ks.spt
    if ( -f lc93ks.inf ) rm lc93ks.inf
```

```
if ( -f lc93ks.dci ) rm lc93ks.dci
if ( -f lc93ks.con ) rm lc93ks.con

#    change next 4 line and replace 107.* by newstar.*
cp 107.inf lc93ks.inf
cp 107.dci lc93ks.dci
cp 107.con lc93ks.con
if ( -f 107.spt )  cp 107.spt lc93ks.spt

if ( -f DUMMY    ) rm DUMMY
lc93ks >& 107.log
if ( -f lc93ks.trace ) rm lc93ks.trace
if ( -f core     ) rm core
if ( -f lc93ks.spo   ) mv lc93ks.spo 107.spo
if ( -f lc93ks.spt   ) then
  if ( -f 107.spt ) rm 107.spt
  mv lc93ks.spt 107.spt
endif
if ( -f lc93ks.out   ) then
  if ( -f 107.out ) rm 107.out
  mv lc93ks.out 107.out
endif

echo  Just finished running '107' !

exit


CLEAN:
    if ( -f DUMMY    ) rm DUMMY
    if ( -f core     ) rm core
    if ( -f C.01     ) rm C.*
    if ( -f O.01     ) rm O.*
    if ( -f R.01     ) rm R.*
    if ( -f lc93ks.spo ) rm lc93ks.spo
    if ( -f lc93ks.spe ) rm lc93ks.spe
    if ( -f lc93ks.spt ) rm lc93ks.spt
    if ( -f lc93ks.inf ) rm lc93ks.inf
    if ( -f lc93ks.dci ) rm lc93ks.dci
    if ( -f lc93ks.out ) rm lc93ks.out
    if ( -f lc93ks.con ) rm lc93ks.con
    if ( -f lc93ks.log ) rm lc93ks.log
    if ( -f 107.log ) rm 107.log
    echo 'dummy' > dummy.out
    rm *.out
    ls
```